SMC Bulletin

ISSN 2394-5087

A Publication of the Society for Materials Chemistry

Volume 10 No. 3 December 2019

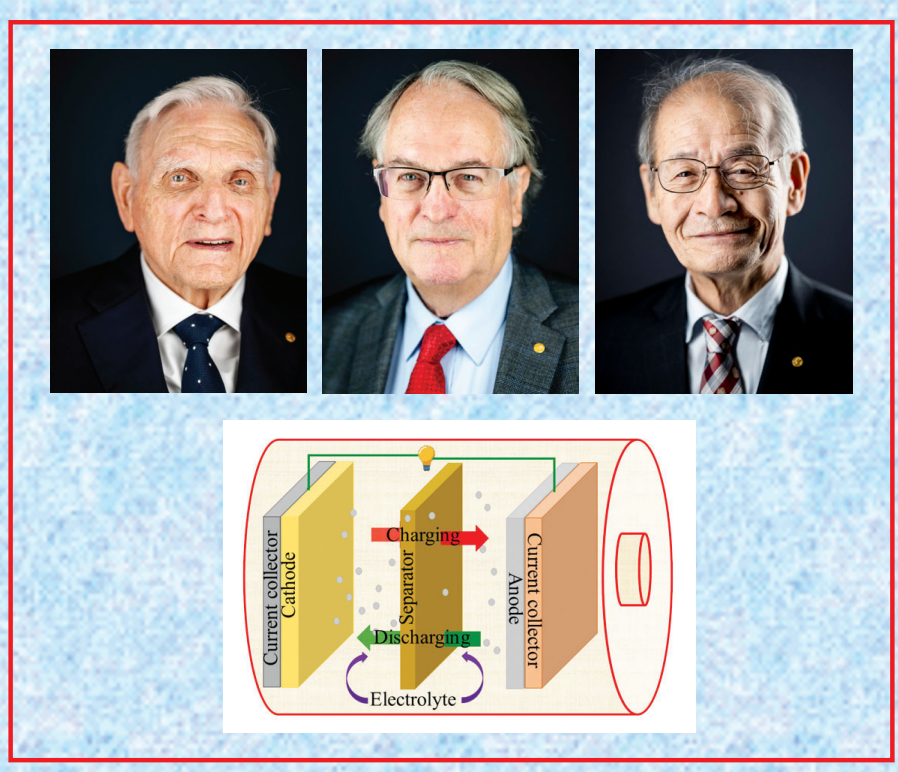

Special Issue on

Energy storage devices (Lithium ion batteries)

SOCIETY FOR MATERIALS CHEMISTRY

Society for Materials Chemistry

Society for Materials Chemistry was mooted in 2007 with following aims and objectives:

(a) to help the advancement, dissemination and application of the knowledge in the field of materials chemistry,

(b) to promote active interaction among all material scientists, bodies, institutions and industries interested in achieving the advancement, dissemination and application of the knowledge of materials chemistry,

(c) to disseminate information in the field of materials chemistry by publication of bulletins, reports, newsletters, journals.

(d) to provide a common platform to young researchers and active scientists by arranging seminars, lectures, workshops, conferences on current research topics in the area of materials chemistry,

(e) to provide financial and other assistance to needy deserving researchers for participation to present their work in symposia, conference, etc.

(f) to provide an incentive by way of cash awards to researchers for best thesis, best paper published in journal/national/international conferences for the advancement of materials chemistry,

(g) to undertake and execute all other acts as mentioned in the constitution of SMC

Executive Committee

Contact address
Society for Materials Chemistry
C/o Chemistry Division
Bhabha Atomic Research Centre, Trombay, Mumbai, 400 085, India
Tel: +91-22-25592001, E-mail: socmatchem@gmail.com

SMC Bulletin

A Publication of the Society for Materials Chemistry

Volume 10 **No. 3** **December 2019**

Special Issue on

Energy storage devices (Lithium ion batteries)

SOCIETY FOR MATERIALS CHEMISTRY

SMC Bulletin

Vol. 10 **No.3** **December 2019**

Guest Editor

Dr. Sandeep Nigam
Chemistry Division
Bhabha Atomic Research Centre
Trombay, Mumbai 400 085
e-mail: snigam@barc.gov.in

Dr. Vinita G. Gupta
Chemistry Division
Bhabha Atomic Research Centre
Trombay, Mumbai 400 085
e-mail: vinita@barc.gov.in

Dr. Balaji P. Mandal
Chemistry Division
Bhabha Atomic Research Centre
Trombay, Mumbai 400 085
e-mail: bpmandal@barc.gov.in

Published by

Society for Materials Chemistry
C/o. Chemistry Division
Bhabha Atomic Research Centre, Trombay, Mumbai, 400 085
E-mail: socmatchem@gmail.com,
Tel: +91-22-25592001

Front cover shows schematic of a Li-ion battery and photographs of John B. Goodenough, M. Stanly Whittingham and Akira Yoshino, who were awarded the Noble Prize in 2019 for their remarkable contributions towards the development of Li-ion batteries.

Guest Editorial

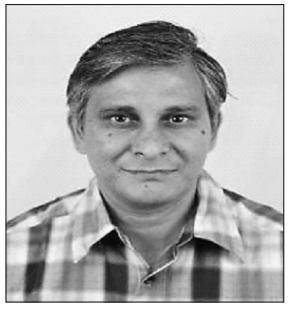

Dr. Sandeep Nigam

Dr. Vinita G. Gupta

Dr. Balaji P. Mandal

If there is one technology that has truly impacted the modern day life, it is lithium ion battery (LIB) technology. It involves the lightest solid element Li which has been derived from the Greek word "Lithos" (meaning stone). In today's world, where obtaining energy from cleaner sources is matter of priority as well as urgency for Governments around the world, Li-ion battery technology has come to the rescue. There is no denying the fact that Lithium-ion batteries have brought the greatest benefit to humankind. They are used globally to power the aids that we us in our day-to-day life for working, communicating, studying, entertainment and effectively in all the spheres of our life. Not only this, they have made possible the storage of energy from other renewable sources such as solar and wind thus enabling the mankind to step towards fossil fuel-free world. This has been duly recognised and John B. Goodenough, M. Stanly Whittingham and Akira Yoshino were honoured with Nobel Prize in 2019 for their remarkable contribution towards the development of Li-ion batteries.

The fundamental research and development in solid state chemistry and physics, particularly during 1970s and 1980s, has contributed immensely to development of Li-ion battery. Discovery of new materials and an evolving fundamental understanding of the structure-composition-property-performance relationships have been at the heart of advancement of this particular field. Lithium ion battery is composed of cathode, anode, electrolyte and separator. While all the components of the battery are important, the quality of battery is hugely dependent on electrodes, therefore, research focus is on development or designing of new electrode materials. Today's research is thus focussed on designing new battery materials with high energy density, higher power density, enhanced cycle life and increased level of safety. The innovation in synthesis and processing strategies well supported by advanced characterisation techniques could also pave way for the discovery of better and safer materials.

To honour this great discovery and to celebrate the tireless efforts of the Nobel prize winners of year 2019, a special issue of SMC Bulletin is being presented. This issue brings together eminent battery researchers, form various parts of country, working on different aspects of Li-ion battery who have shared their work and invaluable experience in this field.

The article from Dr. Manjusha Shelke's group discusses about different conversion- type anode materials for LIBs. It is a lucid review on various metal oxide, sulphide and phosphide-based anode materials and their electrochemical performance in context of LIBs. Different challenges like safety, environment compatibility, cost, ease of fabrication etc. have to be addressed for industrial applications. Prof. Dixit has painstakingly summarized the development of cathode materials from first generation $LiMO_2$ cathode materials to present day third generation complex oxide based cathode materials. This would be an interesting account for the researchers working in this field. In the recent years, "alloying reactions" of Li with some of the elements such as Si, have been investigated to overcome the several drawbacks associated with graphitic C-based materials. In this context, Prof. Mukhopadhyay's article focuses on various electro-chemo-mechanical aspects of Si-based anodes for Li-ion batteries. Prof. Nagaraju's article discusses about electrochemical performance of vanadium oxides with different morphology and oxidation states. Dr. Dutta et al review a totally novel material, 3D graphene, as host for Li-S battery.

We are sure that this collection of different aspects of Li-ion battery research would present a contemporary and a wholesome view to the readers. We extend our heartfelt gratitude to all the contributors for sharing their research. We are also thankful to Society of materials chemistry for giving us this opportunity to be the guest editors for this very special issue which we have thoroughly enjoyed.

From the desks of the President and Secretary

Dr. V. K. Jain
President

Dr. R. K. Vatsa
Hon. Secretary

Dear colleagues,

Warm greetings from Executive Council of Society for Materials Chemistry!

Society for Materials Chemistry and Editorial Board of SMC bulletin have been regularly publishing thematic issues on contemporary topics of materials chemistry. Materials for Lithium Ion Battery (LIB) is one such topic which has gained unprecedented attention in recent times due to its wide-ranging applications.Nearly 1.5 billion mobile phones are annually manufactured worldwide and all of these run on LIB.The development of LIB has neither been simple nor easy due to safety problems associated with handling of lithium metal and its deposition recharging. It required breakthrough in materials chemistry for anode, cathode and non-aqueous electrolytes to accomplish the desired goal. The first patent entitled "Transition metal oxides as cathode, $LiCoO_2$" towards LIB development was filed by Prof. Goodenough on 31 March 1980, and thereafter there was an outbreak in this field. The outstanding and remarkable contributions in the development of LIB based energy storage systems for practical applications have been dually recognized with the award of 2019-Nobel Prize in Chemistry to three scientists Prof. J. B. Goodenough, Prof. M. S. Whittingham and Prof. A. Yoshino.

It is hard to imagine today's world without LIB which finds its application in different fields like telecommunications, automobiles, space, defence, etc. Constant effortsare being made to improve the energy density, power density, safety and long cycle life of LIB.A variety of electrode materials have been designed with improvised behaviour. Along with the electrode materials, the search for electrolyte materials with superior stability is also aggressively pursued. The next generation Li-Sulfur battery has great potential in this regard as its energy density is much higher than LIB. The cycle stability and capacity fading are some other issues that are being researched to obtain superior systems. As the world is aiming for the fossil fuel-free world, Li-ion based devices are invaluable devices for energy storage.

To commemorate the success of LIBs, current issue of SMC bulletin is being published. This issue contains five invited articles focussing recent developments on electrode materials such as metal oxides/ sulfides/ phosphides, 3D graphene sponge-based materials for high energy density LIBs. We place on record our sincere appreciation to Drs. Sandeep Nigam, Vinita G. Gupta and Balaji Prasad Mandal, Guest Editors, who have taken keen interest to bring out this special issue. We also thank all the members of SMC for their continued support and cooperation in the growth of the Society.

CONTENTS

Metal Oxides/Sulphides/phosphides: High specific energy conversion anodes for Li ion batteries

Pravin K. Dwivedi[a,b], Poonam Yadav[a,b], Golu Parte[a,b] and Manjusha V. Shelke*[a,b]
[a]*Physical and Materials Chemistry Division, CSIR-National Chemical Laboratory, Pune 411008, MH, India*
[b]*Academy of Scientific and Innovative Research (AcSIR), Gaziabad-200112, UP, India*
**Corresponding author: Dr. Manjusha V. Shelke (mv.shelke@ncl.res.in)*

Abstract

Development of high-performance Li-ion batteries (LIBs) are green solution to meet the future energy demands and combat environmental pollution problems. Various nanostructured high capacity anodes starting from Li metal, graphite, metal oxides, sulphides and phosphides have been developed. Graphite is a stable anode but with low capacity. On the other hand, oxides, sulphides and phosphides are high capacity anodes but this capacity is not very stable over cycling. In this review, we summarise developments and strategies used to stabilise high capacity of anode materials and their charge storage mechanisms.

1. Introduction

Research on electrode materials for rechargeable battery is very important considering the increasing need of high specific energy storage devices especially for the storage and transport of the energy from resources like solar and wind [1-4]. LIB is an energy storage device which has gained attention due to its high electrochemical performance [5, 6]. Li-ion cell consists of positive electrode (cathode) and negative electrode (anode) separated by polymeric separator dipped in the electrolyte. The reaction with lower potential occurs at anode and reaction at higher potential occurs at cathode [7]. Due to the lowest standard potential and the lowest atomic weight, the metallic lithium offers extremely high energy density, so it becomes the material of choice for anode in next generation LIBs [8]. But due to non-uniformity of Li deposition and dissolution, Li dendrite structure forms which causes safety issues and short circuit of the cell [9].

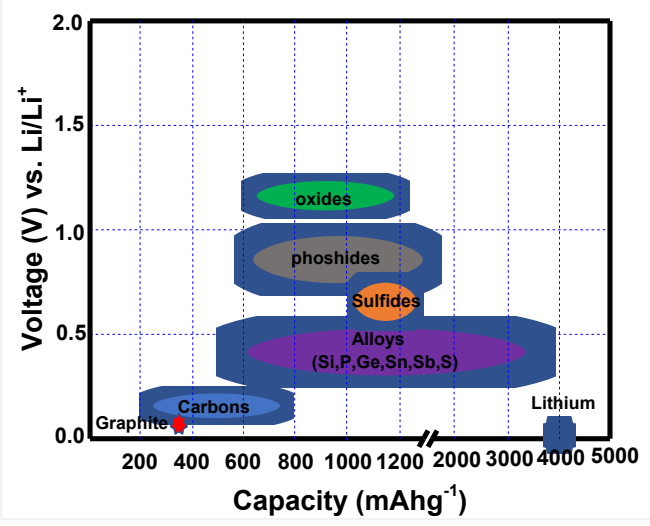

Figure 1: *Performance comparison of different anodes for LIB.*

Carbon based insertion materials provide reasonable alternative to lithium metal anode considering the safety and cyclability of anodes [10]. Capacity vs. reaction potential comparison of various anodes is shown in figure1. One such example of carbon material is graphite which is inexpensive, easy to handle, and abundant with good safety and stability. Li intercalation into graphite occurs at ~100 mV, voltage enough to prevent plating of Li and dendrites formation. But graphite, an intercalation type of anode has limited specific capacity (~ 375 mAh g^{-1} theoretically). Various alternative materials to graphite; such as metal oxides, sulphides and phosphides have been explored for their higher specific capacity that are based on conversion chemistry. It is also observed that the polarization (V) decreases from fluorides (V~ 1.1 V) to oxides (V~ 0.9 V), sulfides (V~ 0.7 V) and phosphides (V~0.4 V) [11]. The reason lies in the strength of bond between metal and anion. As the electronegativity of the anion decreases, localization of charges diffuses away from metal centre and electron transfer also occurs into the bands with strong anion contribution. This allows the tuning of reaction potential using different anionic species and resulting energy density according to required application. In this review, we focus on different anode materials, their synthesis and LIB performances.

1. Basics of anode: mechanism, voltage, energy density

Li batteries are rechargeable batteries which reversibly interconvert electrical and chemical energy via a 'rocking-chair' mechanism [12]. Charge storage takes place via reversible insertion/extraction of Li-ions between the electrodes separated by a Li-ion conducting but electrically insulating polymer membrane dipped in electrolyte

medium. So, basic components of an electrochemical cell are cathode (positive electrode), anode (negative electrode), electrolyte, separator and current collector. In the commercial batteries, graphitic carbon is most commonly used anode and $LiCoO_2$ is most commonly used cathode material. The Li storage occurs at respective electrodes according to following equations:

$$\text{At Anode: } C + xLi^+ + xe^- \rightarrow Li_xC$$

$$\text{At Cathode: } LiCoO_2 - xLi^+ - xe^- \rightarrow Li_{1-x}CoO_2$$

At the time of charging, reduction of cathode materials takes place, Li ions moves through ionically conducting electrolyte and electron transport takes place via external circuit. The reverse reactions occur at the time of discharging at respective electrode. Total number of Li ions exchanged between cathode and anode decides the capacity of the cell. The theoretical specific capacity (C^{th}) can be calculated by following equation:

$$C^{th} = nF/M$$

Where, n is the number of moles of electrons involved in the electrochemical reaction, F is the Faraday constant, and M is the molecular weight of the active electrode material.

2. Metal Oxides:

Transition metal oxides are the potential candidate as an anode material for LIBs for the substitution of graphite electrode due to very high theoretical specific capacity. Additionally, reversible reactions with Li metal reduce the metal-lithium alloy formation as follows:

$$M + xLi^+ + xe^- \leftrightarrow 4Li_2O + M \ (M = Fe, Co, Ni, Cu)$$

The above forward reaction is thermodynamically feasible and involves multi electron transfer per metal atom, leads to high theoretical capacity [13]. However, the backward reaction, formation of the Li ion from Li_2O is a thermodynamically unfavourable and facilitated by metal nanoparticles (M) synthesis during the reaction. This reversibility of the above reaction is well maintained in the nanoscale system and improves the capacity retention as well as the thickness of SEI film at high current density. In conversion mechanism, the normal reaction voltage range is within 0.5-1.0 V, which increases with the iconicity of the M-O bond [14]. So the higher reversible specific capacity and safer lithiation potential of these materials are important parameters for high performance LIBs but poor reaction kinetics, large volume expansion and large potential hysteresis, related to the energy barrier in the breaking of the M-O bond and the change of electronic conductivity, diminish the electrochemical performance and long term cycle life of LIBs for large scale applications [14]. In this context, several researchers have developed nanostructured porous materials and their nanocomposites with improved reaction kinetics to enhance the cycle life and capacity retention in LIBs.

2.1 Manganese Oxide

Conversion reaction based materials especially nanostructured transition metal oxides such as Fe-, Co-, Ni-, Sn-, and Mn-oxides are considered promising anode materials for LIBs. Among these Mn-oxides (MnOx) have received tremendous interest due to their high specific capacity, low toxicity, abundance, low cost and lower operating voltage [15]. However, poor cycling stability due to volume change and particle aggregation during lithiation/ delithiation which leads to loss of electrical contact and mechanical failure consequently decreases the rate capability [16]. To counter these issues different strategies were implicated such as hybridizing MnOx with carbon, construction of nanostructures, i.e., nanowires, nanorods, nanotubes and nanosheets etc. Manganese oxides are found in different phases such as MnO (756 $mAhg^{-1}$), MnO_2 (1223 $mAhg^{-1}$), Mn_2O_3 (1019 $mAhg^{-1}$), and Mn_3O_4 (937 $mAhg^{-1}$) [17]. Various MnOx-carbon nanocomposites such as MnOx with carbon nanofibers, graphene, carbon nanosheets and nanotubes have been investigated to improve the electrochemical performance of MnOx.

Liu et al prepared MnO nanocrystals embedded in carbon nanofibers (MnO/CNFs) through an electrospinning process. The as-formed MnO/CNFs were used as an anode material for lithium-ion batteries, the MnO/CNFs display high discharge capacity of 1082 $mAhg^{-1}$ after 100 cycles at 100 mAg^{-1} with coulombic efficiency of 99% which indicates the excellent cyclic performance. The MnO/CNFs delivered specific capacity of 575 $mAhg^{-1}$ at 1 Ag^{-1} even after 200 cycles reflects the superior rate capability of material. The excellent rate capability and cyclic performance is due to the CNFs which increases the contact area between the electrode and electrolyte as well as accommodate the volume change of MnO during lithiation/delithiation [18]. Xu et al. prepared MnO/C nanotube as an anode for LIBs by hydrothermal method followed by annealing. It shows a reversible capacity of 763.3 $mAhg^{-1}$ after 100 cycles at a current density of 100 mAg^{-1} [19]. Gao et al. anchored MnO nanowires homogeneously on both sides of the cross-linked rGO [20]. Many other studies were carried out on

MnO/CNFs/GO/CNTs/C nanocomposites to mitigate the drawback to increase the electrochemical performance of MnO [21-29].

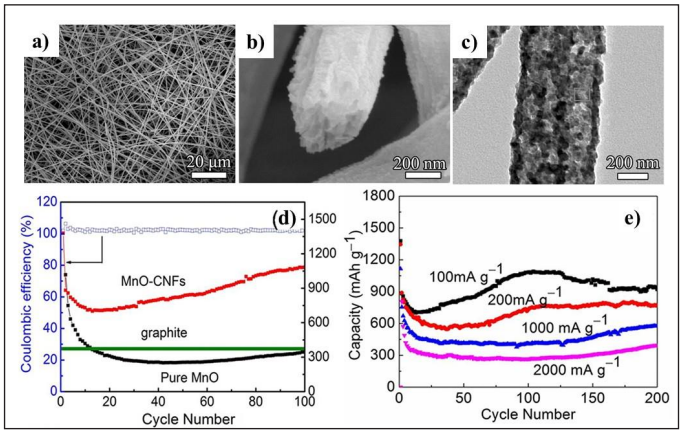

Figure 2: *(a,b) FESEM images of the MnO/CNFs; (c) TEM image of the porous MnO/CNFs; (d) Capacity-cycle number curves of MnO/CNFs and bare MnO nanoparticles at a current density of 100 mAg^{-1} (e) Cycling performance of MnO/CNFs electrode at various current densities.[18]*

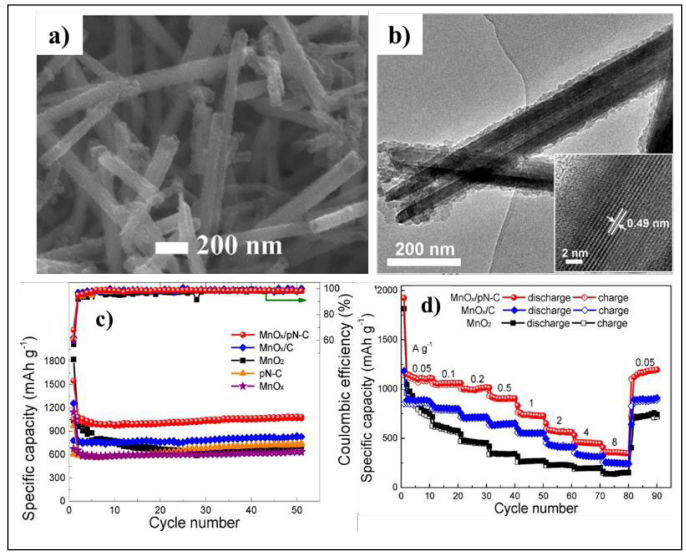

Figure 3: *(a) SEM image of MnOx/pN-C nanocomposites; (b) TEM image of MnOx/pN-C nanocomposite and (b, inset) the corresponding HRTEM. [30]*

Wang et al. coated nitrogen-enriched porous carbon (pN-C) onto the MnO_2 nanotubes and used as anode material for LIBs. The MnO_2/pN-C shows reversible capacity of 1068 mAhg^{-1} at 100mAg^{-1} and delivers a specific capacity of 361 mAhg^{-1} even at high current density of 8 A g^{-1} and provides a stable cycling performance of 606 mAhg^{-1} for 300 cycles at current density of 2Ag^{-1}. The pN-C increases the electrochemical performance by improving electron transfer kinetics and alleviating the volume change of MnO_2 during cycling [30]. Wu et al. prepared MnO_2/CNTs nanocomposite membrane by chemical vapor deposition and electrodeposition [31]. Asif et al. reported Ni-doped manganese oxide/CNT nanostructures as a cathode for magnesium/lithium hybrid ion battery [32]. Li et al. reported 3D multilevel porous conductive structure of rGO wrapped CNTs and MnO_2 nanosheets surrounding rGO via vacuum freeze-drying [33]. There are considerable reports on modifying the nanostructure composites of MnO_2/C/CNTs/CNH/graphene hybrids with an objective for high reversible capacity, excellent cycling stability and rate capability of LIBs [34-39].

Hwang Ko et al. have added PEDOT: PSS (poly (3, 4-ethylenedioxythiophene) polystyrene sulfonate) to Mn_2O_3 nanowires to overcome the capacity fading of LIBs during cycling. PEDOT: PSS was coated onto Mn_2O_3 nanowires which delivered excellent cyclability with a reversible capacity of 1450 mAhg^{-1} at a current density of 100 mAg^{-1} after 200 cycles [40]. To improve the electrochemical performance of Mn_2O_3 mixed metal oxides and metal doping was also adopted [41-45]. For example, Jie Quiong Li et al. preparaed $FeMnO_3$/ Mn_2O_3 hybrid, this shows reversible discharge capacity of 1580 mAhg^{-1} and retain capacity of 995 mAhg^{-1} at current density of 200 mAg^{-1} for 170 cycles. $FeMnO_3$ nanocubes and Mn_2O_3 nanotubes synergistically improved overall structure stability and hence increase in the electrochemical performance [46].

Park et al. synthesized a flexible and free standing porous Mn_3O_4 nanorod/reduced graphene oxide (pMn_3O_4 NR/rGO) paper. pMn_3O_4 NR/rGO paper as LIBs anode exhibited the first discharge capacity of 943 mAhg^{-1}, and remained constant at 573 mAhg^{-1} even after 100 cycles at 100 mAhg^{-1} [47]. Ma et al. synthesized composite of vapour grown carbon fibers with Mn_3O_4 (Mn_3O_4/VGCFs). This composite exhibits a reversible capacity of 950 mAhg^{-1} at 200 mAg^{-1} current density [48]. There are significant number of reports on tailoring and designing of the nanostructures of Mn_3O_4/C/graphene/CNFs/CNTs nanocomposites with an aim of increasing rate capability and cyclic life [49-59].

3.2 Iron oxides

Among all transition metal oxides, iron oxides like hematite (Fe_2O_3), magnetite (Fe_3O_4) and ferrous oxide (FeO) drawn particular attention because of their high theoretical capacity of ≈1000 mAhg^{-1}, non-toxicity, high abundance, high corrosion resistance, and low processing cost [60,61]. The higher lithium insertion voltage and the inflammable behaviour of iron-oxide-based anodes make safer LIBs for

large-scale applications. In all three forms of iron oxides, Fe_2O_3 used as promising anode material due the most thermodynamically stable nature and its high theoretical capacity of 1007 $mAhg^{-1}$ following the general reaction mechanism $Fe_2O_3 + 6Li^+ + 6e^- \leftrightarrows 2Fe + 3Li_2O$ as reported firstly by Tarascon and co-workers [13]. Nanosized α-Fe_2O_3 nanoparticles (approx. ~ 20 nm) can retain their structural integrity during conversion reaction and react reversibly with 0.5 mol of Li within the potential range of 4.0 to 1.5 V (vs Li). Up to 0.9 V (vs Li) discharge of the cell, 2 mol of Li ion can be intercalated, however, on the delithiation process, this amount of Li cannot be electrochemically extracted without obliterating the crystal structure. Further the deep discharge up to 0.005 V (vs Li^+/Li), causes reaction of 6 mol of Li ions with 1 mol of Fe_2O_3 and the leftover Li ions could be causing the electrolyte degradation on the surface of hematite nanoparticles. The reaction of lithiation process is explained as follows [62].

$$Fe_2O_3 + 2Li^+ + 2e^- \rightarrow Li_2(Fe_2O_3)(4.0 - 0.9\ V)$$

$$Li_2(Fe_2O_3) + 4Li^+ + 4e^- \rightarrow 2Fe^0 + 3Li_2O\ (0.9 - 0.005\ V)$$

Formation of the insulative Li_2O matrix on the surface of electrode cause higher capacity loss on further delithiation process, and form the amorphous iron oxide by oxidation of metallic Fe. Hence the reversible reaction mechanism is proposed as follows [62].

$$2Fe^0 + 2xLi_2O \leftrightarrow 2FeOx + 4xLi^+ + 4xe^-\ (0.005 - 3.0\ V, 0 \leq x\ \leq 1.5)$$

Moreover, there are several limitations like poor cycle life caused by the volume expansion during the lithiation-delithiation process. The low electronic conductivity of iron oxides also degrades the battery performance at high current rate. So design and synthesis of the electrode material in the nanoscale level with various morphology, porous structure, different configuration, which promote the electrochemical process and maintain the good structural integration is important to enhance the battery performance [63]. Tarascon et al. studied the effect of size of the α-Fe_2O_3 nanoparticles in the lithiation-delithiation process for the 1st time and observed that large particles (0.5mm) took up only a small amount of lithium ($Li_xFe_2O_3$, x < 0.1), whereas nanosized α-Fe_2O_3 (20 nm) inserted up to one Li per formula unit ($Li_xFe_2O_3$, x =1) without any phase transformation. To avoid the use of additives and improving the electron transport efficiency, it is more preferred to grow the Fe_2O_3 nanostructured onto the conductive substrate like Cu and Ti foil directly, which provide the direct attachment of the nanostructured to the current collector. Reddy et al synthesized α-Fe_2O_3 nanoflakes on copper substrates by a simple thermal treatment technique which exhibits a stable capacity of 680 $mAhg^{-1}$, corresponding to the 4.05 moles of Li per mole of α-Fe_2O_3. There is no noticeable capacity fading after 80 cycles of charge-discharge at 65 mAg^{-1} (0.1 C rate) of current density [64]. Lin et al. developed monocrystalline hematite nanorods by hydrothermal method which exhibit high initial reversible capacities of 908 $mAhg^{-1}$ at 0.2 C rate and 837 $mAhg^{-1}$ at 0.5 C rate [65]. Zhang and co-workers synthesized a facile lysine-assisted template-free approach to fabricate hierarchical porous Fe_2O_3 microspheres consisting of interconnected Fe_2O_3 nanoparticles and deliver large initial charge specific capacity of 1079 $mAhg^{-1}$ at a current density of 100 mAg^{-1}. Interestingly, the capacity of the product remains 705 $mAhg^{-1}$ after 430 cycles [66]. Zhang and co-workers synthesized the highly pure α-Fe_2O_3 nanoparticles with abundant mesopores with a large surface-to-volume ratio deliver a high capacity of 1009 $mAhg^{-1}$ at 100 mAg^{-1} over 230 cycles and superior high-rate performance attributed to the unique 3D pore-solid architecture [67].

Carbon is playing effective role in hybrid nanomaterials anode for LIB, as it improves the electrochemical performance by enhancing the conductivity while buffering the volume expansion and contraction of the electrode material during the charge discharge process. Zhu et al. reported a simple two-step process to fabricate RGO platelet/ Fe_2O_3 nanoparticle composite which exhibits 1693 and 1227 $mAhg^{-1}$ of the first discharge and charge capacities, respectively, at a current density of 100 $mAhg^{-1}$. It shows a good capacity retention with 1027 $mAhg^{-1}$ after the 50th discharge, as well as ~800 $mAhg^{-1}$ of discharge capacity even at the current density of 800 mAg^{-1} (based on the mass of Fe_2O_3 in the composite) indicating a positive synergistic effect of RGO and Fe_2O_3 on the improvement of electrochemical performance [68]. Jin Kan and co-worker reported a new Fe_2O_3-graphene sheet-on-sheet composite which exhibited a high reversible capacity of 1074.9 $mAhg^{-1}$ with good cycling performance at 0.1 C. A high reversible capacity of 622.4 $mAhg^{-1}$ was retained after 100 cycles at a high current rate of 1 C [69].

Nan Yan and coworkers designed a novel hybrid nanostructure by coating Fe_2O_3 nanoparticles with multi-walled carbon nanotubes (Fe_2O_3@MWCNTs) which exhibit reversible discharge capacity of 515 $mAhg^{-1}$ after 50 cycles at a density of 100 mAg^{-1} and maintain its reversible discharge capacity of 515 $mAhg^{-1}$ after 50 cycles at a density

of 100 mAg^{-1} [70]. Improved electrochemical performance is due to the hollow interiors of MWCNTs providing enough space for the accommodation of large volume expansion of inner Fe_2O_3 nanoparticles. Zhang et al report quasi 1D Fe_2O_3-carbon composite nanofibers via. Electrospinning method, which exhibits a reversible capacity of 820 $mAhg^{-1}$ at a current rate of 0.2 C up to 100 cycles [71]. At a higher current density of 5 C, the cells still exhibit a specific capacity of 262 $mAhg^{-1}$ due to the homogenous dispersed Fe_2O_3 nanocrystals on the carbon nanofiber support.

Recently, several researchers reported composites of active/synergetic electrode materials with hybrid nanostructures having large empty space to accommodate volume expansion during lithiation-delithiation. This also helps to maintain the efficient electrolyte penetration and act as structural stabilizers to improve the electrochemical performance as well as stability of the electrode material. Gu and co-workers fabricate the branched nanocomposite with β -MnO_2 nanorods as the back-bone and porous α -Fe_2O_3 nanorods as the branches by a high-temperature annealing of FeOOH epitaxial grown on the β -MnO_2 nanorods [72]. The branched nanorods of β -MnO_2 / α-Fe_2O_3 delivers a reversible specific capacity of 1028 $mAhg^{-1}$ at a current density of 1 Ag^{-1} up to 200 cycles and excellent rate performance (881 $mAhg^{-1}$at 4 Ag^{-1}). Here Fe_2O_3 is designed to coat the surface of MnO_2, to bridge it with the electrolyte. Meanwhile, the surface coating of Fe_2O_3 on MnO_2 might restrain the potential dissolution of Mn species into electrolyte during lithiation/delithiation. Hao wu et al has developed the branched nanowire hetero structure of Co_3O_4/ α-Fe_2O_3 on a Ti substrate by simple two step hydrothermal procedure which exhibit high initial discharge specific capacity of 1534 $mAhg^{-1}$ at 0.1 Ag^{-1} of current density [73]. Additionally, this heterostructure possess enhanced reversible capacity of 980 $mAhg^{-1}$ over 60 cycles. Here Ti substrate enables the fast charge transfer pathways and the Co_3O_4 nanowire arrays allow the efficient electronic and ionic transport while α-Fe_2O_3 branches provide large surface area with high theoretical specific capacity. α-Fe_2O_3 branches act as volume spacers in between the Co_3O_4 nanowires arrays to reduce the aggregation and maintain the electrolyte penetration during lithiation and delithiation.

Liu et al. developed a three-dimensional (3D) reduced graphene oxide (rGO)/multi-walled carbon nanotubes (MWCNTs)/Fe_2O_3 ternary composite via one-step urea-assisted hydrothermal synthesis [74]. rGO/MWCNTs/Fe_2O_3 exhibits highly enhanced specific capacity (initial discharge and charge capacities of 1692 and 1322 $mAhg^{-1}$ at 100 mAg^{-1}, respectively), high rate capability (1118 $mAhg^{-1}$ after 50 cycles at 100 mAg^{-1} and 785 $mAhg^{-1}$ at 1 Ag^{-1}) due to the strong synergistic effects among the individual components. Xia and co-workers synthesized a ternary composites of rGO/Fe_2O_3/SnO_2 via in situ precipitation of Fe_2O_3 nanoparticles on GO nanosheets, then followed by a subsequent chemical reduction of GO with $SnCl_2$ [75]. The novel nanocomposite exhibited initial discharge and charge capacities of 1179 and 746 $mAhg^{-1}$, respectively, at 400 mAg^{-1} with stable cycle life for 100 cycles with more than 700 $mAhg^{-1}$. The conductive matrix of graphene facilitates the transfer of lithium ions and electrons, also buffers the stress caused by volume expansion and prevents the accumulation of Fe_2O_3 particles during Li uptake/release. The dispersion of Fe_2O_3 and SnO_2 particles on graphene mitigates the degree of stacking of graphene sheets.

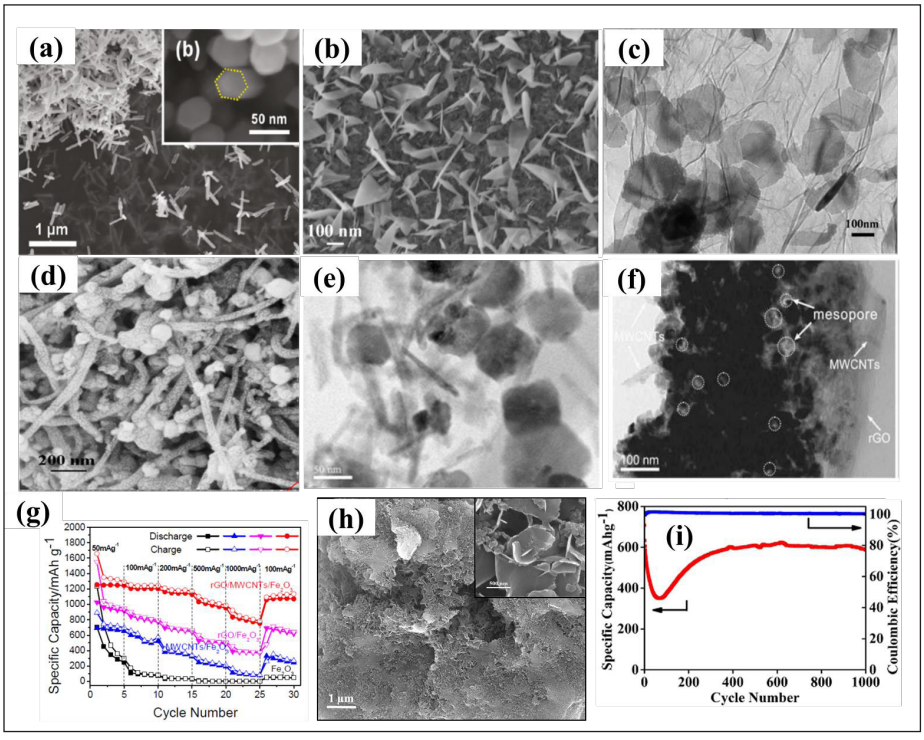

Figure 4: *(a) SEM image of a-Fe_2O_3 nanorods; [65] (b) SEM image of a-Fe_2O_3 nanoflakes; [64] (c) TEM image of Fe_2O_3-graphene sheet-on-sheet composite [69] (d) SEM of the MWNT/Fe_2O_3 composite; [70] (e) TEM image of RG-O/Fe_2O_3 branched NWs; [68] (f) TEM image and Rate capabilities of 3D rGO/MWCNTs/Fe_2O_3 composite; [74] (h) SEM image of NFOC-20,(inset: showing high magnification image); (i) Cycling stability of NFOC-20 composite. [76]*

In addition, SnO_2 particles hinder the agglomeration of Fe_2O_3 nanoparticles. Dwivedi et al. synthesized a ternary hybrid composite of $Ni(OH)_2$-Fe_2O_3/Carbon Nano Onions (NFOC) by using two-step solution phase method which delivers reversible discharge capacity of 928 $mAhg^{-1}$ at 50 $mAg^{-1}$and 673 $mAhg^{-1}$ at a 1 Ag^{-1} with excellent rate performance [76]. Additionally, it shows stable cycle life up to 1000 cycles with 96% capacity retention and more than 99% of coulombic efficiency. The reversible reaction of Fe_2O_3 and $Ni(OH)_2$ with Li, maintains its long cycle life with higher reversible discharge capacity and CNOs improve the efficient electronic transfer, accommodate substantial volume expansion and maintain the structural integrity of the material during lithiation-delithiation process.

Besides Fe_2O_3, Fe_3O_4 also attracted several researchers' interest as anode material for LIBs, because of its high theoretical capacity as well (925 $mAhg^{-1}$). Similar to Fe_2O_3, nanostructured particle architectures and composition with conducting material has been considered as an efficient way to enhance its electrochemical properties. For instance, Liu et al. fabricated uniform pomegranate-like nanoclusters composed of ultrafine Fe_3O_4@nitrogen-doped carbon (Fe_3O_4@N-C) subunits with a diameter of around 4 nm. As prepared pomegranate-like Fe_3O_4@N-C showed 1063.0 $mAhg^{-1}$ of specific capacity and 98.4% capacity retention after 1000 cycles at specific currents of 1 Ag^{-1}, and also exhibit 92% and 91.7% capacity retention at 10 Ag^{-1} and 20 Ag^{-1} of current density after 1000 cycles [77].

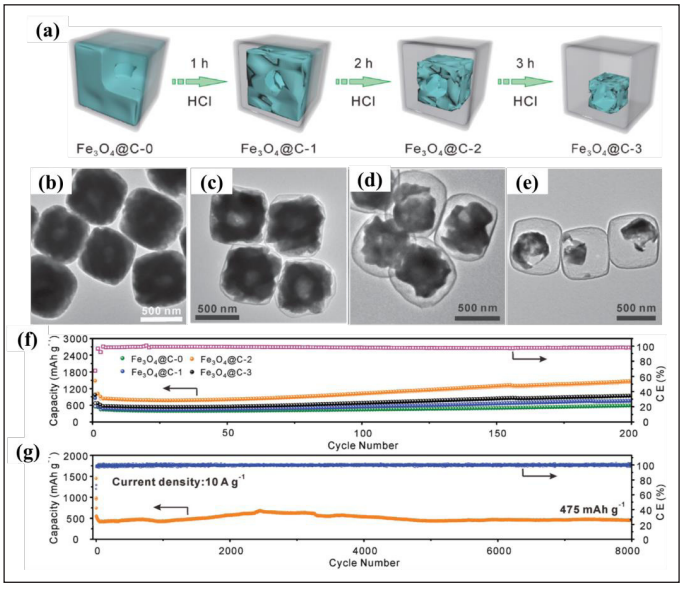

Figure 5: *(a) Schematic representation of the formation of Fe_3O_4@C yolk-shelled nanocubes with different etching times. (b-e) TEM images of Fe_3O_4@C yolk–shelled nanocubes with different etching times (a, 0 h; b, 1 h; c, 2 h; d, 3 h); cycling performance of the four obtained samples at 0.5 A g^{-1} (e) and the Fe_3O_4@C-2 yolk–shelled nanocubes at 10 Ag^{-1} (f). [81]*

Wei et al. described a novel approach to synthesize 3D graphene foams (GF) cross-linked with Fe_3O_4 nanospheres (Fe_3O_4 NSs) and encapsulated in graphene sheets which delivers a high reversible capacity of 1059 $mAhg^{-1}$ over 150 cycles with excellent rate capability [78]. Wan and co-workers synthesized carbon-coated Fe_3O_4 nanospindles via the partial reduction of carbon-coated hematite nanospindles. The resulting Fe_3O_4-C nanospindles revealed a stable capacity of ≈600 $mAhg^{-1}$ at C/2 and fully retained after 80 cycles [79]. He et al. fabricated carbon-encapsulated Fe_3O_4 nanoparticles embedded in 2D highly conducting porous graphitic carbon nanosheets (NSs) (Fe_3O_4@C@PGC nanosheets) using NaCl as template [80]. Fe_3O_4@C@PGC nanosheets displayed 3.47% capacity loss with 556 $mAhg^{-1}$ after 350 cycles at a high rate of 10 C. Here, thin carbon layers act as a barrier to prevent the direct contact between the Fe_3O_4 and the electrolyte. Electronically conductive and flexible PGC nanosheets can alleviate the volume changes of the Fe_3O_4@C nanoparticles and prevent their deleterious aggregation through maintaining the electrical and overall structural integrity of the composite electrode upon cycling. Liu et al. synthesized unique Fe_3O_4@C yolk-shelled nanocubes via an etching-in-a-box strategy which generate inner cavities in Fe_3O_4 cores (figure 5a-5e). As prepared Fe_3O_4@C yolk-shelled nanocubes achieved ultralong life cycles at 10 Ag^{-1} up to 8000 cycles with significant capacity of 475 mAh g^{-1} as shown in figure 5f-5g [81].

3.3 Cobalt oxides

CoO and Co_3O_4 are the main phases of cobalt oxides that are used as an anode material for LIBs. CoO exhibit high theoretical specific capacities of 715 $mAhg^{-1}$ on reaction with Li by transferring 2 electrons per mole according to the equation ($CoO + 2Li^+ + 2e^- \leftrightarrow Co + Li_2O$). Cao and co-workers synthesized CoO nanowire clusters (NWCs) consisting of ultrasmall nanoparticles (≈10 nm) via a hydrothermal synthesis on the copper current collector. It delivered a high capacity of 1516 $mAhg^{-1}$ at 1 C rate and maintained 1331 mAh g^{-1} of specific capacity even at 5 C rate [82]. Passerini et al. synthesized a CoO-Co-C nanocomposite via in situ carbothermal reduction of Co_3O_4 which showed long term cycle life and coulombic efficiency [83]. Huang and co-workers synthesized the binder-free mechanically strong CoO/graphene nanocomposites through a novel electrostatic induced spread growth method. As prepared electrode shows stable cycle over 5000 cycles at 1Ag^{-1} and excellent rate performance with 172 $mAhg^{-1}$ at 20 Ag^{-1} of high current density [84].

Co_3O_4 exhibit high theoretical specific capacity of 890 $mAhg^{-1}$ and on reaction with Li it transfers 8 electrons per mole of Li. There are two different observation on reaction

of Co_3O_4 with Li. One is that the reaction is highly reversible and occurs as follows [85-89]:

$$Co_3O_4 + 8Li^+ + 8e^- \leftrightarrow 3Co + 4Li_2O$$

Meanwhile, the other outlook is that this reaction is not fully reversible and that the lithiation product Co nanograins should be reoxidated to CoO, not Co_3O_4 [90-91]. Su et al. synthesized Co_3O_4 nanoplates/graphene and studied the dynamic structure changes during cycling. They have observed that the conversion of highly crystalline Co_3O_4 nanoplates transformed it into numerous Co nanograins and Li_2O during the first lithiation.[10] A reversible conversion reaction occur in between Co nanograins and CoO nanograins. The whole reaction can be expressed as follows:

$$Co_3O_4 + 8Li^+ + 8e^- \leftrightarrow 3Co + 4Li_2O \text{ (first lithiation)}$$

$$Co + Li_2O \leftrightarrow CoO + 2Li^+ + 2e^-$$

Volume expansion and low conductivity are major drawbacks of Co_3O_4 for practical applicability. Development of hybrid nanocomposites with carbon and tuning the morphology of electrode material has potentially countered above mentioned problems [92-95]. For example, Wang et al developed triple-shelled Co_3O_4 microspheres by controlling the size and diffusion rate of the hydrated Co^{2+} as well as the absorption capability of the carbonaceous microspheres (CMSs) as displayed in figure 6e [92]. As prepared multishell Co_3O_4 hollow microspheres exhibit high specific capacity of 1615.8 $mAhg^{-1}$ after 30th cycle at 50 mAg^{-1} of current density. Yao et al. developed mesoporous Co_3O_4 nanowires (figure 6d) confined by N-doped graphene aerogel anode via hydrothermal reaction followed by topotactic calcination process which delivered high capacity of ~1200 $mAhg^{-1}$ after 200 cycles [96].

Self-adhesive Co_3O_4/expanded graphite paper and Co_3O_4 nanoparticles-embedded carbonaceous fibers are also developed as an anode for LIB which showed excellent electrochemical performance [97-99]. High surface area and well-designed pore structures are beneficial for shortening diffusion path length of the Li^+ and to accommodate large volume expansion strain during cycling. Hou et al. prepared Co_3O_4/N-doped porous carbon dodecahedrons by Co-based zeolitic imidazolate frameworks (ZIF-67) at room temperature which exhibit a charge capacity of 892 $mAhg^{-1}$ that is retained after 100 cycles with a coulombic efficiency close to 100% [100]. Fang et al synthesized Co_3O_4/3D nickel foam (Co_3O_4/3DNF) hybrid binder-free electrode which possesses the advantages of porous nanostructures and a 3D conductive substrate. Co_3O_4/3DNF showed long-term cyclic stability over 2000 cycles at current density of 5 Ag^{-1} and 20 Ag^{-1} [101]. Chen and co-workers synthesized the hierarchical CNT/Co_3O_4 microtubes from polyacrylonitrile (PAN)-cobalt acetate ($Co(Ac)_2$) composite nanofibers (PAN-$Co(Ac)_2$). As prepared CNT/Co_3O_4 microtubes exhibit a high reversible capacity of 1281 $mAhg^{-1}$ at 0.1 Ag^{-1} with exceptional rate capability and long cycle life of over 200 cycles as an anode material for lithium-ion batteries (figure 6a-6c) [102].

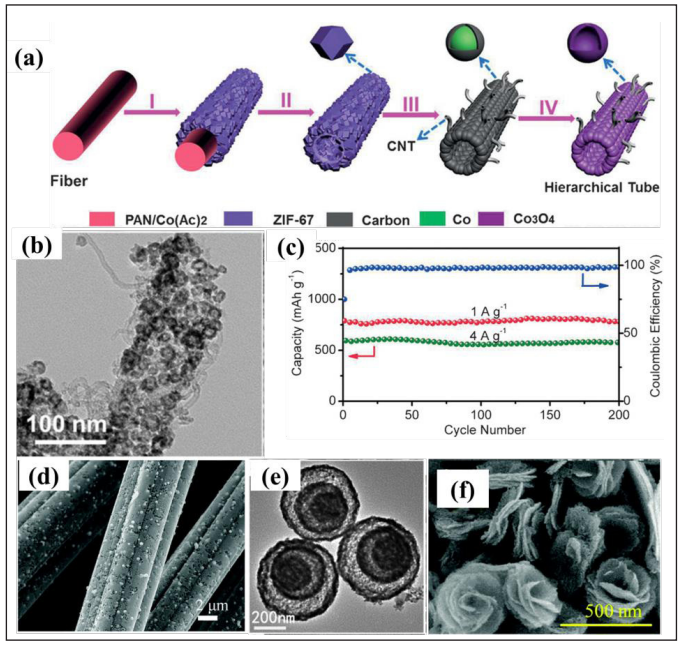

Figure 6: *(a, b, c) Schematic of synthesis, TEM image and cycling performance and Coulombic efficiency of the synthesized hierarchical CNT/Co_3O_4 microtube, respectively; [102] (d) SEM image of Co_3O_4/CF-60; (96) (e) TEM image of triple shelled Co_3O_4 hollow microspheres; [92] (f) FESEM image Co_3O_4 nanoflowers (Co_3O_4-NFs). [85]*

3.4 Nickel Oxide

Recently Nickel oxide (NiO), a p-type wide bandgap semiconductor, has drawn much attention as an anode for LIB due to its chemical stability, high theoretical specific capacity (718 $mAhg^{-1}$) and low cost [103]. Nevertheless, low electrical conductivity ($\rho > 10^{15}$ Ωm at 25 °C) and reduced surface area prevent its practical application for LIB. Additionally, large volume expansion associated with conversion of NiO to Li_2O during charge-discharge process is another problem. Therefore, to overcome all those issues nanostructure engineering of NiO, like variation in morphology, size and porous nature has been carried out to facilitate the li ion diffusion, to enhance the mechanical integrity and to enhance the surface to volume ratio. Incorporation of conducting carbon into NiO increases its electrical and mechanical properties [104-107]. Hierarchical porous NiO nanosheet arrays synthesized by Chen et al. via hydrothermal process. These NiO nanosheet array delivered 511 $mAhg^{-1}$ of specific

capacity at high current density of 3 Ag^{-1} because of unique 3D hierarchical porous structure of NiO [108]. Sun and co-workers synthesized 3-dimensinal curved nanomembrane of NiO which exhibit high capacity of 721 $mAhg^{-1}$ at 1.5 C, with long cycle life up to 1400 cycles as shown in figure 7a-7b [109]. Free standing core shell nanofibre structure of Ni-NiO was fabricated by Bell et al. by electrospinning process followed by thermal oxidation. The Ni–NiO nanofiber cloth exhibit specific capacity of 1054 mA h g^{-1} at 3 C rate (1 C=718 mAg^{-1}) and shows exceptional stable cycle life up to 1500 cycles [110].

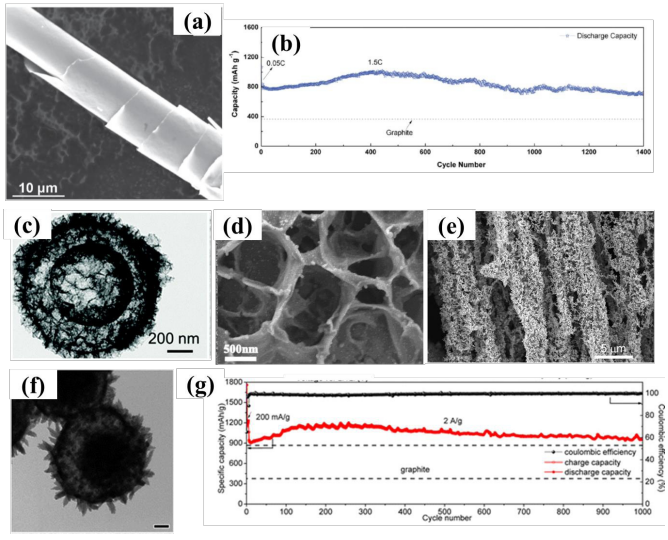

Figure 7: *(a) SEM image of curved NiO nanomembrane; (b) Reversible Li discharge capacity of the curved NiO nanomembrane electrode versus cycle number in comparison with the theoretical capacity of graphite; [109] (c) TEM image of an individual bowl-like NiO NSs@C particle; [111] (d) SEM image of sandwiched NiO/C arrays on Ti foil; [112] (e) SEM image of NiO nanowire foam; [113] (f) TEM image (scale bar: 200 nm) of the NiO/Ni/Graphene sphere; (g) Cycle performance of the NiO/Ni/Graphene at a current density of 2 A/g for 1000 cycles. [114]*

Liang et al developed hybrid bowl-like nanostructure morphology by anchoring NiO nanosheets on flat carbon hollow particles (NiO NSs@C composite) which delivers 1012 $mAhg^{-1}$ of specific capacity at 0.2 Ag^{-1} of current density with 94% capacity retention after 150 cycles [111]. Feng et al. synthesized novel 2D sandwich-like NiO/C arrays on Ti foil by using hydrothermal process which delivers high specific capacity of 1458 $mAhg^{-1}$ at 0.5 Ag^{-1} with 95.7% capacity retention after 300 cycles [112]. Liu et al synthesized template free and binder less NiO-decorated Ni nanowires from Ni wire backbone and achieved specific capacity of 680 $mAhg^{-1}$ at 0.5 C after 1000 cycles [113]. Zou and co-workers developed graphene coated hierarchical NiO/Ni nanocrystals which shows 1144 $mAhg^{-1}$ of reversible capacity with stable cycle life upto 1000 cycles and excellent rate performance (805 $mAhg^{-1}$ at 15 Ag^{-1}) [114].

3.5 Copper Oxide

Like other TMOs, CuO has also attracted researcher's attention as an anode material for LIB because of its high theoretical specific capacity (674 $mAhg^{-1}$) and less toxic nature. Associated problems with CuO like low conductivity (p-type semiconductor) and large volume expansion (174%) impair its battery performance. Micro-/nano-structural morphology of CuO like nanowires, nanorods, nanofibers, nanosheets, nanoribbons, 3D hierarchical mesocrystals, hollow structures and development of hybrid materials with conducting carbon can improve its electrochemical performance [115-125]. By tuning structural morphology of CuO in nano level can relieve mechanical strain and reduce the diffusion length of Li ions which increase the Li storage capacity of electrode. For example, Zhang et al. synthesized vertically aligned single crystalline CuO nanowires on nickel foam via. one-step thermal oxidation which shows specific capacity of 692 $mAhg^{-1}$ after 50 cycles at 0.1 Ag^{-1} and also at higher current density of 1 Ag^{-1} it is showing 445 $mAhg^{-1}$ up to 600 cycles [117]. Fan and co-workers synthesized graphene quantum dots (GQD) coated CuO nanowires on Cu foam (the CuO-Cu-GQD) where surface conductivity and stability of the nanowire arrays has been increased by unique GQD coating [116]. The CuO-Cu-GQD triaxial nanowire arrays deliver a high reversible capacity 780 $mAhg^{-1}$ at 1/3 C, excellent rate performance with 330 $mAhg^{-1}$ at 30 C with no capacity loss up to 1000 cycles. Hybrid nanostructures of CuO with conducting carbon and metal are also developed to improve the conductivity and to buffer the volume expansion/contraction during cycling. Liu and co-workers synthesized encapsulated CuO nanoparticles in mesoporous carbon multi-yolk-shell octahedra by using a solvothermal process followed by thermal treatment. This composite showed high reversible capacity (598 $mAhg^{-1}$) at 0.25 Ag^{-1} as an anode for LIB [126]. Additionally, it exhibited excellent rate capacity (365 $mAhg^{-1}$ at 3Ag^{-1} of current density) and long-term cycle life of 300 cycles at 0.5 Ag^{-1} with 512 $mAhg^{-1}$ of specific capacity. Here novel multi-yolk–shell structure can accommodate large volume variations, prevent the aggregation of CuO nanoparticles during cycling. Ko et al. developed a CuO/MWCNTs nanocomposite where mesoporous CuO nanoparticles particles are threaded by MWCNTs. This composite exhibited a reversible capacity of 650 $mAhg^{-1}$ at 0.1 C rate with an excellent rate performance (580 $mAhg^{-1}$ at 5 C, and 500 $mAhg^{-1}$ at 10 C) [127]. Wang's group fabricated carbon-coated CuO hollow spheres via a feasible aerosol spray pyrolysis method which delivers 670 $mAhg^{-1}$ of specific capacity at 1 C and excellent rate capacity

(400 $mAhg^{-1}$ at 50 C retained after 300 cycles) [128]. Tan et al. reported synthesis of hollow copper nanoparticles supported by N-doped carbon nanosheets (Cu@NCSs) on Cu foil by chemical vapor and solid deposition strategy. The resulting product displayed stable cycle life with specific capacity value of 688 $mAhg^{-1}$ over 1000 cycles at 2 Ag^{-1} of current density and also exhibit 400 $mAhg^{-1}$ of specific capacity at high current density of 4 Ag^{-1}. In well-designed hollow CuO@NCS composites NCS improve the electrical conductivity of electrode and alleviates the volume expansion during cycling as shown in figure 8h-8i [129].

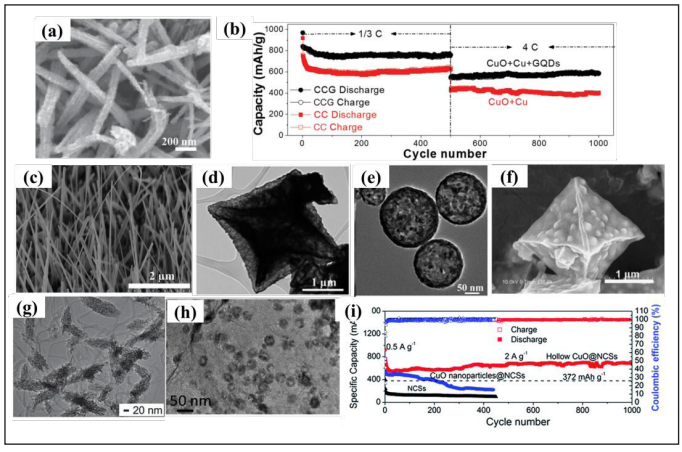

Figure: 8 *(a) SEM image of CuO + Cu + GQD triaxial nanowires; (b) Cycling performance at 1/3 C for the first 500 cycles and 4 C for the second 500 cycles; [116] (c) SEM images of a Cu film on nickel foam heated at 400 °C for 12 h; [117] (d) TEM image of CuO hollow octahedral; [126] (e) TEM image of the nano-structured carbon-coated CuO hollow spherical particles; [128] (f) SEM images of CuO@C multi-yolk-shell octahedral; [126] (g) TEM image of the CuO/CNT nanocomposite produced by transformation of the $Cu(OH)_2$ coating layer into the CuO particles;[127] (h) TEM image of the hollow CuO@ NCS composites; (i) The long-term cycling performance and coulombic efficiencies of NCS, CuO nanoparticles@NCS and the hollow CuO@ NCS electrodes at 2 Ag^{-1} [129].*

3.6 Tin Oxide

Tin oxide (SnO_2) is very attractive candidate as anode material for LiBs because of its natural abundance, high theoretical Li-ion storage capacity and environmental benignity. However, large volume expansion (>300%) during lithiation/delithiation leads to pulverization and aggregation of particles consequently rapid capacity fading [130, 131]. To overcome these intrinsic problems various methods are deployed [132-139].

Abouali et al. encapsulated SnO_2 NPs in mesoporous carbon to suppress the capacity decay [140]. Liang and co-workers synthesized a flexible free-standing graphene/SnO_2 nanocomposite paper by a simple filtration method followed by thermal reduction [141]. Jin Liang et al. designed SnO_2 nanoparticles on to the bowl like carbon hollow nanostructures to get bowl-like SnO_2@ carbon hollow particles as shown in figure 9a-9c. This simple strategy of bowl like deflated hollow spheres increases the packing density of nanoparticles as these excludes the unnecessary void space in conventional hollow particles, consequently increases the Li storage capacity of the electrode. Bowl-like SnO_2@C composite showed a first reversible discharge capacity of 1212 $mAhg^{-1}$ and even after 100 cycles at 400mAg^{-1} exhibited specific capacity of 963 $mAhg^{-1}$. Bowl-like SnO_2@C composite at high current density of 1600 mAg^{-1} displayed specific capacity of 850 $mAhg^{-1}$ and specific capacity of 1282 $mAhg^{-1}$ was recovered at 100mAg^{-1} after cycling with capacity retention of 90% (figure 9d-9e) [142].

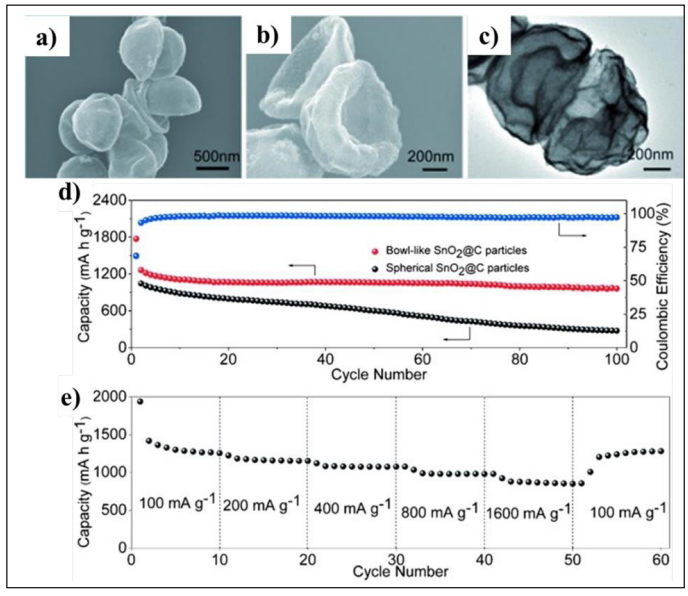

Figure 9: *FESEM and TEM images of (a–c) bowl-like SnO2@C nanocomposites; (d) cycling performance at a current density of 400 mA g^{-1} SnO2@C nanocomposite; (e) rate performance of SnO2@C nanocomposite. [142]*

Ye et al. synthesized SnO_2 nanotubes using one-dimensional (1D) silica mesostructures as effective sacrificial templates by hydrothermal method. SnO_2 nanotubes as an anode for LIBs showed excellent electrochemical performance. It shows initial discharge specific capacity of 1724 $mAhg^{-1}$. They showed that average capacity fading for SnO_2 nanotubes is about 1.7% compared to the 3.1% of SnO_2 nanopowder. This shows that nanostructure designing play important role in achieving stable capacity [143]. Jiang et al. coated polydopamine to SnO_2 nanoparticles to stabilize solid electrolyte interface

and counter volume expansion [144]. In summary, SnO_2 nanostructures and its composite with carbon have been vastly explored for the fundamental understanding as well as to bring into practical LIBs applications.

3. Metal Sulphides:

Sulfides usually have higher conductivities and smaller volume expansions during cycling than those of oxides, means better ion transport. Moreover, the chemical bond between metal and sulfur is weaker than that of metal oxides which is advantageous for reversible conversion reactions. Different metal sulphides, their material design and LIB performances are discussed in the following section.

3.1 Nickel Sulphide

The lithium storage performance of metal sulfides is restricted by their intrinsic poor conductivity and large volumetric expansion. These issues can be addressed using nanostructured metal sulfides grown on self-standing conductive templates. Conductive carbonaceous matrix can be one such substrate to achieve high reversible capacities and long cycling life which can buffer the volume expansion/contraction and a separator as well to inhibit sulfide particles from aggregating during cycling. Nickel Sulfide nanoparticles anchored on electrospun carbon nanofibers have been reported as binder-free anodes for high-performance lithium-ion batteries. This 3D macroporous architecture offers open channels for rapid diffusion of lithium ions to access the nanoparticles of nickel sulphide [145]. The hybrid membranes exhibited a high reversible capacity of 1149.4 mAhg $^{-1}$ with good cycling and high rate capability of 664.3 mAhg $^{-1}$ at a high current density of 3 Ag $^{-1}$.

Further, NiS_x@C yolk–shell microboxes were reported by Lu et al. with excellent electrochemical performance in LIBs. These nano-boxes delivered impressive cycle stability of 2000 cycles at 1 Ag^{-1} with a capacity of 460 $mAhg^{-1}$ after 2000 cycles and superior rate performance with a capacity of 225 $mAhg^{-1}$ at 20 Ag^{-1}. This confined yolk–shell structure is a new strategy to create advanced electrode materials for high performance [146].

3.2 Cobalt Sulphide

The Cobalt sulphide exists in many phases such as CoS_2, Co_3S_4, CoS and Co_9S_8. Cobalt sulfides have attracted great attention due to their unique physical and chemical properties. Many approaches have been used to synthesize metal sulfides, including solid-state reaction, hydrothermal/solvothermal method, an arc-discharge method, a catalyzed transport method and chemical vapor decomposition. Among these methods, the solid-state reaction is widely used in industry and easily scalable. Cobalt sulfide phases with different stoichiometry can be synthesized using combined approach of solid-state assembly and heat treatment. The sulphide reacts with Li according to following reaction:

$$M_aS_b + xLi^+ + xe^- \leftrightarrow a\,M + bLi_2S$$

These cobalt sulphide materials when used as the electrodes of lithium ion batteries, showed good cycling stability with the discharge capacities of 929 and 835 $mAhg^{-1}$ for CoS_2 and CoS respectively [147]. Cobalt sulphide-rGO composite synthesised by low temperature wet chemical method was reported by Lee et al as LIB anode. Sulfide particles were homogeneously distributed on the surface of rGO forming an ultrathin sheet like structure. The composite showed superior lithium storage properties with high capacity of 994 $mAhg^{-1}$ after 150 cycles at a current density of 200 mAg^{-1} [148].

3.3 Iron Sulfide

Iron sulphides are promising as anode materials for rechargeable batteries for having combined advantages of iron such as abundance, low cost and of sulphides such as low polarization. Iron have many sulphide phases such as FeS, FeS_2, Fe_3S_4, and Fe_7S_8.

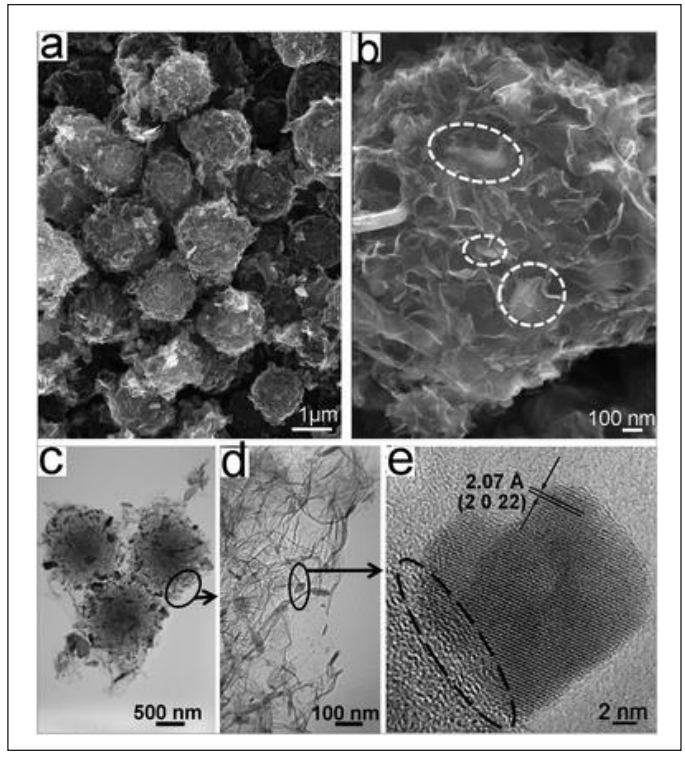

Figure 10: *SEM (a and b) and TEM images (c, d and e) of iron sulphide embedded in carbon microspheres [149].*

The FeS have theoretical capacity of 609 $mAhg^{-1}$ which is much higher than that of commercial graphite. FeS microspheres decorated carbon nanosheets show a high capacity and high-rate capabilities. The first discharge capacity obtained was 1564 $mAhg^{-1}$ and a capacity of 736 $mAhg^{-1}$ was maintained after 50 cycles at 50 mAg^{-1}. Reversible capacities of 783, 734 and 541 $mAhg^{-1}$ can be obtained at 0.5, 1, and 5 Ag^{-1}, respectively [149]. The enhanced electrochemical data of composite than bare FeS can be ascribed to the addition of carbon nanosheets which increases the surface contact between electrode and electrolyte, and the wettability of electrode. Furthermore, polysulfides are more difficult to dissolve in the electrolyte in the carbon nanosheet-wrapped FeS structure. Sandwich type graphene-wrapped FeS-graphene nanoribbon (G@ FeS-GNR) was reported by Tour et. al to address the stability degradation problem and polysulfide dissolution into electrolyte. In this composite, FeS nanoparticles were sandwiched between graphene and graphene nanoribbons, reducing the solubility of the intermediate polysulfide during cycling thus improving its electrochemical stability. The reversible discharge capacity of 536 $mAhg^{-1}$ was retained after 100 cycles at 0.4 Ag^{-1}[150].

3.4 Copper Sulfide

Copper sulphide is interesting material for LIBs due to its high electrical conductivity (10^{-3} S cm^{-1}), good theoretical capacity (560 $mAhg^{-1}$) and flat discharge curves. But rapid capacity fading, and Lithium polysulfide formation are the issues related with CuS. Nano-structuring has been tried to increase the number of reaction sites, shorten the diffusion path length and enhance charge transport. Nanostructured CuS of size in the range of 10 nm has been used as anode material for LIB. The initial discharge and charge capacities of 775 and 561 $mAhg^{-1}$ were obtained, respectively and a capacity of ~182 $mAhg^{-1}$ at a high current rate of 5.0 C was obtained [151].

3.5 Zinc Sulfide

Zinc Sulfide have high theoretical capacity of 962 $mAhg^{-1}$ based on conversion and alloying reaction shown below:

$$ZnS + 2Li^+ + 2e^- \rightarrow Zn + Li_2S$$

$$Zn + 4Li^+ + 4e^- \rightarrow Li_4Zn$$

Zinc sulphide-N-doped porous carbon (ZnS-NPC) synthesised from carbonization and sulfurization of zeolitic imidazolate framework-8 (ZIF-8) was used as anode for LIB [152].

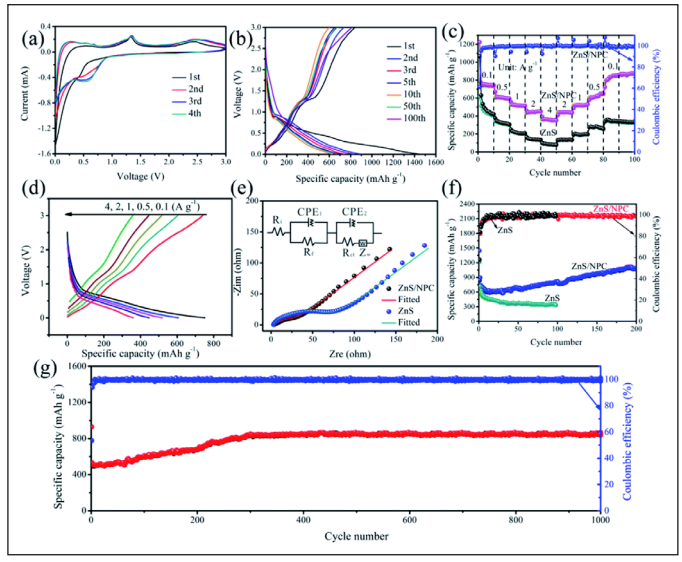

Figure 11: Zinc Sulfide synthesised from ZIF for LIB. [152]

This synthesis gives unique polyhedral morphology and large size of about 2 mm. The ZnS-NPC composite displayed the reversible specific capacity of 1067.4 $mAhg^{-1}$ at 0.1 Ag^{-1} after 200 cycles and excellent rate capability with a capacity of 364.6 $mAhg^{-1}$ at 4 Ag^{-1}), and long-term cycling performance with a capacity of 856.8 $mAhg^{-1}$ at 1 Ag^{-1} after 1000 cycles.

3.6 Tin Sulfide

Sn-based materials are interesting anode materials for LIBs due to their low cost, lower reaction potential and high theoretical capacity. Tin sulphide is high capacity anode material as it shows conversion cum alloying reaction mechanism. It exists in two phases SnS and SnS_2. SnS has orthorhombic structure and this crystallographic feature helps in facilitating faster Li^+ diffusion. SnS stores Li according to following reactions:

$$SnS + 2Li^+ + 2e^- \rightarrow Sn + Li_2S$$

$$Sn + Li^+ + e^- \rightarrow Li_{4.4}Sn$$

Theoretical capacity of SnS and SnS_2 is 1138 $mAhg^{-1}$ and 1230 $mAhg^{-1}$, respectively. First reaction is not reversible in SnS (Li_2S formation) case. SnS nanobelts are synthesised using controlled hydrothermal approach and applied as anode materials for LIBs [153]. SnS nanobelts delivered a discharge capacity of 889.9 $mAhg^{-1}$ after 50 cycles at a current density of 0.1 Ag^{-1}. It has been suggested that SnS_2 can realize a reversible conversion (formation and decomposition of Li_2S). In another work, hierarchical assemblies of thin SnS_2 nanosheets were prepared using solvothermal approach and further surface modified to increase its structure stability. c-SnS_2 nanosheet assembly

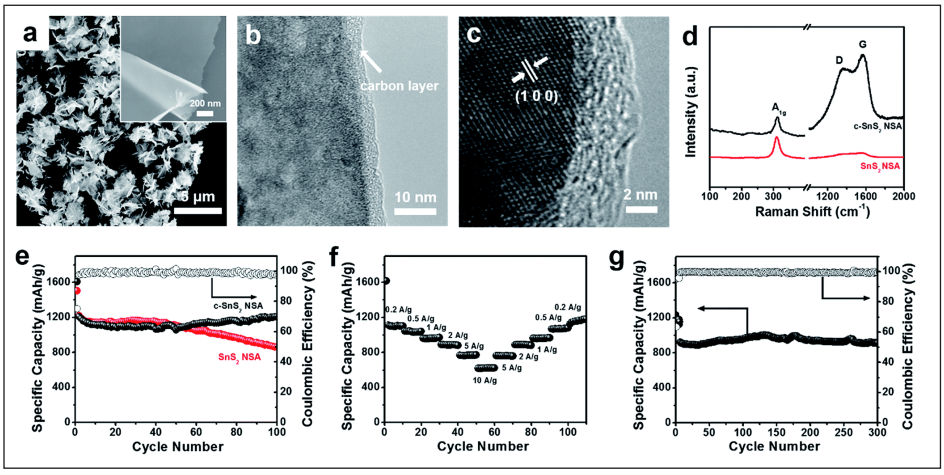

Figure 12: *(a) SEM images (b, c) TEM images (d) Raman spectrum (e) Cycling stability at 0.2 Ag^{-1}. (f) Rate capability (g) Cycling stability at 1 Ag^{-1} of c-SnS_2. [154]*

showed a high capacity of 1300 mA h g^{-1} at 200 $mAhg^{-1}$ after 100 cycles [154]. It also exhibited a remarkable rate capability with a capacity of 1109 $mAhg^{-1}$, 1042 $mAhg^{-1}$, 967 $mAhg^{-1}$, 893 $mAhg^{-1}$, 770 $mAhg^{-1}$ and 620 $mAhg^{-1}$ at current density of 200 mAg^{-1} to 500 mAg^{-1}, 1 Ag^{-1}, 2 Ag^{-1}, 5 $Ag^{-1}$and 10 Ag^{-1}, respectively.

4. Metal phosphides: Ni, Co, Fe and Sn

Charge storage in metal phosphides takes place by following conversion reaction

$$M_aP_b + xLi^+ + xe^- \leftrightarrow a\,M + bLi_3P$$

Phosphorous (P)-based materials come under conversion-type LIB anodes which exhibit an ultrahigh theoretical capacity of ~2600 $mAhg^{-1}$ for red P but shows poor cycling stability owing to the structural pulverization caused by over 300% volume variation during lithiation/delithiation processes and low electrical conductivity. In metal phosphides (MP), P is bonded with metal elements, MPs usually exhibit improved electric conductivity and electrochemical stability when compared to pure P. MPs can store Li ions via conversion reactions in the form of Li_3P. Metal phosphides are high capacity anode materials but suffer with low rate capability and rapid capacity fading limiting its application for next generation LIBs. Synthesis of unique structure/morphologies of various phosphides and methods for their stabilization as high capacity anode are discussed in the following sections.

4.1 Nickel Phosphide

Nickel based nanostructured phosphides have very interesting properties such as low polarization, low resistivity and high charge density. Various nickel phosphide phases such as Ni_2P, Ni_5P_4 and Ni_3P are reported so far for LIBs; e.g. highly ordered porous Ni_3P film was electrodeposited through a self-assembled monodisperse polystyrene sphere template on copper substrate. Well-ordered and closely packed pores of 800 nm are obtained after removal of polystyrene. The nanostructured porous Ni_3P film exhibited better rate capability and reversibility than dense film. The reversible capacity of the porous Ni_3P film is 403 $mAhg^{-1}$ and 239 $mAhg^{-1}$ at 0.2 C and 2 C, respectively [155]. The enhanced electrochemical performance of the porous film is attributed to the better contact between Ni_3P and electrolyte, which provides more sites for Li^+ accommodation, shortens the diffusion length of Li^+ and enhances the kinetics of electrode process. A monophase nickel phosphide/carbon (Ni_5P_4/C) composite with carbon coating is controllably synthesized via a two-step process of wet chemistry reaction and a solid-state reaction. During the solid-state reaction, further diffusion of phosphorus is possibly responsible for a chemical transformation from a binary phase of Ni_5P_4 -Ni_2P to monophase Ni_5P_4. The Ni_5P_4/C composite exhibits a high rate capability and good cycling stability [156]. The capacity value of 644.1 $mAhg^{-1}$ was retained after 50 cycles at a 0.1 C rate and the specific capacity of 357.1 $mAhg^{-1}$ was obtained at 3C. Hierarchical nanostructured nickel phosphide (h-Ni_2P) spheres of 5-20 nm size are synthesized using oleyl ammine as surfactant and filled by amorphous carbon. The hierarchical structure increases the contact area between Ni_2P and electrolyte significantly, which provides more sites for Li^+ storage, shortens the diffusion path length of Li^+, and enhances the reactivity of the electrode. The amorphous carbon and the hierarchical Ni_2P nanostructures can buffer volume expansion and thus increase the electrode stability during cycling. The reversible capacity of h-Ni_2P spheres was 365.3 $mAhg^{-1}$ at 0.5 C and 257.8 $mAhg^{-1}$ at 1 C which was higher than Ni_2P spheres (97.2 $mAhg^{-1}$at 0.5 C). Rational design of 1-D Ni_2P peapod array with graphitized carbon is reported with a capacity as high as 618 $mAhg^{-1}$ after 300 cycles which was 97% of that of the second cycle [157]. The graphitized carbon fiber layer around the Ni_2P nanoparticles can effectively prevent the adjacent nanoparticles from coming in contact with each other and minimize the aggregation of the particles in the charge/discharge processes. Moreover, the carbon layer forms an elastic active matrix that can buffer the large volume expansion and contraction during the electrochemical cycling.

4.2 Cobalt Phosphide

Theoretical capacity of CoP is 894 $mAhg^{-1}$. Co_xP nanostructures with controlled size, phase, and shape are studied as anode for LIBs. CoP and Co_2P cobalt phosphide phases with an amorphous carbon layer obtained by the carbonization of organic surfactants are reported.

The CoP hollow nanoparticle with carbon coating showed good capacity retention and high rate capability. The specific capacity of 630 $mAhg^{-1}$ at 0.2 C after 100 cycles, and a reversible capacity of 256 $mAhg^{-1}$ was achieved at current rate of 5 C [158]. A composite of ultrafine CoP nanoparticles in nitrogen-doped carbon matrix was obtained from phosphorization of zeolitic imidazolate framework 67 (ZIF-67) template. Due to their unique structural characteristics, CoP exhibited a specific capacity of 522.6 $mAhg^{-1}$ at a current density of 200 mAg^{-1} after 750 cycles and excellent cycling stability up to 2000 cycles at 500 mAg^{-1} [159].

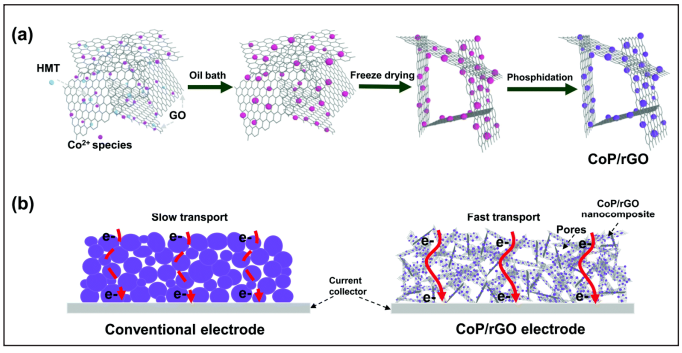

Figure 13: CoP-rGO composite for LIB. [160]

Further, CoP-rGO nanocomposite is reported with stable network structure, good electrical conductivity relatively high surface area and porosity in contrast to bulk CoP which suffers from particle stacking/agglomeration, low conductivity and hindered electron/ion transport pathways resulting into rapid capacity degradation. The specific capacity of 1154 $mAhg^{-1}$ at 100 mA h g^{-1} of current density was obtained which is much higher than the theoretical value of CoP. A capacity of 840 $mAhg^{-1}$ at 2Ag^{-1} was reported with excellent rate capability and ultralong cycle life of 2000 stable cycles [160].

4.2 Iron phosphide

Another attractive material i.e. FeP, with two step reversible insertion and conversion anode mechanism, is synthesized and electrochemical studies were done. The transition metal phosphides reported till now show different redox reactions based on the 3d transition metal. With early transition metals such as Ti and V, lithium reaction proceeds through insertion mechanisms whereas with middle and late transition metals such as Mn, Fe, Co and Ni, it generally proceeds through the conversion of MPy into a composite electrode made of metallic particles in nanosize embedded in a Li_3P matrix. To avoid the agglomeration of Fe and low electronic conductivity issue of FeP anode, a simple route using metal organic framework (MOF) phosphorization has been explored for in-situ encapsulation of FeP nanoparticles in porous carbon framework (FeP-C). The MOF derived FeP-C anode can inhibit the coarsening of small Fe particles, improve the electron conductivity and moderate the volume expansion of electrode, leading to superior rate capability and excellent cycling performance for Li-ions storage [161]. The FeP-C anode delivered a high reversible capacity of 700 $mAhg^{-1}$ at 0.1 Ag^{-1} after 180 cycles. The studies such as kinetic analysis, calculated diffusion coefficient and partial density of states (PDOS) were also done supporting the advantages of this in-situ synthesis for alkali ion diffusion.

4.3 Copper Phosphide

Copper forms three phosphorus compounds Cu_3P, CuP_2 and Cu_2P_7 but only Cu_3P is air stable. The Li uptake occurs according to the reaction

$$Cu_3P + 3Li \rightarrow 3Cu + Li_3P$$

Gravimetric capacity of Cu_3P is 377 $mAhg^{-1}$ which is lower than graphite (372 $mAhg^{-1}$) but it shows volumetric capacity of 2778 AhL^{-1} which is higher than that of graphite (800 AhL^{-1}). The electrochemical properties of the Cu_3P synthesized via mechanochemical method (ball milling) using n-dodecane as solvent were studied. Improved performance was obtained when the charge potential was limited to 0.50 V (vs. Li/Li^+) instead of 0.02 V and restricting the formation of the Li_3P phase. Capacity almost equal to the theoretical capacity was obtained during the first cycle when charged to 0.02 V but this capacity faded with prolonged cycling. Electrochemical performance was increased when cell was cycled with a voltage range of 2.0 to 0.50 V (vs. Li/Li^+). When reversibly charged to lower cut-off potentials (0.02 V), capacity decay is due to the type of the products formed (Li_3P and Cu) and which is difficult to convert to pristine materials because of energy barrier needed to reconvert back. This energy barrier is smaller for the products formed when the potential is cut-off to 0.50 V and was visible in the good capacity retention of the cells [162].

Another copper phosphide phase i.e. CuP_2 was used as anode in nanowires form synthesised via a supercritical fluid–liquid–solid growth (SFLS). It showed a high

discharge capacity of 945 $mAhg^{-1}$ after 100 cycles and a high rate capability with a capacity of 600 $mAhg^{-1}$at 6 C [163].

4.4 Zinc Phosphide

ZnP_2 and Zn_3P_2 are two phases of zinc phosphide reported in the literature which have been used as LIB anode. ZnP_2 has a higher theoretical capacity of 1581 $mAhg^{-1}$ and zinc-rich Zn_3P_2 has capacity of 1241 $mAhg^{-1}$ which are higher than commercial graphite (372 mA h g^{-1}). ZnP_2 nanowires synthesised via solvothermal method has been reported as an anode material for lithium batteries with first discharge capacity of 1415 $mAhg^{-1}$ at 0.3 C (1C = 1581 mA h g^{-1}). The discharge capacity of 1066 $mAhg^{-1}$ was obtained after 500 cycles [164]. The insertion reaction for Zn and Li has following two steps:

$$ZnP_2 \rightarrow LiZnP + LiP \rightarrow Li_3P + LiZn$$

In first step, ZnP_2 undergoes conversion reaction and second step involves Li and Zn alloy formation. Well aligned Zn_3P_2 nanowire arrays grafted on carbon fabric cloth were synthesised using CVD method and it was used as a novel self-supported binder-free anode for lithium ion batteries (LIBs) [165]. The hierarchical three-dimensional anode showed excellent electrochemical performances with a lithium storage capacity of 1200 $mAhg^{-1}$ upto 200 cycles. It has displayed a high rate capability with the capacity of 400 $mAhg^{-1}$ at current rate of 15 Ag^{-1} and an ultrahigh rate performance with a capacity of 300 $mAhg^{-1}$ at 20 Ag^{-1}.

4.5 Tin phosphide

SnP_3 and Sn_4P_3 phases of tin phosphides are explored as LIB anode. The Li storage takes place according to following reaction leading to a theoretical capacity of 1255 $mAhg^{-1}$.

$$Sn_4P_3 + 9Li^+ + 9e^- \rightarrow 4Sn + 3Li_3P$$

$$5Sn + 22Li^+ + 22e^- \rightarrow Li_{22}Sn_5$$

Sn_4P_3 hollow spherical microstructures are synthesized by a facile Solvothermal approach and applied as anode material for LIBs. The initial discharge capacity of 1478 $mAhg^{-1}$ was obtained at 100mAg^{-1} and it decreased to 261$mAhg^{-1}$ after 20 cycles. [166].

All-solid-state LIB was studied using Sn_4P_3 as electrode which was prepared by mechanical ball milling. The working electrode was consisting of Sn_4P_3, solid electrolyte (SE) and acetylene black (AB) and showed the first discharge capacity of 1080 $mAhg^{-1}$. The working electrode without SE and AB showed the first discharge capacity of 670 $mAhg^{-1}$. In further studies, doping into tin phosphide system has been tried and their efficiency for LIBs was studied [167].

Manganese (Mn)-doped Sn_4P_3 nanoparticles were synthesized via ultrasonic assisted hydrothermal method. The Mn content crucially determines the electrochemical performances of Sn_4P_3 nanoparticles. The Sn_4P_3 nanoparticles with 0.10 mol% concentration of Mn dopant gives the best cycling performances. The discharge capacity of 488 $mAhg^{-1}$ was obtained after 150 cycles at the current density of 100 mA g^{-1}, 420 $mAhg^{-1}$ at 200 mAg^{-1} and 255 $mAhg^{-1}$ at 1000 mAg^{-1}. This proves that concept of doping improves the structure stability and electrochemical properties of Sn_4P_3. Capacity fading issue in tin phosphide was addressed by making a composite with rGO [168]. The performance was stable with a reversible capacity of 651 $mAhg^{-1}$ after 100 cycles in comparison

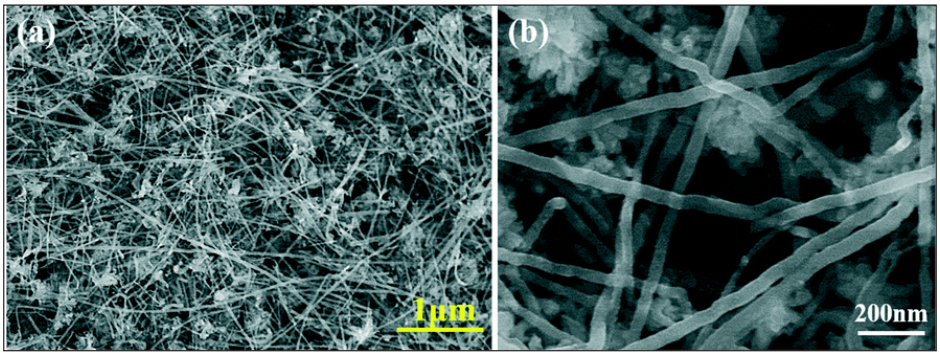

Figure 14: ZnP_2 nanowires synthesized by solvothermal method [164]

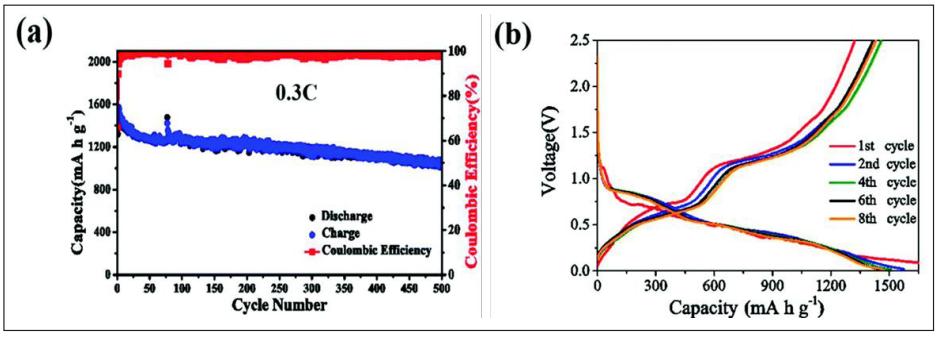

Figure 15: *(a) Cycle performance of ZnP_2 nanowires at a rate of 0.3C between 0.01 and 2.5 V. (b) Galvanostatic charge/discharge profiles of ZnP2 nanowire at 0.1C. for the first cycle, and 0.3C for the 1st, 2nd, 4th, 6th and 8th cycles. [164]*

to pure Sn_4P_3. Another interesting layered crystalline tin phosphide i.e. SnP_3 was also studied as anode for LIB. SnP_3 is expected to show interesting Li insertion/extraction behaviour due to layered structure. The SnP_3 electrode showed sequential topotactic and conversion reactions. In topotactic reaction region (0.7–2.0 V) a high volumetric capacity of 663 $mAhcm^{-3}$ was obtained and a good capacity retention of 636 $mAhcm^{-3}$ over 100 cycles with high C-rate with a capacity of 550 $mAhcm^{-3}$ at 3 C [169].

5. Summary

This review summarizes conversion type of anode materials explored for LIBs. Various metal oxide, sulphide and phosphide-based anode materials and their electrochemical performance for LIBs are discussed. Furthermore, different strategies such as synthesis of nano-dimensional materials, composite materials and intermetallic materials to increase and stabilize the capacity and stability of anode materials is discussed in detail. Several strategies to fabricate advanced energy storage materials have been developed, such as Nano-structuring, hybridization, pore-structure control, surface modification and composition optimization. Tremendous progress has been made in recent years in terms of the capacity, rate capability, and cycling life of electrode materials for LIBs. But issues of safety, environment compatibility, cost, ease of fabrication and suitability for high energy requirements e.g. electric vehicles, are the challenges still needs to be addressed for industrial applications.

References

1. C. T. Tugcu, I. Ozturk, A. Aslan, *Energy Econ.* 2012, *34*, 1942-1950.
2. K. Ellegård, J. Palm, *Appl. Energy* **2011**, *88*, 1920-1926.
3. B. Guo, M. Niu, X. Lai, L. Chen, *Glob. Energy Interconnect.* **2018**, *1*, 79-86.
4. V. Steinbach, F.-W. Wellmer, *Sustain.* **2010**, *2*, 1408-1430.
5. D. N. Buckley, C. O'Dwyer, N. Quill, R. P. Lynch, in *Energy Storage Options Their Environ. Impact*, **2019**, 115-149.
6. J.-M. Tarascon, *Philos. Trans. R. Soc. A Math. Phys. Eng. Sci.* **2010**, *368*, 3227-3241.
7. J. Liu, J. Wang, C. Xu, H. Jiang, C. Li, L. Zhang, J. Lin, Z. X. Shen, *Adv. Sci.* **2018**, *5*, 1700322.
8. Z. A. Ghazi, Z. Sun, C. Sun, F. Qi, B. An, F. Li, H.-M. Cheng, *Small* **2019**, *15*, 1900687.
9. Y. Zhang, T.-T. Zuo, J. Popovic, K. Lim, Y.-X. Yin, J. Maier, Y.-G. Guo, *Mater. Today* **2019**.
10. S. Goriparti, E. Miele, F. De Angelis, E. Di Fabrizio, R. Proietti Zaccaria, C. Capiglia, *J. Power Sources* **2014**, *257*, 421-443.
11. J. Lu, Z. Chen, F. Pan, Y. Cui, K. Amine, *Electrochem. Energy Rev.* **2018**, *1*, 35-53.
12. B. Scrosati, *J. Electrochem. Soc.*, **1992**, 10, 2776-2781
13. M. V. Reddy, G. V. Subba Rao, & B V. R. Chowdari, *Chem. rev.*, **2013**, *113*, 5364-5457.
14. L. S. G. Poizot, S. Laruelle, S. Grugeon, L. Dupont, & J. M. Tarascon, *Nature*, **2000**, *407*, 496.
15. Y. Deng, L. Wan, Y. Xie, X. Qin, G. Chen, *RSC Adv.* **2014**, *4*, 23914-23935.
16. J. Cabana, L. Monconduit, D. Larcher, M. R. Palacín, *Adv. Mater.* **2010**, *22*, E170-192.
17. X. Liu, C. Chen, Y. Zhao, B. Jia, *J. Nanomater.* **2013**, *2013*.
18. B. Liu, X. Hu, H. Xu, W. Luo, Y. Sun, Y. Huang, *Sci. Rep.* **2014**, *4*, 4229.
19. G.-L. Xu, Y.-F. Xu, H. Sun, F. Fu, X.-M. Zheng, L. Huang, J.-T. Li, S.-H. Yang, S.-G. Sun, *Chem. Commun.* **2012**, *48*, 8502-8504.
20. L. Gao, C. Gu, J. Zhao, X. Song, J. Huang, *Ceram. Int.* **2019**, *45*, 3425-3434.
21. L. Sheng, S. Liang, T. Wei, J. Chang, Z. Jiang, L. Zhang, Q. Zhou, J. Zhou, L. Jiang, Z. Fan, *Energy Storage Mater.* **2018**, *12*, 94-102.
22. P. Xia, H. B. Lin, W. Q. Tu, X. Q. Chen, X. Cai, X. W. Zheng, M. Q. Xu, W. S. Li, *Electrochim. Acta* **2016**, *198*, 66-76.
23. C. C. Li, H. Yu, Q. Yan, H. H. Hng, *Electrochim. Acta* **2016**, *187*, 406-412.
24. D.-S. Liu, D.-H. Liu, B.-H. Hou, Y.-Y. Wang, J.-Z. Guo, Q.-L. Ning, X.-L. Wu, *Electrochim. Acta* **2018**, *264*, 292-300.
25. J. Liu, N. Chen, Q. Pan, *J. Power Sources* **2015**, *299*, 265-272.
26. K. Li, F. Shua, X. Guo, D. Xue, *Electrochim. Acta* **2016**, *188*, 793-800.
27. Y. Lin, S. Zhao, J. Qian, N. Xu, X.-Q. Liu, L.-B. Sun, W. Li, Z. Chen, Z. Wu, *J. Mater. Sci.* **2020**, *55*, 2139-2154.
28. T. Chen, Z. Wu, W. Xiang, E. Wang, T. Chen, X. Guo, Y. Chen, B. Zhong, *Electrochim. Acta* **2017**, *246*, 931-940.
29. X. Fan, S. Li, L. Lu, *Electrochim. Acta* **2016**, *200*, 152-160.
30. J. Wang, C. Zhang, F. Kang, *ACS Appl. Mater. Interfaces* **2015**, *7*, 9185-9194.
31. Y. Wu, X. Li, Q. Xiao, G. Lei, Z. Li, J. Guan, *J. Electroanal. Chem.* **2019**, *834*, 161-166.
32. M. Asif, M. Rashad, Z. Ali, H. Qiu, W. Li, L. Pan, Y. Hou, *Mater. Today Energy* **2018**, *10*, 108-117.
33. S. Li, Y. Zhao, Z. Liu, L. Yang, J. Zhang, M. Wang, R. Che, *Small* **2018**, *14*, 1801007.
34. Y. Wang, Z. J. Han, S. F. Yu, R. R. Song, H. H. Song, K. (Ken) Ostrikov, H. Y. Yang, *Carbon* **2013**, *64*, 230-236.
35. L. Shen, Q. Dong, G. Zhu, Z. Dai, Y. Zhang, W. Wang, X. Dong, *Adv. Mater. Interfaces* **2018**, *5*, 1800362.
36. M. Rana, V. Sai Avvaru, N. Boaretto, V. A. de la Peña O'Shea, R. Marcilla, V. Etacheri, J. J. Vilatela, *J. Mater. Chem. A* **2019**, *7*, 26596-26606.
37. H. Lai, J. Li, Z. Chen, Z. Huang, *ACS Appl. Mater. Interfaces* **2012**, *4*, 2325-2328.
38. A. Yu, H. W. Park, A. Davies, D. C. Higgins, Z. Chen, X. Xiao, *J. Phys. Chem. Lett.* **2011**, *2*, 1855-1860.
39. L. Li, A.-R. O. Raji, J. M. Tour, *Adv. Mater.* **2013**, *25*, 6298-6302.
40. I.-H. Ko, S.-J. Kim, J. Lim, S.-H. Yu, J. Ahn, J.-K. Lee, Y.-E. Sung, *Electrochim. Acta* **2016**, *187*, 340-347.
41. Q. Zhou, M. Zeng, X. Wu, Y. Zhang, G. Qin, *J. Alloys Compd.* **2019**, *786*, 368–376.
42. W. Ren, D. Liu, C. Sun, X. Yao, J. Tan, C. Wang, K. Zhao, X. Wang, Q. Li, L. Mai, *Small* **2018**, *14*, 1800659.

43. Q. Li, L. Yin, Z. Li, X. Wang, Y. Qi, J. Ma, *ACS Appl. Mater. Interfaces* **2013**, *5*, 10975-10984.
44. S. Yuan, W. Chen, L. Zhang, Z. Liu, J. Liu, T. Liu, G. Li, Q. Wang, *Small* **2019**, *n/a*, 1903311.
45. S. Chandel, S. Lee, S. Kim, S. P. Singh, J. Gim, J. Kim, A. K. Rai, *New J. Chem.* **2019**, *43*, 12916-12922.
46. J.-Q. Li, F.-C. Zhou, Y.-H. Sun, J.-M. Nan, *J. Alloys Compd.* **2018**, *740*, 346-354.
47. S.-K. Park, C.-Y. Seong, S. Yoo, Y. Piao, *Energy* **2016**, *99*, 266-273.
48. F. Ma, A. Yuan, J. Xu, *ACS Appl. Mater. Interfaces* **2014**, *6*, 18129-18138.
49. Z. Bai, X. Zhang, Y. Zhang, C. Guo, B. Tang, *J. Mater. Chem. A* **2014**, *2*, 16755-16760.
50. Y. Jiang, J.-L. Yue, Q. Guo, Q. Xia, C. Zhou, T. Feng, J. Xu, H. Xia, *Small* **2018**, *14*, 1704296.
51. M. S. Akhtar, P. T. M. Bui, Z.-Y. Li, O.-B. Yang, B. J. Paul, S. Kim, J. Kim, A. K. Rai, *Solid State Ion.* **2019**, *336*, 31-38.
52. Z. Li, N. Liu, X. Wang, C. Wang, Y. Qi, L. Yin, *J. Mater. Chem.* **2012**, *22*, 16640-16648.
53. C. Wang, L. Yin, D. Xiang, Y. Qi, *ACS Appl. Mater. Interfaces* **2012**, *4*, 1636-1642.
54. L. Wang, L. Li, H. Wang, J. Yang, F. Wu, R. Chen, *ACS Appl. Energy Mater.* **2019**, *2*, 5206-5213.
55. Z. Cai, L. Xu, M. Yan, C. Han, L. He, K. M. Hercule, C. Niu, Z. Yuan, W. Xu, L. Qu, et al., *Nano Lett.* **2015**, *15*, 738-744.
56. L. Guo, Y. Ding, C. Qin, W. Song, S. Sun, K. Fang, W. Li, J. Du, F. Wang, *J. Alloys Compd.* **2018**, *735*, 209-217.
57. J.-G. Wang, D. Jin, R. Zhou, X. Li, X. Liu, C. Shen, K. Xie, B. Li, F. Kang, B. Wei, *ACS Nano* **2016**, *10*, 6227-6234.
58. D. Zhang, G. Li, J. Fan, B. Li, L. Li, *Chem. - A Eur. J.* **2018**, *24*, 9632-9638.
59. S. Luo, H. Wu, Y. Wu, K. Jiang, J. Wang, S. Fan, *J. Power Sources* **2014**, *249*, 463-469.
60. J. Cabana, L. Monconduit, D. Larcher, M. R. Palacín, *Adv. Mater.* **2010**, *22*, E170-E192.
61. N. Kang, J. H. Park, J. Choi, J. Jin, J. Chun, I. G. Jung, J. Jeong, J. Park, S. M. Lee, H. J. Kim, *Angew. Chemie Int. Ed.* **2012**, *51*, 6626–6630.
62. P. Poizot, S. Laruelle, S. Grugeon, L. Dupont, J.-M. Tarascon, *Nature* **2000**, *407*, 496.
63. J. B. Goodenough, K.-S. Park, *J. Am. Chem. Soc.* **2013**, *135*, 1167-1176.
64. M. V Reddy, T. Yu, C.-H. Sow, Z. X. Shen, C. T. Lim, G. V Subba Rao, B. V. R. Chowdari, *Adv. Funct. Mater.* **2007**, *17*, 2792-2799.
65. Y.-M. Lin, P. R. Abel, A. Heller, C. B. Mullins, *J. Phys. Chem. Lett.* **2011**, *2*, 2885-2891.
66. J. Zhang, Y. Sun, Y. Yao, T. Huang, A. Yu, *J. Power Sources* **2013**, *222*, 59-65.
67. J. Zhang, T. Huang, Z. Liu, A. Yu, *Electrochem. commun.* **2013**, *29*, 17-20.
68. X. Zhu, Y. Zhu, S. Murali, M. D. Stoller, R. S. Ruoff, *ACS Nano* **2011**, *5*, 3333-3338.
69. J. Kan, Y. Wang, *Sci. Rep.* **2013**, *3*, 3502.
70. N. Yan, X. Zhou, Y. Li, F. Wang, H. Zhong, H. Wang, Q. Chen, *Sci. Rep.* **2013**, *3*, 3392.
71. X. Zhang, H. Liu, S. Petnikota, S. Ramakrishna, H. J. Fan, *J. Mater. Chem. A* **2014**, *2*, 10835-10841.
72. X. Gu, L. Chen, Z. Ju, H. Xu, J. Yang, Y. Qian, *Adv. Funct. Mater.* **2013**, *23*, 4049-4056.
73. H. Wu, M. Xu, Y. Wang, G. Zheng, *Nano Res.* **2013**, *6*, 167-173.
74. J. Liu, J. Jiang, D. Qian, G. Tan, S. Peng, H. Yuan, D. Luo, Q. Wang, Y. Liu, *RSC Adv.* **2013**, *3*, 15457-15466.
75. G. Xia, N. Li, D. Li, R. Liu, C. Wang, Q. Li, X. Lü, J. S. Spendelow, J. Zhang, G. Wu, *ACS Appl. Mater. Interfaces* **2013**, *5*, 8607-8614.
76. P. K. Dwivedi, V. K. A. Muniraj, R. R. Devarapalli, M. V Shelke, *ChemistrySelect* **2018**, *3*, 2286-2292.
77. B. Liu, Q. Zhang, Z. Jin, L. Zhang, L. Li, Z. Gao, C. Wang, H. Xie, Z. Su, *Adv. Energy Mater.* **2018**, *8*, 1702347.
78. W. Wei, S. Yang, H. Zhou, I. Lieberwirth, X. Feng, K. Müllen, *Adv. Mater.* **2013**, *25*, 2909-2914.
79. W. Zhang, X. Wu, J. Hu, Y. Guo, L. Wan, *Adv. Funct. Mater.* **2008**, *18*, 3941-3946.
80. C. He, S. Wu, N. Zhao, C. Shi, E. Liu, J. Li, *ACS Nano* **2013**, *7*, 4459-4469.
81. Z. Liu, X.-Y. Yu, U. Paik, *Adv. Energy Mater.* **2016**, *6*, 1502318.
82. W. Y. Li, L. N. Xu, J. Chen, *Adv. Funct. Mater.* **2005**, *15*, 851-857.
83. D. Bresser, E. Paillard, P. Niehoff, S. Krueger, F. Mueller, M. Winter, S. Passerini, *ChemPhysChem* **2014**, *15*, 2177-2185.
84. X. Huang, R. Wang, D. Xu, Z. Wang, H. Wang, J. Xu, Z. Wu, Q. Liu, Y. Zhang, X. Zhang, *Adv. Funct. Mater.* **2013**, *23*, 4345-4353.
85. B. Wang, X.-Y. Lu, K. Y. Wong, Y. Tang, *Mater. Chem. Front.* **2017**, *1*, 468-476.
86. S. Sun, X. Zhao, M. Yang, L. Wu, Z. Wen, X. Shen, *Sci. Rep.* **2016**, *6*, 19564.
87. N. S. Marzuki, N. U. Taib, M. F. Hassan, N. H. Idris, *Electrochim. Acta* **2015**, *182*, 452-457.
88. G. Huang, F. Zhang, X. Du, Y. Qin, D. Yin, L. Wang, *ACS Nano* **2015**, *9*, 1592-1599.
89. Y. Kim, J.-H. Lee, S. Cho, Y. Kwon, I. In, J. Lee, N.-H. You, E. Reichmanis, H. Ko, K.-T. Lee, et al., *ACS Nano* **2014**, *8*, 6701-6712.
90. L. Luo, J. Wu, J. Xu, V. P. Dravid, *ACS Nano* **2014**, *8*, 11560-11566.
91. Q. Su, J. Zhang, Y. Wu, G. Du, *Nano Energy* **2014**, *9*, 264-272.
92. J. Wang, N. Yang, H. Tang, Z. Dong, Q. Jin, M. Yang, D. Kisailus, H. Zhao, Z. Tang, D. Wang, *Angew. Chemie Int. Ed.* **2013**, *52*, 6417-6420.
93. L. Yu, H. Hu, H. Bin Wu, X. W. (David) Lou, *Adv. Mater.* **2017**, *29*, 1604563.
94. J. Wang, H. Tang, L. Zhang, H. Ren, R. Yu, Q. Jin, J. Qi, D. Mao, M. Yang, Y. Wang, et al., *Nat. Energy* **2016**, *1*, 16050.
95. L. Zhou, Z. Zhuang, H. Zhao, M. Lin, D. Zhao, L. Mai, *Adv. Mater.* **2017**, *29*, 1602914.
96. J. Sun, D. Li, Y. Xia, X. Zhu, L. Zong, Q. Ji, Y. (Alec) Jia, D. Yang, *Chem. Commun.* **2015**, *51*, 16267-16270.
97. X. Yao, G. Guo, Y. Zhao, Y. Zhang, S. Y. Tan, Y. Zeng, R. Zou, Q. Yan, Y. Zhao, *Small* **2016**, *12*, 3849-3860.

98. S. Abouali, M. Akbari Garakani, B. Zhang, H. Luo, Z.-L. Xu, J.-Q. Huang, J. Huang, J.-K. Kim, *J. Mater. Chem. A* **2014**, *2*, 16939-16944.
99. Y. Zhao, C. Ma, Y. Li, H. Chen, Z. Shao, *Carbon* **2015**, *95*, 494-496.
100. Y. Hou, J. Li, Z. Wen, S. Cui, C. Yuan, J. Chen, *Nano Energy* **2015**, *12*, 1-8.
101. G. Fang, J. Zhou, C. Liang, A. Pan, C. Zhang, Y. Tang, X. Tan, J. Liu, S. Liang, *Nano Energy* **2016**, *26*, 57-65.
102. Y. M. Chen, L. Yu, X. W. (David) Lou, *Angew. Chemie Int. Ed.* **2016**, *55*, 5990-5993.
103. U. Boesenberg, M. A. Marcus, A. K. Shukla, T. Yi, E. McDermott, P. F. Teh, M. Srinivasan, A. Moewes, J. Cabana, *Sci. Rep.* **2014**, *4*, 7133.
104. S. Yang, X. Feng, S. Ivanovici, K. Müllen, *Angew. Chemie Int. Ed.* **2010**, *49*, 8408-8411.
105. Y. Zou, Y. Wang, *Nanoscale* **2011**, *3*, 2615-2620.
106. X. Xu, H. Tan, K. Xi, S. Ding, D. Yu, S. Cheng, G. Yang, X. Peng, A. Fakeeh, R. V. Kumar, *Carbon* **2015**, *84*, 491-499.
107. Q. Liang, L. Z. Gao, Q. Li, S. H. Tang, B. C. Liu, Z. L. Yu, *Carbon* **2001**, *39*, 897-903.
108. M. Chen, X. Xia, M. Qi, J. Yuan, J. Yin, Q. Chen, *Electrochim. Acta* **2015**, *184*, 17-23.
109. X. Sun, C. Yan, Y. Chen, W. Si, J. Deng, S. Oswald, L. Liu, O. G. Schmidt, *Adv. Energy Mater.* **2014**, *4*, 1300912.
110. J. Bell, R. Ye, K. Ahmed, C. Liu, M. Ozkan, C. S. Ozkan, *Nano Energy* **2015**, *18*, 47-56.
111. J. Liang, H. Hu, H. Park, C. Xiao, S. Ding, U. Paik, X. W. (David) Lou, *Energy Environ. Sci.* **2015**, *8*, 1707-1711.
112. Y. Feng, H. Zhang, W. Li, L. Fang, Y. Wang, *J. Power Sources* **2016**, *301*, 78-86.
113. C. Liu, C. Li, K. Ahmed, Z. Mutlu, C. S. Ozkan, M. Ozkan, *Sci. Rep.* **2016**, *6*, 29183.
114. F. Zou, Y.-M. Chen, K. Liu, Z. Yu, W. Liang, S. M. Bhaway, M. Gao, Y. Zhu, *ACS Nano* **2016**, *10*, 377-386.
115. R. Zhang, J. Liu, H. Guo, X. Tong, *Mater. Lett.* **2015**, *139*, 55-58.
116. C. Zhu, D. Chao, J. Sun, I. M. Bacho, Z. Fan, C. F. Ng, X. Xia, H. Huang, H. Zhang, Z. X. Shen, et al., *Adv. Mater. Interfaces* **2015**, *2*, 1400499.
117. Q. Zhang, J. Wang, D. Xu, Z. Wang, X. Li, K. Zhang, *J. Mater. Chem. A* **2014**, *2*, 3865-3874.
118. H. Huang, Y. Liu, J. Wang, M. Gao, X. Peng, Z. Ye, *Nanoscale* **2013**, *5*, 1785-1788.
119. H. Zhang, G. Zhang, Z. Li, K. Qu, L. Wang, W. Zeng, Q. Zhang, H. Duan, *J. Mater. Chem. A* **2016**, *4*, 10585-10592.
120. Q. Zhang, D. Xu, X. Zhou, X. Wu, K. Zhang, *Small* **2014**, *10*, 935-943.
121. Y. F. Yuan, Y. B. Pei, J. Fang, H. L. Zhu, J. L. Yang, S. Y. Guo, *Mater. Lett.* **2013**, *91*, 279-282.
122. K. Chen, D. Xue, *Phys. Chem. Chem. Phys.* **2013**, *15*, 19708-19714.
123. X. Duan, H. Huang, S. Xiao, J. Deng, G. Zhou, Q. Li, T. Wang, *J. Mater. Chem. A* **2016**, *4*, 8402-8411.
124. J. Wang, Y. Liu, S. Wang, X. Guo, Y. Liu, *J. Mater. Chem. A* **2014**, *2*, 1224-1229.
125. R. Wu, X. Qian, F. Yu, H. Liu, K. Zhou, J. Wei, Y. Huang, *J. Mater. Chem. A* **2013**, *1*, 11126-11129.
126. T. Chen, Y. Hu, B. Cheng, R. Chen, H. Lv, L. Ma, G. Zhu, Y. Wang, C. Yan, Z. Tie, et al., *Nano Energy* **2016**, *20*, 305-314.
127. S. Ko, J.-I. Lee, H. S. Yang, S. Park, U. Jeong, *Adv. Mater.* **2012**, *24*, 4451-4456.
128. Y. Xu, G. Jian, M. R. Zachariah, C. Wang, *J. Mater. Chem. A* **2013**, *1*, 15486-15490.
129. Y. Tan, Z. Jia, J. Sun, Y. Wang, Z. Cui, X. Guo, *J. Mater. Chem. A* **2017**, *5*, 24139-24144.
130. W. Wang, Y. Liang, Y. Kang, L. Liu, Z. Xu, X. Tian, W. Mai, H. Fu, H. Lv, K. Teng, et al., *Mater. Chem. Phys.* **2019**, *223*, 762-770.
131. V. Etacheri, G. A. Seisenbaeva, J. Caruthers, G. Daniel, J. Nedelec, V. G. Kessler, V. G. Pol, *Adv. Energy Mater.* **2015**, *5*, 1401289.
132. X. W. Lou, C. M. Li, L. A. Archer, *Adv. Mater.* **2009**, *21*, 2536-2539.
133. H. Li, Q. Su, J. Kang, M. Huang, M. Feng, H. Feng, P. Huang, G. Du, *Mater. Lett.* **2018**, *217*, 276-280.
134. X. Zhou, L. Yu, X. W. Lou, *Adv. Energy Mater.* **2016**, *6*, 1600451.
135. J. Yan, A. Sumboja, E. Khoo, P. S. Lee, *Adv. Mater.* **2011**, *23*, 746-750.
136. L. Chang, Z. Yi, Z. Wang, L. Wang, Y. Cheng, *Appl. Surf. Sci.* **2019**, *484*, 646-654.
137. N. Palaniyandy, M. A. Kebede, K. I. Ozoemena, M. K. Mathe, *Electrocatalysis* **2019**, *10*, 314-322.
138. L. Yi, L. Liu, G. Guo, X. Chen, Y. Zhang, S. Yu, X. Wang, *Electrochim. Acta* **2017**, *240*, 63-71.
13. M. Sahoo, S. Ramaprabhu, *Carbon* **2018**, *127*, 627-635.
140. S. Abouali, M. Akbari Garakani, J.-K. Kim, *Electrochim. Acta* **2018**, *284*, 436-443.
141. J. Liang, Y. Zhao, L. Guo, L. Li, *ACS Appl. Mater. Interfaces* **2012**, *4*, 5742-5748.
142. J. Liang, X.-Y. Yu, H. Zhou, H. Bin Wu, S. Ding, X. W. (David) Lou, *Angew. Chemie Int. Ed.* **2014**, *53*, 12803-12807.
143. J. Ye, H. Zhang, R. Yang, X. Li, L. Qi, *Small* **2010**, *6*, 296-306.
144. B. Jiang, Y. He, B. Li, S. Zhao, S. Wang, Y.-B. He, Z. Lin, *Angew. Chemie Int. Ed.* **2017**, *56*, 1869-1872.
145. L. Zhang, Y. Huang, Y. Zhang, H. Gu, W. Fan, T. Liu, *Adv. Mater. Interfaces* **2016**, *3*, 1500467.
146. Q. Li, L. Li, P. Wu, N. Xu, L. Wang, M. Li, A. Dai, K. Amine, L. Mai, J. Lu, *Adv. Energy Mater.* **2019**, *9*, 1901153.
147. Y. Wang, J. Wu, Y. Tang, X. Lü, C. Yang, M. Qin, F. Huang, X. Li, X. Zhang, *ACS Appl. Mater. Interfaces* **2012**, *4*, 4246-4250.
148. Z. Li, W. Li, H. Xue, W. Kang, X. Yang, M. Sun, Y. Tang, C.-S. Lee, *RSC Adv.* **2014**, *4*, 37180-37186.
149. B. Wu, H. Song, J. Zhou, X. Chen, *Chem. Commun.* **2011**, *47*, 8653-8655.
150. L. Li, C. Gao, A. Kovalchuk, Z. Peng, G. Ruan, Y. Yang, H. Fei, Q. Zhong, Y. Li, J. M. Tour, *Nano Res.* **2016**, *9*, 2904-2911.
151. M. Zhou, N. Peng, Z. Liu, Y. Xi, H. He, Y. Xia, Z. Liu, S. Okada, *J. Power Sources* **2016**, *306*, 408-412.
152. J. Li, D. Yan, X. Zhang, S. Hou, T. Lu, Y. Yao, L. Pan, *J. Mater. Chem. A* **2017**, *5*, 20428-20438.

153. K. Li, S. Yan, Z. Lin, Y. Shi, *J. Alloys Compd.* **2016**, *681*, 486-491.
154. Y. Wang, J. Zhou, J. Wu, F. Chen, P. Li, N. Han, W. Huang, Y. Liu, H. Ye, F. Zhao, et al., *J. Mater. Chem. A* **2017**, *5*, 25618-25624.
155. J. Y. Xiang, X. L. Wang, X. H. Xia, J. Zhong, J. P. Tu, *J. Alloys Compd.* **2011**, *509*, 157-160.
156. Y. Lu, J.-P. Tu, Q.-Q. Xiong, J.-Y. Xiang, Y.-J. Mai, J. Zhang, Y.-Q. Qiao, X.-L. Wang, C.-D. Gu, S. X. Mao, *Adv. Funct. Mater.* **2012**, *22*, 3927-3935.
157. Y. Bai, H. Zhang, L. Fang, L. Liu, H. Qiu, Y. Wang, *J. Mater. Chem. A* **2015**, *3*, 5434-5441.
158. D. Yang, J. Zhu, X. Rui, H. Tan, R. Cai, H. E. Hoster, D. Y. W. Yu, H. H. Hng, Q. Yan, *ACS Appl. Mater. Interfaces* **2013**, *5*, 1093-1099.
159. K. Zhu, J. Liu, S. Li, L. Liu, L. Yang, S. Liu, H. Wang, T. Xie, *Adv. Mater. Interfaces* **2017**, *4*, 1700377.
160. Y. Yang, Y. Jiang, W. Fu, X.-Z. Liao, Y.-S. He, W. Tang, F. M. Alamgir, Z.-F. Ma, *Dalt. Trans.* **2019**, *48*, 7778-7785.
161. X. Xu, J. Feng, J. Liu, F. Lv, R. Hu, F. Fang, L. Yang, L. Ouyang, M. Zhu, *Electrochim. Acta* **2019**, *312*, 224-233.
162. M. C. Stan, R. Klöpsch, A. Bhaskar, J. Li, S. Passerini, M. Winter, *Adv. Energy Mater.* **2013**, *3*, 231-238.
163. G.-A. Li, C.-Y. Wang, W.-C. Chang, H.-Y. Tuan, *ACS Nano* **2016**, *10*, 8632-8644.
164. J.-Y. Chen, L.-C. Chin, G.-A. Li, H.-Y. Tuan, *CrystEngComm* **2017**, *19*, 975-981.
165. W. Li, L. Gan, K. Guo, L. Ke, Y. Wei, H. Li, G. Shen, T. Zhai, *Nanoscale* **2016**, *8*, 8666-8672.
166. S. Liu, H. Zhang, L. Xu, L. Ma, *J. Cryst. Growth* **2016**, *438*, 31-37.
167. A. Ueda, M. Nagao, A. Inoue, A. Hayashi, Y. Seino, T. Ota, M. Tatsumisago, *J. Power Sources* **2013**, *244*, 597-600.
168. Y. Ding, Z.-F. Li, E. V Timofeeva, C. U. Segre, *Adv. Energy Mater.* **2018**, *8*, 1702134.
169. J.-W. Park, C.-M. Park, *Sci. Rep.* **2016**, *6*, 35980.

Dr. Manjusha Shelke *is a Principal Scientist at CSIR-National Chemical Laboratory, Pune. She is a materials' chemist and her research interests are in the development of high energy electrode materials for storage devices like rechargeable batteries (Li-ion, Li-sulphur, Na-ion, multivalent chemistries) and supercapacitors for stationary and mobility applications. She completed her PhD in chemistry in the year from CSIR-Advanced Materials and Processes Research Institute, Bhopal, MP, India. She had worked as postdoctoral researcher at Institutd'électronique de microélectronique et de nanotechnologie (IEMN), Lille, France during 2007-08 sponsored by Embassy of France in India. She had been awarded a visiting scholarship in chemical sciences for the year 2013 by Indo-US Science & Technology Forum (IUSSTF) and worked at Rice University, Houston, TX, USA. She has been selected as Kavli Fellow by National Academy of Sciences (NAS), USA in 2015 and as a Fellow of Maharashtra Academy of Sciences (MAS) in 2018. She has also been invited as visiting faculty by Automotive Research Association of India's Academy (ARAI) since 2020.*

Pravin Kumari Dwivedi *received her B.Sc. degree in 2010 and M.Sc. degree in 2012 in Chemistry from Banasthali University, Rajasthan, India. She has defended her Ph.D. degree under the supervision of Dr.Manjusha V. Shelke at Physical and material Chemistry Division, CSIR-National Chemical Laboratory, Pune, India on Feb, 2020. She is pursuing postdoctoral research work on Na-ion batteries at Indian Institute of Technology Delhi, New Delhi, India. Her current research interests include Material Chemistry, energy storage devices like Li ion Battery, Sodium ion Battery and Supercapacitor.*

Poonam Yadav *received her integrated B.TECH-M.TECH degree in 2014 in Nanotechnology from University of Rajasthan, India. She is currently pursuing AcSIR-RMIT Joint Ph.D. in Chemical Sciences under the supervision of Dr. Manjusha V. Shelkeat CSIR-National Chemical Laboratory (CSIR-NCL), Pune, India and Dr. Lathe Jones at RMIT University, Melbourne, Australia. Her current research interests include material's chemistry for energy storage devices like Alkali ion Battery, solid state electrolyte and supercapacitor.*

Golu Parte *received his BS-MS degree in 2015 in Chemistry from IISER, Pune India. Currently, he is pursuing Ph.D. degree under the supervision of Dr.Manjusha V. Shelke atPhysical and material Chemistry Division, CSIR-National Chemical Laboratory, Pune, India. His research interests include energy storage devices like Li ion Battery, Sodium ion Battery and Supercapacitor.*

Cathode Materials for Lithium Ion Batteries (LIBs): A Review on Materialsrelated aspects towards High Energy Density LIBs

Ambesh Dixit*
Department of Physics & Center for Solar Energy, Indian Institute of Technology Jodhpur, Jodhpur 342037, India
**ambesh@iitj.ac.in*

Abstract

This article reviews the development of cathode materials for secondary lithium ion batteries since its inception with the introduction of lithium cobalt oxide in early 1980s. The time has passed and numerous cathode materials are designed and developed to realize not only the enhanced capacity but also the power density simultaneously. However, there are numerous challenges such as the cyclic stability of cathode materials, their structural and thermal stability, higher operating voltage together with high ionic and electronic conductivity for efficient ion and charge transport during charging and discharging. This article will cover the development of materials in chronological order classifying as the lithium ion cathode materials in different generations. The ternary oxides such as LiTMOx (TM=Transition Metal) are considered as the first generation materials, whereas modified ternary and quaternary oxide systems are considered as the second generation materials. The current i.e. third generation includescomplex oxide systems with higher lithium content such as Li_2TMSiO_4 aiming for higher energy density. Further, developments are heading towards lithium metal based batteries with very high energy densities.

Keywords: Energy storage; Secondary batteries; Li-ion battery, Cathode materials; Electrochemistry; Charge dynamics; Cyclability.

Introduction:

The demand of energy consumption per person is continuously increasing not only because of comfort living but also to meet every day necessities such as mobiles, laptops, and other electronic gadgets for every day communication, commuting, power electronics, and house hold accessories especially in remote areas. Thus, batteries, particularly rechargeable ones, are becoming essential and integral part of everyone's life. Further, with these applications energy demand especially for movable platforms such as buses, rickshaws, cars, trains and even planes currently rely on uses of conventional non-renewable i.e. fossil fuels. The use of fossil fuels is also impacting our environment and severely polluting with various toxic and greenhouse gases, leading to adverse effect on living beings. That's' why there is a continuous compulsion to use renewable/green energy sources, such as solar, wind, thermal and geothermal, not only because of limited conventional fossil fuel sources depleting every day but also because of large pollution after consuming conventional fossil fuel products, causing environmental degradation and thus, life threatening consequences. Most of the megacities are facing such environmental degradation because of toxic exhaust gases from regular vehicles and other exhausts such as conventional power plants, burnings, and industries using conventional fuel sources. The situation is worse in developing and under developed countries, where there is no guidelines and policies on using conventional fossil fuels. The alarming situation is that the consumption of conventional fuel is increasing every day even after knowing the consequences. Further, there are intrinsic challenges with renewable energy sources such as their availability, e.g. Sun light is available during day time and energy requirement is equally or even more important for off-Sun hours, unpredictability, uncontrollability, and intermittency apart from day and night cycles. In spite of all these, the development of solar photovoltaics led to the installation of large scale PV power plants producing GW (Giga Watts) poweracross the globe and providing useful electrical energy from the freely available Sun light. This directly converted electrical energy can be either fed to the grid or used in distributed applications. However, after Sun hours, the generation of electricity is not possible and thus, there is a stringent requirement of storing electrical energy simultaneously for its use during off-Sun hours. This relies on the energy storage systems i.e. batteries in terms of large specific capacity and power density together with cyclability. The energy needs for various applications such asoff-Sun hour grid, distributed off grid, and small scale energy applications,can be met by using efficient electrical energy storage devices. Considering such constraints, large efforts are put in the development of secondary rechargeable batteries to meet some of these requirements.

The large energy storage requirements are currently met by lead acid batteries in general, which are not safe to handle because of lead as the toxic elements and also suffer from lower operating voltage and specific energy density, as illustrated schematically in Ragone plot, Fig 1.

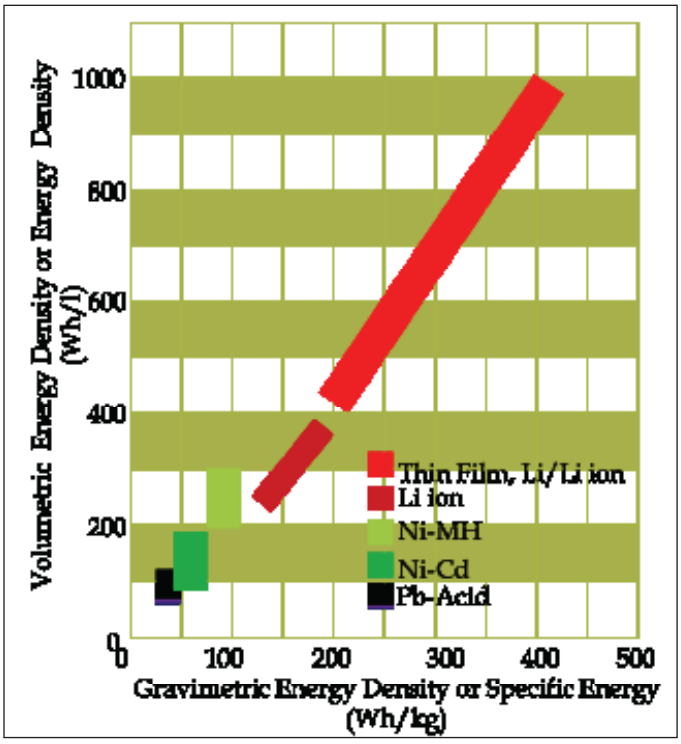

Figure 1. Ragone plot, showing gravimetric and volumetric energy densities of different rechargeable batteries

This provides opportunities to innovate materials which can offer high energy density, cyclability without capacity fading, together with safety against environmental factors. The lithium ion batteries are considered as one of the probable solution towards mitigating the intermittency of renewable energy sources by replacing the widely used toxic lead acid batteries. However, currently lithium ion rechargeable batteries are mostly used in portable electronic devices and in its matured state, which replaced the initially used nickel-cadmium rechargeable batteries. These Ni-Cd batteries were offering relatively poor energy and power density with respect to lithium ion batteries, Fig 1, and also suffering from memory issues, ending with relatively shorter life time. Thus, lithium ion batteries are far superior from their counter systems such as lead acid (Pb-acid), nickel-cadmium (Ni-Cd), and nickel-metal hydride (Ni-MH) batteries, Fig 1. The relatively high gravimetric and volumetric energy density of lithium ion batteries replaced other batteries in todays' consumer electronics and leading steps towards green energy. 2019 Nobel Prize in chemistry is awarded to Professor John Goodenough (The University of Texas at Austin, USA), M. Stanley Whittingham (Binghamton University, State University of New York, USA), and Akira Yoshino (Asahi Kasei Corporation, Tokyo, Japan, &Meijo University, Nagoya, Japan), for the development of lithium ion battery, Fig 2.

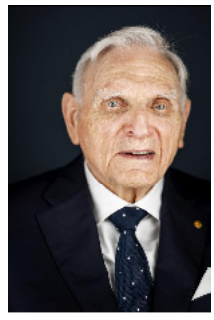		
John B. Goodenough The University of Texas at Austin, USA	**M. Stanley Whittingham** Binghamton University, State University of New York, USA	**Akira Yoshino** Asahi Kasei Corporation, Tokyo, Japan & Meijo University, Nagoya, Japan
Metal oxides as lithium intercalating cathodes e.g. Lithium cobalt oxide	Metal sulphide as lithium intercalating cathode e.g. titanium disulphide	Carbon material as an alternative anode material

Figure 2: Nobel prize winners and their contribution in the field of rechargeable energy storage, especially in lithium ion batteries, **Reference: https://www.nobelprize.org/prizes/chemistry/2019/summary/**

The development of battery, especially lithium battery was initiated 1970 and accelerated onwards to explore efficient rechargeable electrical energy storage system, which can overcome the low gravimetric and volumetric energy density issues with contemporary rechargeable batteries. The work was fueled by these Nobel Prize winners' work, which revolutionized the field of electrical energy storage. Professor Whittingham, around 1970s, discovered titanium disulphide as a cathode material which can host and intercalate lithium ions efficiently in lithium ion batteries. Further, around 1980s, the work on metal oxide i.e. lithium cobalt oxide by Professor Goodenough provided an alternative cathode material to metal sulphide for lithium ion batteries which can operate at higher voltage ~.3.5 - 4V and thus, providing higher energy/power density. In these work metallic lithium was used as anode, which is highly reactive and explosive material, thus was not a common choice for battery applications. Later around 1985, Professor Akira Yoshino used a carbon material (petroleum coke) as an anode in place of lithium together

with lithium cobalt oxide as cathode material to fabricate a lithium ion battery. This is considered as the birth point for the current commercially used lithium ion batteries. The advantage of such lithium ion batteries is that these are not based on any chemical reaction but intercalation of lithium ions via lithium ion movement between cathode and electrode during charging and discharging. The use of such rechargeable lithium ion batteries is increasing and most of the portable electronic devices are using only lithium ion batteries providing long hour power backups together with longer charge/discharge cyclability and thus, longer life span. With the advent of lithium ion batteries, there are continuous efforts in developing new battery materials, which can provide enhanced energy and power density, an essential requirement for power electronics and towards the development of electric and hybrid electric vehicles (cars, buses and even planes). However, there are still limited or negligible uses of lithium ion batteries for large power applications such as energy storage in solar photovoltaic power plants, hybrid electric vehicles i.e. plug-in electric vehicles and other such power applications. Further, large energy to power density aspect ratio together with higher operating voltage, large charge-discharge cyclability without capacity fading and safety issues are other important points to be considered towards developing such high energy and power density materials. Thus, large efforts are required to innovate such materials which can meet these requirements. The present article discusses the chronological development of cathode materials together with issues and challenges in realizing efficient rechargeable lithium ion batteries.

Working Mechanism of a Lithium Ion Battery:

A battery stores electrical energy in the form of electrochemical energy, which can be converted back into electrical energy whenever required. It consists of four essential components (i) cathode (e.g. $LiFePO_4$), anode (e.g. nanocarbon based materials such as graphene), electrolyte (e.g. $LiPF_6$) a material allowing ions to travel through while electrically insulating avoiding electrical conduction through it, and a separator, a mesoporous material, allowing ions and also prevents electrical shorting between cathode and anode. All these components with representative materials are shown in Fig 3. The process is similar for other electrode materials. The respective lithium ion positions together with its relative motion are shown in Fig 3 for these charging, Fig 3(a), and discharging, Fig 3(b) states of a lithium ion battery. The insertion of lithium ion in cathode and anode is known as intercalation and mostly these cathode and anode materials are materials allowing easy intercalation rather chemical reaction. The charging and discharging are accompanied by lithium ion intercalation and deintercalation at the electrodesas illustrated below for $LiFePO_4$ cathode and carbon anode electrode materials.

At cathode or positive electrode

$$LiFePO_4 \underset{Discharging}{\overset{Charging}{\rightleftharpoons}} Li_{1-x}FePO_4 + x\,Li^+ + x\,e$$

At anode or negative electrode

$$C + x\,Li^+ + x\,e \underset{Discharging}{\overset{Charging}{\rightleftharpoons}} Li_xC$$

Total process = Sum of processes at cathode and anode

$$LiFePO_4 + C \underset{Discharging}{\overset{Charging}{\rightleftharpoons}} Li_{1-x}FePO_4 + Li_xC$$

The lithium ion forms complexes like LixC with carbon at anode ends during charging, whereas lithium atoms are at respective crystallographic sites in the cathode materials, which are mostly transition metals oxides, in the discharge states, Fig 3. The respective electron and current motions are shown in respective figures through load while discharging and through a voltage source

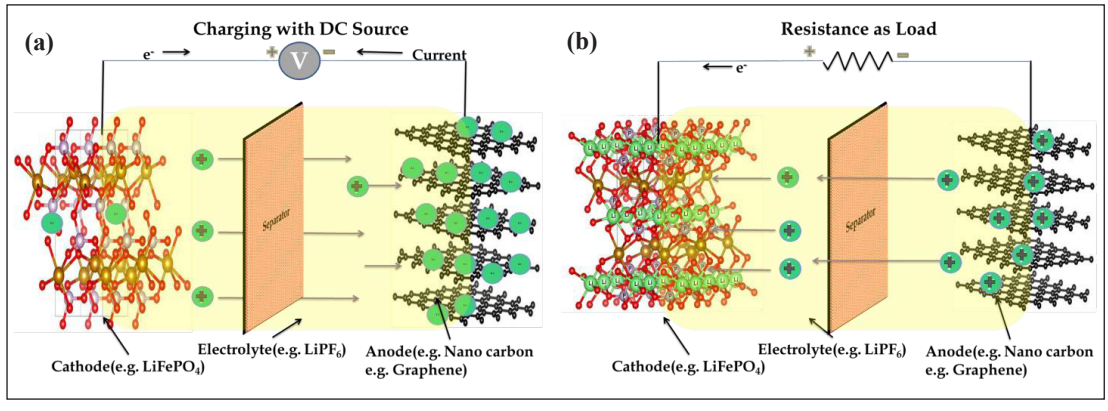

Figure 3: Schematic representation of (a) charging using an external DC source and (b)discharging using an external load for a rechargeable Li-ion battery.

while charging. The lithium chemical potential is lower in cathode than that of anode, which facilitates release of stored electrochemical energy into electrical energy while discharging. The most common electrolyte is $LiPF_6$ based organic liquid and stable upto 4.5 V and at higher voltage i.e. > 4.5 V, it may degrade or decompose into its constituents as well. Further, the operating voltage and energy density or battery capacity are limited by the electronic properties of cathode materials together with efficient ionic i.e. lithium ion transport. Thus, the development of suitable cathode material is very important not only to meet the high energy and power density requirements but also the operational safety.

Configurations of rechargeable lithium ion batteries:

The increasing demand and compulsion towards green energy accelerated the development of rechargeable lithium ion batteries. Initially only smaller electronic systems/machineries were targeted and success can be noticed as lithium ion batteries replaced nearly completely its counterparts such nickel-cadmium and nickel-metal hydride rechargeable batteries. However, lithium ion batteries are still struggling to replace the conventional lead-acid batteries, which are mostly used in power sectors such as electric or hybrid-electric vehicles, power electronic equipment, and power plants. Considering the potential of lithium ion batteries and mitigating this gap, lithium ion batteries are developed in different configurations, as illustrated in Fig 4.

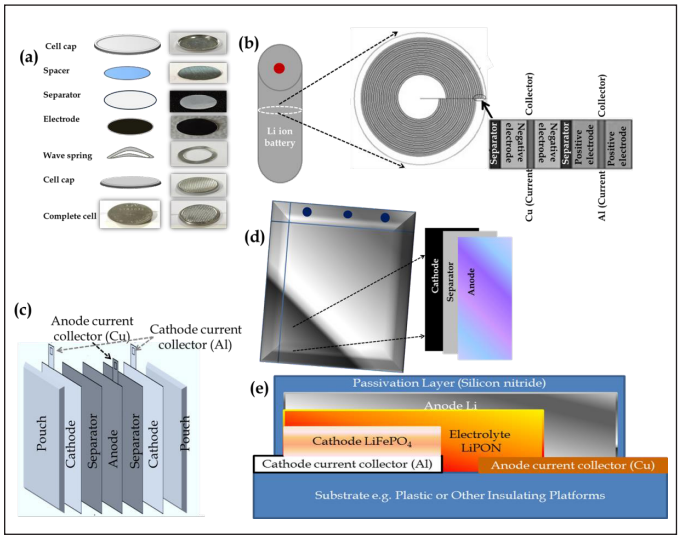

Figure 4: The schematic diagrams for different configurations of lithium ion battery (a) coin or button cell, (b) cylindrical cell, (c) pouch cell, (d) prismatic cell, and (e) thin film cell

The coin or button cell, Fig 4(a), is mostly used in laboratory to characterize the electrochemical performance of electrode materials. Here, each component of coin cell is shown schematically together with corresponding actual photographs from the authors' laboratory. The coin cell is also developed for commercial applications as well; however, it is mostly suitable for low power devices. The cylindrical cell is shown schematically in Fig 4(b)and used for powering devices with higher power requirements. These cells are combined in suitable (series and parallel) combinations to achieve the desired voltage and current. These coin and cylindrical cells use metallic casing and thus increasing overall weight of battery system. In this regard, pouch, Fig 4(c), may provide better solutions, as there is no metallic casing is used like coin cells. .Thus, these cells achieve the highest packing density and thus providing more energy density. The pouch cells are much larger than coin and cylindrical cells and used in various strategic applications such as space and military together with common electric and hybrid electric vehicles. Another similar cell is prismatic cell and shown schematically in Fig 4(d). These cells uses polymer and usually known as lithium-polymer cells. These pouch and prismatic cells may provide high power and very suitable for high current based applications. However, sometimes, swelling issues are noticed with pouch cells. Another interesting configuration is the thin film battery configuration. The geometrical configuration of thin film lithium ion battery is shown in Fig 4(e). This cell may offer a better solution to the present day power needs for miniaturized electronic devices and also probably may be integrated in the chip or devices itself.

Development of cathode materials for lithium ion batteries and their classification:

The importance of lithium ion batteries compels to develop efficient batteries meeting the todays' electrical energy demand in all sectors including low power everyday applications to hybrid electrical vehicles and power plants. That's why there are continuous efforts in developing efficient materials to realize a miniaturized powerful battery together with operational safety. The inception of lithium ion battery in research can be noticed even in late 1950s with preliminary work on LiTMOx (TM = Co, Ni, Mn, Fe and V) and much emphasis was given on materials properties and their electrochemical performance. Further efforts ever made to develop new class of materials, as classified in Table 1.

Table 1: Classification of cathode materials based on different properties and time period for the development of lithium ion batteries

S. No.	Generation	Cathode Materials	Operating Voltage range (V)	Capacity (mAh g^{-1})	Time period
1.	Generation I	Mono Li atom based transition metal (TM) ternary oxides	1.2 – 3.5	≤ 150	1950 - 1985
2.	Generation II	Mono Li atom based TM ternary oxides	3.5 – 4.0	150 – 200	1985 - 2000
3.	Generation III	Higher Li atom based TM ternary and quaternary oxides and oxifluorides	3.5 – 5.0	200 – 330 or more	2001 - 2020
4.	Generation IV	Li-S or Li-Air systems	1.5 - 2.5	>1000	May be up to 2025

The development of new materials led to the enhanced operating voltage and energy density, Table 1, making lithium ion batteries suitable for various applications including electric vehicles and power plants. Further, pristine lithium ion based batteries are showing potential for very high energy density in both large and thin film geometries, Fig 1, however, large safety concerns are yet to address together with various technological issues before using in real applications. The next section will review the various materials developed over period with their salient materials and electronic features, suitable for lithium ion battery applications.

1st Generation materials for rechargeable lithium ion batteries (Since 1950- 1985):

The materials developed up to 1985 are classified as 1st generation cathode materials for rechargeable lithium ion batteries. These materials are summarized in Table 2. The crystallographic structures, their synthesis procedure adopted for fabricating such cathode materials are listed in Table 2 together with battery capacity and remarks, if any, with respective references.

This was the era to explore new potential cathode materials for rechargeable lithium ion batteries; that's

Table 2: 1st Generation cathode materials used in lithium ion batteries (Time period 1950 – 1985)

S. No.	Material	Year	Configuration / structure	Method	Cathode/ Anode	Capacity (mAhg^{-1})	Remark	Refs.
1.	$Li_xCo_{1-x}O$ (x=.5)	1958	Rhombohedral	Solid state	Cathode	Not reported	First Commercial Li-ion battery material	1
2.	$LiMnO_2$	1956	Orthorhombic	Sintering	Cathode	Not reported	One of earliest material	2
3.	$LiNiO_2$	1958	Rhombohedral	Solid State	Cathode	Not reported	None	3
4.	Li_xCoO_2	1980	Hexagonal	Electrochemical extraction	Cathode	4.7 Volt at X=0.1	None	4
5.	$Li_{1-x}MnO_2$	1983	Tetragonal	Lithiation of β-MnO_2	Cathode	Not Reported	None	5
6.	$Li_{1.5}Fe_3O_4$	1982	Cubic	Chemical & electrochemical	Cathode	1.3 Volt	None	6
7.	$Li_{1.7}Fe_2O_3$	1982	Cubic	Chemical & electrochemical	Cathode	1.2 Volt	None	6
8.	$LiMn_2O_4$	1983	Cubic	Solid state	Cathode	Not reported	None	7
9.	$Li_2Mn_2O_4$	1983	Tetragonal	Solid state	Cathode	Not reported	None	7
10.	$LiMn_3O_4$	1983	Tetragonal	Solid state	Cathode	Not reported	None	7
11.	$Li_{1-x}V_2O_4$ (0<x<.34)	1985	Cubic	Solid state	Cathode	Not reported	None	8
12.	$Li_{1.5}V_2O_4$	1985	Cubic	Solid state	Cathode	Not reported	None	8
13.	$Li_2V_2O_4$	1985	Cubic	Solid state	Cathode	Not reported	None	8

why nearly all the transition metals are explored in the periodic table. As an essential condition, a multivalent ion based cathode material is required to compensate the charge during lithium insertion and extraction from the cathode material. The materials should show structural stability during lithium transport during charging/ discharging process to realize large cycling stability. The manganese and vanadium based compounds show structural stability with relatively large specific capacity, which became the material of choice for next generation cathode materials. Most of these materials are transition metal based ternary oxides and mostly the materials and electrochemical properties are evaluated in their bulk forms. This is the reason of observing poor capacity with respect to their theoretical capacity at even much lower operating voltages. The main reason of lower capacity is their insulating nature together with relatively lower ionic conductivity and longer diffusion paths in bulk materials.

2nd Generation materials for rechargeable lithium ion batteries (Since 1986- 2000):

The introduction of transition metal oxides based cathode materials by Professor J. B. Goodenough and his team already showed the potential of lithium ion batteries in 1st generation. However, the limited capacity and lower operating voltages compelled to innovate the modification strategies of 1st generation cathode materials or design and develop new materials for desired electrochemical properties to achieve the optimal performance. The issues with the first generation materials were their poor electrical and ionic conductivity and efforts were put to mitigate these issues in second generation. The doping strategies were adopted to modify the ionic conductivity together with electronic conductivity. The most of ternary oxides from 1st generations are followed in second generation with suitable dopants. The doping of high valent either transition metals or non-transition metals at second cation sites led to enhanced electronic conductivities of these materials. The 2nd generation cathode materials are summarized in Table 2 together with their synthesis process, crystallographic phases, electrochemical capacity together with some noticeable properties as remarks.

Further, in contrast to the bulk materials, nanostructured e.g. nanoparticle, nanotubes, nanorods or two dimensional (2D) sheets like structures are synthesized for these materials and used for electrochemical studies. The reduced dimensions of these materials showed improved

Table 3: 2nd Generation cathode materials used in lithium ion batteries (Time period 1986 – 2000)

S. No.	Material	Year	Configuration / structure	Method	Cathode/ Anode	Capacity ($mAhg^{-1}$)	Remark	Refs.
1.	$Li(Co_{1-x}Li_{x/3}Mn_{2x/3})O_2(x=.0)$ x = 0.1, 0.2, 0.3	1999	Monoclinic	Solid state	Cathode	160$mAhg^{-1}$	Stable	9
2.	$LiCoO_2$, $LiNiO_2$	1990	Hexagonal	Solid state	Cathode	Not reported	None	10
3.	LT-$LiCoO_2$ [Layered] (low temperature)	1993	Trigonal, Cubic	Nitrate method, Carbonate method	Cathode	Not reported	Prepared at low temp.	11
4.	$LiCoO_2$	1996	Cubic	Microwave heating	Cathode	140 $mAhg^{-1}$	Stable and good cyclability	12, 13
5.	$LiCoO_2$	1996	Trigonal	Sol-gel	Cathode	98 $mAhg^{-1}$	None	14
6.	$LiCoO_2$ (Pseudo spinel)	1996	Cubic	Solid state	Cathode	Not reported	None	14
7.	$LiCoO_2$[Layered]	1998	Trigonal	Solid state	Cathode	150$mAhg^{-1}$	None	15
8.	$LiCoO_2$	1998	Hexagonal	Solid state	Cathode	142$mAhg^{-1}$	Stable, good rate capability & good cyclability	16
9.	$LiCoO_2$	1998	Hexagonal, Trigonal	Solid state, Sol-gel	Cathode	145$mAhg^{-1}$ -165$mAhg^{-1}$	None	17, 18, 19
10.	$LiCoO_2$	1999	Hexagonal	Sol-gel	Cathode	120$mAhg^{-1}$	None	20, 21

11.	Corrugated layer $LiFeO_2$	1996	Orthorhombic	Sol-gel	Cathode	110mAhg^{-1}	Synthesized at 90 ^oC	22
12.	Goethite type $LiFeO_2$	1996	Orthorhombic	Sol-gel	Cathode	65mAhg^{-1}	Synthesized at 170 ^oC	22
13.	$Li_3Fe_2(PO_4)_3$	1997	Monoclinic	Solid state	Cathode	105 mAhg^{-1}	None	23
14.	$LiFeP_2O7$	1997	Monoclinic	Solid state	Cathode	65 mAhg^{-1}	None	23
15.	$LiFePO_4$	1997	Hexagonal	Solid state	Cathode	130 mAhg^{-1}	High capacity	23, 24
16.	$LiFePO_4$	1999	Orthorhombic	Solid state	Cathode	125 mAhg^{-1}	None	25
17.	$LiMn_2O_4$	1991	Trigonal	Solid state	Cathode	Not reported	None	26
18.	$LiNiO_2$	1991	Rhombohedral	Solid state	Cathode	Not reported	None	26
19.	$LiCoO_2$	1991	Trigonal	Solid state	Cathode	Not reported	None	26
20.	$LiMn_2O_4$	1996	Cubic	Solid state	Cathode	75mAhg^{-1}	None	27, 28
21.	$LiMnO_2$	1996	Monoclinic	Solid state	Cathode	280mAhg^{-1}	Pure material, High capacity & less fading	29
22.	$LiNiO_2$	1990	Hexagonal	Solid state	Cathode	.009Ahg^{-1}	Long cycle life	30,31
23.	$LiNiO_2$	1995	Hexagonal	Solid state	Cathode	260mAhg^{-1}	High capacity	32
24.	TiO_2 ($LiCoO_2$ as cathode)	1995	Tetragonal	As prepared	Anode	46 mAhg^{-1}	None	33
25.	LiV_2O_4	1986	Trigonal	Solid state	Cathode	Not reported	None	34
26.	$LiVO_2$	1988	Cubic	Solid state	Cathode	Not reported	None	35
27.	Li_2MnO_2	1990	Trigonal, Hexagoanl	Solid state	Cathode	Not reported	Changes in phase by Li insertion	36
28.	LiV_2O_4	1991-99	Cubic	Solid state	Cathode	.117Ahg^{-1}, 135AhKg^{-1}	Initial structure retained after 500 cycle,70% retention after 800 cycle	35, 37, 38, 39, 40

ionic conductivities as it resulted in the reduced diffusion paths for lithium ions in case of nanomaterials with respect to bulk materials. The electronic conductivities of these materials are also improved by designing cathode material as core and graphitic carbon as shell, leading to several orders of magnitude higher electrical conductivity. In addition to the first generation cathode materials, emphasis was also given to the vanadium based ternary oxide materials as potential cathode materials, Table 2, due to their layered structures having large potential for easy intercalation and deintercalation, showing moderated ~ 150 mAh g^{-1} capacity. The structural instability associated with these materials for complete removal of lithium hampered the use of full capacity of these cathode materials. Most interestingly, again from Professor J. B. Goodenough's group, a quaternary oxide $LiFePO_4$ as cathode material was reported during 1997, as a potential candidate in its olivine structure and showed electrochemical capacity, very close to the theoretical limits, 170 mAh g^{-1}, after modifying its electronic and ionic conductivities. Olivine $LiFePO_4$ system among its derivatives with other crystallographic structures is very robust, showing no crystallographic degradation even after complete deintercalation of lithium and showed very high stability. Thus, $LiFePO_4$ can exhibit very large charge/discharge cycles without any capacity fading.

The second generation materials showed guidelines to modify the ionic and electronic properties of cathode materials showing improved performance. However, the power density was still limited not only in terms of energy density but also in terms of operating voltage and current. The operating voltage of 2nd generation materials is limited to 3.5 V, whereas there are some studies showing high current extraction using nanostructured cathode materials in lithium ion batteries.

3rd Generation materials for rechargeable lithium ion batteries (Since 2001- 2020):

The initially developed cathode materials showed their potential in the development of commercial lithium ion batteries, and are widely used today for powering everyday electronics in general together with applications in strategic areas such as space and defence. However, limited energy density and relatively lower operating voltage motivated to explore new cathode materials, which may probably mitigate such issues. In third generation, emphasis was given to develop cathode materials with very high electrochemical capacity (250mAh g^{-1} or more) with good charge/discharge cyclability. These requirements led to the surge in the development of cathode materials, as can be seen in Table 4, listing the developed cathode materials during this period. A large number of cathode materials are reported in table 4, showing relatively higher electrochemical capacities.

Table 4: 3rd Generation cathode materials used in lithium ion batteries (Time period 2001 – 2020)

S. No.	Material	Year	Configuration /structure	Method	Cathode/ Anode	Capacity ($mAhg^{-1}$)	Remark	Refs.
1.	$LiVPO_4OH$	2016	Monoclinic, Triclinic	Hydrothermal	Cathode	280$mAhg^{-1}$	New tavorite type composition	41
3.	$LiVPO_4F$	2003, 2014	Triclinic	Carbothermal reduction	Cathode	116$mAhg^{-1}$	None	42 - 44
4.	$LiVPO_4F$ (Ti doped)	2014	Triclinic	Carbothermal reduction	Cathode	128 $mAhg^{-1}$	None	43,44
5.	$LiVPO_4F$,$LiVPO_4F$ /Ag	2015	Triclinic	Sol-gel	Cathode	102$mAhg^{-1}$ - 117$mAhg^{-1}$	None	45
6.	$LiVPO_4F$/ C,$LiVPO_4F$/C-N	2016, 2019	Triclinic	Sol-gel	Cathode	140$mAhg^{-1}$	None	46, 47
7.	$Li_4Ti_5O_{12}$	2007	Cubic	Sol-gel	Anode	170$mAhg^{-1}$	None	48
8.	$Li[Cr_xLi_{(1-x)}Mn_{2(1-x)}]O_2$	2007	Hexagonal	Sol-gel	Cathode	195 $mAhg^{-1}$	Stable cycling performance at x=.290	49
9.	$LiVPO_4F$, $LiY_xV_{(1-x)}$ PO4F(x=0.04)	2009	Triclinic	Carbothermal reduction	Cathode	119 $mAhg^{-1}$ - 134 $mAhg^{-1}$	Stable cyclic performance	50
10.	$LiVPO_4F$	2010	Triclinic	Sol-gel	Cathode	134 $mAhg^{-1}$	None	51
11.	$Li_4Ti_5O_{12}Li_4Ti_5O_{12}$/ Sn	2011	Cubic	Solid-state	Anode	165 – 321 $mAhg^{-1}$	None	52
12.	$LiVPO_4F$/grphene	2017	Triclinic	Ionothermal process	Cathode	129 - 153$mAhg^{-1}$	Good cycling stability and good discharge efficiency	53
13.	$LiVPO_4F/C$	2018	Triclinic	Sol-gel	Cathode	135.3$mAhg^{-1}$	Stability in cyclability	54
14.	$LiVPO_4F/C$	2018	Triclinic	Sol-gel	Cathode	140$mAhg^{-1}$	None	55
15.	LiV_2O_4	2004	Cubic	Solid state	Cathode	Not reported	None	56
16.	$LiNi_{0.5}Co_{0.2}Mn_{0.3}O_2$, LiV_2O_4 coated $LiNi_{0.5}Co_{0.2}Mn_{0.3}O_2$	2019	Hexagonal	Solid-state	Cathode	145 - 164$mAhg^{-1}$	None	57
17.	$LiNi_{1-x}Sb_xO_2$(x=0, 0.1, 0.15, 0.2)	2011	Hexagonal	Solid-state	Cathode	105 -117$mAhg^{-1}$	Structure stability and good cyclability	58
18.	$LiMnPO_4/C$	2011	Orthorhombic	Spray pyrolysis	Cathode	149 $mAhg^{-1}$	None	59

19.	$Li[Li_{0.2}Mn_{0.54}Ni_{0.13}Co_{0.13}]O_2$	2011	Trigonal	Co-precipitation	Cathode	250 - 268 $mAhg^{-1}$	None	60
20.	$Li_{1.2}Mn_{.56}Ni_{.16}Co_{.08}O_2$	2014	Monoclinic & Rhombohedral	Solid-state	Cathode	245 $mAhg^{-1}$	Good cyclability	61
21.	$Li[Li_{0.2}Mn_{0.54}Ni_{0.13}Co_{0.13}]O_2$ (nanoplate)	2016	Hexagonal	Co-precipitation	Cathode	307.9 $mAhg^{-1}$	Excellent cyclability	62
22.	$Li_{1.1}Ni_{35}Mn_{65}O_2$	2017	Hexagonal	Solid-state	Cathode	210 $mAhg^{-1}$	None	63
23.	$Li_{1.2}Mn_{.6}Ni_{.2}O_2$-SG	2018	Hexagonal	Sol-gel	Cathode	230.38 $mAhg^{-1}$	None	64
24.	$Li_{1.17}Mn_{0.56}Ni_{0.14}Co_{0.13}O_2$ (PEG2000-LMNCO)	2015	Hexagonal	Sol-gel	Cathode	228 $mAhg^{-1}$	None	65
25.	$LiCoO_2$($Li_4Ti_5O_{12}$ coated)	2007	Hexagonal	Sol-gel	Cathode	179 $mAhg^{-1}$	None	66
26.	$Li_4Ti_5O_{12}$	2008	Cubic	Solid-state	Cathode	170 $mAhg^{-1}$	None	67
27.	$Li_4Ti_5O_{12}/B_0$-C, $Li_4Ti_5O_{12}/B_{0.1}$-C, $Li_4Ti_5O_{12}/B_{0.3}$-C,$Li_4Ti_5O_{12}/B_{0.5}$-C	2016	Cubic	Solid-state	Cathode	154 $mAhg^{-1}$	Good cyclability	68
28.	$LiCoO_2$(Pristine and Al_2O_3 doped)	2017	Hexagonal	Solid-state	Cathode	195 – 202 $mAhg^{-1}$	None	69
29.	$LiCoPO_4$	2010	Orthorhombic	Solid-state Rheological phase method	Cathode	30.9-71.5 $mAhg^{-1}$	None	70
30.	Li_2MnSiO_4 /Pure& carbon coated	2012	Orthorhombic	Sol-gel	Cathode	81 – 144 $mAhg^{-1}$	None	71
31.	$Li_2Mn_{.80}Fe_{.20}SiO_4$ (SiO_2 size 5nm)	2013	Orthorhombic	Hydrothermal	Cathode	95.6 – 129.4 $mAhg^{-1}$	None	72
32.	Li_2MnSiO_4 /C, $Li_2Mn_{.96}Ca_{.04}SiO_4$ /C	2018	Orthorhombic	Solvothermal	Cathode	141.1 $mAhg^{-1}$	None	73
33.	Li_2MnSiO_4 / C$Li_2MnSi_{.75}V_{.25}O_4$ /C	2016	Orthorhombic	Sol-gel	Cathode	60 – 130 $mAhg^{-1}$	None	74
34.	B-Li_2MnSiO_4(Bulk & porous LMS)	2015	Orthorhombic	Hydrothermal	Cathode	120 - 217$mAhg^{-1}$	None	75
35.	Li_2MnSiO_4/C (20AM+3KB+3TAB) AM-Active Material KB-Ketjen Black TAB-Teflonized Acetylene Black	2011	Orthorhombic	Solid State	Cathode	79 – 160 $mAhg^{-1}$	Good cyclability	76
36.	Li_2MnSiO_4 Powder	2012	Orthorhombic	Sol-gel	Cathode	206 - 295 $mAhg^{-1}$	Good cyclability	77
37.	$Li_2MnSiO_4$and derivative systems	2013	Orthorhombic	Hydrothermal	Cathode	185 $mAhg^{-1}$	None	78
38.	Li_2MnSiO_4/C and derivative systems	2016	Orthorhombic	Hydrothermal	Cathode	135 $mAhg^{-1}$	None	79
39.	Li_2MnSiO_4& Mg, Al, Ga doped sample	2013	Orthorhombic	Sol-gel	Cathode	101 – 147 $mAhg^{-1}$	None	80

40.	Li_2MnSiO_4/C nano Composites	2010	Monoclinic	Microwave-solvothermal	Cathode	215 $mAhg^{-1}$	None	81
41.	Li_2MnSiO_4 ($Pmn2_1$)	2011	Orthorhombic	Sol-gel	Cathode	100 $mAhg^{-1}$	None	82
42.	Li_2MnSiO_4 as Cathode	2016	Orthorhombic	Sol-gel	Cathode	405 $mAhg^{-1}$	None	83
43.	Li_2MnSiO_4 as Anode	2016	Orthorhombic	Sol-gel	Cathode	658 $mAhg^{-1}$	High energy density and good cyclability	83
4.	Li_2MnSiO_4 (.5 hwr ball milled)	2007	Orthorhombic	Sol-gel	Cathode	142 $mAhg^{-1}$	None	84
45.	$Li_2MnSiO_{3.97}F_{0.03}$ (X=0.03)	2018	Orthorhombic	Solid-state	Cathode	279 $mAhg^{-1}$	Stable energy density	85
46.	Li_2MnSiO_4(at 55° C)	2014	Orthorhombic	Sol-gel	Cathode	225 $mAhg^{-1}$	None	86
47.	Li_2MnSiO_4(at 700° C)	2014	Orthorhombic	Molten salt	Cathode	165 $mAhg^{-1}$	Good cyclability	87
48.	Li_2MnSiO_4/C	2016	Orthorhombic	Sonochemic-al reaction	Cathode	261 $mAhg^{-1}$	None	88
49.	Li_2MnSiO_4/ C(Carbon wt% 2.1)	2013	Orthorhombic	Sol-gel	Cathode	145 $mAhg^{-1}$	None	89
50.	Li_2MnSiO_4-Pristine	2016	Orthorhombic	Sol-gel	Cathode	203 $mAhg^{-1}$	None	90
51.	Li_2FeSiO_4	2013	Monoclinic	Sol-gel	Cathode	180 $mAhg^{-1}$	Stable structure and good cyclability	91
52.	$Li_2Mn_{0.94}Mo_{.06}SiO_4$	2015	Orthorhombic	Sol-gel	Cathode	207.3 $mAhg^{-1}$	None	92
53.	Amorphous type $Li_2Mn_{0.85}Ti_{0.15}SiO_4$/ C(S-LMST)	2018	Orthorhombic	Hydrothermal	Cathode	185 $mAhg^{-1}$	None	93
54.	$Li_2Mn_{.9}Ti_{0.1}SiO4$	2015	Orthorhombic	Sol-gel	Cathode	211 $mAhg^{-1}$	None	94
55.	Li_2MnSiO_4/C with Ni doping	2014	Orthorhombic	Solvothermal	Cathode	274.5 $mAhg^{-1}$	High energy density	95
56.	$Li_2Mn_8Fe_2SiO_4$	2015	Orthorhombic	Sol-gel	Cathode	122 $mAhg^{-1}$	None	96
57.	$Li_2Mn_9Cu_1SiO_4$	2015	Orthorhombic	Sol-gel	Cathode	206 $mAhg^{-1}$	None	97
58.	CNT@Li_2MnSiO_4@C	2018	Orthorhombic	Sol-gel	Cathode	227 $mAhg^{-1}$	None	98
58.	MP-Li_2MnSiO_4@C (MP- mesoporous morpholosy)	2018	Orthorhombic	*In situ* Template method based on non ionic surfactant F127	Cathode	164 $mAhg^{-1}$	Good cyclability	99
59.	$Li_2Mn_{.99}La_{.01}SiO_4$	2015	Orthorhombic	Hydrothermal	Cathode	257$mAhg^{-1}$ (at.05C)	None	100
60.	$Li_2Mn_{.925}Cr_{.075}SiO_4$	2018	Orthorhombic	Solid-State	Cathode	200 $mAhg^{-1}$	None	101
61.	Li_2(Mn/Fe)SiO4	2007	Orthorhombic	Sol-gel	Cathode	125 $mAhg^{-1}$	None	102
62.	$Li_{1.95}Mn_{.95}Cr_{.05}SiO_4$	2014	Orthorhombic	Sol-gel	Cathode	238 $mAhg^{-1}$	High energy density	103
63.	$Li_{2.05}Mn_{.95}Al_{.05}SiO_4$	2014	Orthorhombic	Sol-gel	Cathode	220 $mAhg^{-1}$	High energy density	103
64.	Li_2MnSiO_4/NC-2	2019	Orthorhombic	Sol-gel	Cathode	276.88 $mAhg^{-1}$	High energy density & good cyclability	104

65.	$Li_2MnSiO_4Li_2FeSiO_4$	2012	Orthorhombic	A rapid one-pot supercritical fluid reaction	Cathode	350 - 320 $mAhg^{-1}$	High energy density and excellent cyclability	105
66.	Annealed Li_2MnSiO_4 (A-LMS)	2012	Orthorhombic	Hydrothermal	Cathode	226 $mAhg^{-1}$	High energy density	106
67.	Li_2MnSiO_4/C-2 (Prepa-red in $(BMIM)BF_4$)	2014	Orthorhombic	Ionothermal	Cathode	218 $mAhg^{-1}$	Good cyclability	107
68.	Li_2MnSiO_4/CNFs	2015	Orthorhombic	Solvothermal	Cathode	350 $mAhg^{-1}$	High energy density & good cyclability	108
69.	$Li/Li_{1.8}MnSi_{0.8}P_{0.2}O_4$	2014	Orthorhombic	Sol-gel	Cathode	155 $mAhg^{-1}$	None	109
70.	Li_2MnSiO_4/C	2014	Orthorhombic	Sol-gel	Cathode	256.86 $mAhg^{-1}$	None	110
71.	$Li_2Mg_{.1}Mn_{.9}SiO_4$/C	2011	Orthorhombic	Sol-gel	Cathode	289 $mAhg^{-1}$	High energy density & low energy density	111
72.	Li_2MnSiO_4	2011 on-wards	Orthorhombic	Solid-State, sol-gel, hydrothermal	Cathode	< 100– 268 $mAhg^{-1}$	poor retention, and unclear cyclic stability	112-126

The 3rd generation materials are also transition metal quaternary oxides and oxyfluorides, Table 4. The vanadium based $LiVPO_4$ and its derivatives showed relatively higher capacities (> 250 mAh g^{-1}). Further, to increase electrochemical storage capacity, emphasis was given to develop materials with higher lithium content with respect to mono-lithium based cathode materials. The theoretical capacity of higher lithium content such as Li_2TMSiO_4 (TM = transition metal e.g. Fe, Co, Ni, Mn, V etc) is around 333 mAh g^{-1}, nearly twice to that of mono-lithium based cathode materials. Further, their large band gap may lead to higher operating voltage as well. These materials are relatively new cathode materials and explorations are still going on. The initial studies showed high electrochemical capacity for such compounds, which starts fading after first complete charge/discharge cycles and showed reduction to very low 50-60 mAh g^{-1} in 10 – 20 charge/discharge cycles. This is attributed to the structural instability of Li_2TMSiO_4 cathode materials. The initial structure is subjected to Jahn-Teller (J-T) distortion during charging/discharging and may lead to permanent crystallographic changes at local levels, causing poor cyclability. However, further studies are needed to understand this degradation mechanism and strategies need to be evolved to overcome this aspect. The nanostructuring and even localized strain by doping may provide some understanding towards mitigating the capacity fading in these cathode materials, which seems to potential candidate for high energy density cathode materials.

4thGeneration materials for rechargeable lithium ion batteries (2020 onwards):

The current developments (up to 3rd generations) in rechargeable are widely suitable and used for low power applications in our everyday life and mostly limited with their specific current density up to 150 – 200 mAh g-1. The scaling of these batteries is realized in terms of large battery packs for specific purposes including electric and hybrid- electric vehicles. The power hungry applications such as electric and hybrid electric vehicles, planes, and other commuting means toward green energy initiatives may need very high energy density (> 1000 mAh g^{-1} or more).

The problem of limited specific capacity can be taken care by innovating new materials and battery designs which can show very high capacity i.e. > 1000 mAh g-1. For example metal air batteries are showing promise to beat the current specific capacity limitations, a hurdle in the present lithium ion batteries. The lithium- air and also lithium – sulfur batteries have shown promise with very high specific energy densities. However, the research and development of such batteries are still in nascent stages and various issues such as safety because of the use of pure lithium, which is highly flammable and cyclability need to address carefully.

Hunt for new lithium ion battery cathode materials and design criteria:

The performance of a lithium battery depends on operating voltage and current, energy density, cyclability, stability, and most importantly safety. The electronic properties of cathode materials such as band gap and relative electronic state positions affect the operating voltage of a lithium ion battery. The relative positions of electronic states in terms of electrochemical potential of respective electrodes are shown in Fig 5 for a lithium ion battery. The electrolyte is a good ionic conductor but electrically insulator, with a large band gap E_g expressed as the difference between the lowest unoccupied molecular orbital (LUMO or also known as conduction band) and the highest occupied molecular orbital (HOMO or valence band), as shown schematically in Fig 5. This band gap of electrolyte is also known as the maximum allowed voltage window as above or below these energy levels, the electrolyte will start dissociating.

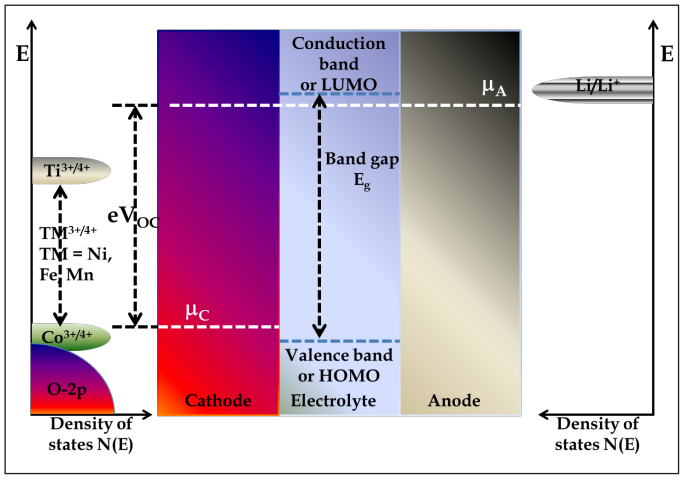

Figure 5: The schematic diagram of electronic states in terms of chemical potential positions of cathode, anode together with band gap of electrolyte. The left most figure shows the relative position of different transition metal elements with respect to oxygen 2p states in transition metal oxides. The right most figure shows the Fermi energy of lithium metal.

Further, the relative chemical potential of cathode and anode are shown with respect to electrolyte HOMO and LUMO positions, suggesting that the open circuit voltage $eV_{OC} = \mu_A - \mu_C$, where e is electronic charge (=1.6x10^{-19} C), V_{OC} is open circuit voltage, μ_A and μ_C are chemical potential of anode and cathode materials, respectively. Thus, the cathode material should be selected in such a way that it's chemical potential i.e. μ_C is located above the valence band (i.e. HOMO) of electrolyte, else the electrolyte will oxidize at the cathode-electrolyte interface, leading to a thin film formation at solid-electrolyte interface and is commonly known as SEI film. On the other hand, the chemical potential of anode i.e. μ_A is located below the conduction band (i.e. LUMO) of the electrolyte, else electrolyte will reduce at the anode-electrolyte interface, causing SEI formation at this interface.Thus, the selection of cathode and anode is limited by the electrochemical window i.e. band gap and relative position of HOMO and LUMO of electrolyte. However, there are continuous efforts to increase the operating voltage of lithium ion batteries and either existing materials are engineered or new materials are being developed to meet the requirements of higher operating voltages together with enhanced electrochemical energy storage capacity. Numerous materials are investigated, as listed in Table 4, where high lithium content materials have shown promise with respect to mono-lithium based cathode materials. However, there are various technological issues and challenges such as their capacity fading in few cycles. Thus, efforts are required to address the capacity fading in high lithium based cathode materials to increase the electrochemical energy density. However, there is a need to develop not only cathode materials with higher operating voltage and enhanced energy density but also compatible electrolyte simultaneously.

Conclusion:

This review addresses the development of cathode materials for rechargeable lithium ion batteries. Large efforts are put to realize the commercial lithium ion batteries, however, there are still issues and challenges to make it more suitable for large scale power applications such as power plants, hybrid electric vehicles. The three generations of cathode materials are discussed covering from its inception to the current state of materials. The large emphasis is given to enhance the electrochemical energy storage density and operating voltage of lithium ion batteries to meet the future demands in all sectors. The associated crystallographic instability in Li_2TMSiO_4 based cathode materials is hampering the full potential of these cathode materials. Further, various layered, spinel, and olivine structured materials are widely explored and also shown potential for future energy needs. However, the success of high voltage and high electrochemical energy density based cathode materials will rely on simultaneous development of suitable electrolytes.

Acknowledgement:

Author acknowledges Mr. Kuldeep Kaswan for his assistance in compiling cathode materials and also funding agency Department of Science and Technology (DST), Government of India (project no. INT/RUS/RFBR/320).

References:

1. Johnston, W. D., R. R. Heikes, and D. Sestrich. "The preparation, crystallography, and magnetic properties of the LixCo (1− x) O system." *Journal of Physics and Chemistry of Solids* 7.1 (1958): 1-13.
2. Johnston, W. D., and R. R. Heikes. "A Study of the LixMn (1-x) O System1." *Journal of the American Chemical Society* 78.14 (1956): 3255-3260.
3. Goodenough, J. B., D. G. Wickham, and W. J. Croft. "Some Ferrimagnetic Properties of the System Li x Ni1− x O." *Journal of Applied Physics* 29.3 (1958): 382-383.
4. Mizushima, K., et al. "LixCoO2 (0< x<-1): A new cathode material for batteries of high energy density." *Materials Research Bulletin* 15.6 (1980): 783-789.
5. David, W. I. F., et al. "Lithium insertion into β□ MnO2 and the rutile-spinel transformation." *Materials research bulletin* 19.1 (1984): 99-106.
6. Thackeray, M. M., W. I. F. David, and John B. Goodenough. "Structural characterization of the lithiated iron oxides LixFe3O4 and LixFe2O3 (0< x< 2)." *Materials Research Bulletin* 17.6 (1982): 785-793.
7. Thackeray, M. M., et al. "Lithium insertion into manganese spinels." *Materials Research Bulletin* 18.4 (1983): 461-472.
8. De Picciotto, L. A., and M. M. Thackeray. "Insertion/extraction reactions of lithium with LiV2O4." *Materials research bulletin* 20.12 (1985): 1409-1420.
9. Numata, Koichi, Chie Sakaki, and Shoji Yamanaka. "Synthesis and characterization of layer structured solid solutions in the system of LiCoO2–Li2MnO3." *Solid State Ionics* 117.3-4 (1999): 257-263.
10. Kemp, J. P., and P. A. Cox. "Electronic structure of LiCoO2 and related materials; photoemission studies." *Journal of Physics: Condensed Matter* 2.48 (1990): 9653.
11. Rossen, E., J. N. Reimers, and J. R. Dahn. "Synthesis and electrochemistry of spinel LT□ LiCoO2." *Solid State Ionics* 62.1-2 (1993): 53-60.
12. Yan, Hongwei, et al. "Microwave synthesis of LiCoO2 cathode materials." *Journal of power sources* 68.2 (1997): 530-532.
13. Sun, Yang-Kook, In-Hwan Oh, and Seong-Ahn Hong. "Synthesis of ultrafine LiCoO 2 powders by the sol-gel method." *Journal of materials science* 31.14 (1996): 3617-3621.
14. Zhecheva, E., et al. "Lithium− cobalt citrate precursors in the preparation of intercalation electrode materials." *Chemistry of materials* 8.7 (1996): 1429-1440.
15. Kim, J., P. Fulmer, and ArumugamManthiram. "Synthesis of LiCoO2 cathodes by an oxidation reaction in solution and their electrochemical properties." *Materials research bulletin* 34.4 (1999): 571-579.
16. Huang, B., et al. "Electrochemical evaluation of LiCoO2 synthesized by decomposition and intercalation of hydroxides for lithium-ion battery applications." *Journal of applied electrochemistry* 28.12 (1998): 1365-1369.
17. Chiang, Yet-Ming, et al. "Synthesis of LiCoO2 by decomposition and intercalation of hydroxides." *Journal of the Electrochemical Society* 145.3 (1998): 887-891.
18. Kumta, P. N., et al. "Synthesis of LiCoO2 powders for lithium-ion batteries from precursors derived by rotary evaporation." *Journal of power sources* 72.1 (1998): 91-98.
19. Peng, Z. S., C. R. Wan, and C. Y. Jiang. "Synthesis by sol–gel process and characterization of LiCoO2 cathode materials." *Journal of Power Sources* 72.2 (1998): 215-220.
20. Yoon, Won-Sub, and Kwang-Bum Kim. "Synthesis of LiCoO2 using acrylic acid and its electrochemical properties for Li secondary batteries." *Journal of Power Sources* 81 (1999): 517-523.
21. Nakamura, T., and A. Kajiyama. "Synthesis of LiCoO2 particles with uniform size distribution using hydrothermally precipitated Co3O4 fine particles." *Solid State Ionics* 123.1-4 (1999): 95-101.
22. Sakurai, Yoji, et al. "Low temperature synthesis and electrochemical characteristics of LiFeO2 cathodes." *Journal of power sources* 68.2 (1997): 711-715.
23. Padhi, A. K., et al. "Effect of structure on the Fe3+/Fe2+ redox couple in iron phosphates." *Journal of the Electrochemical Society* 144.5 (1997): 1609-1613.
24. Padhi, Akshaya K., Kirakodu S. Nanjundaswamy, and John B. Goodenough. "Phospho-olivines as positive-electrode materials for rechargeable lithium batteries." *Journal of the electrochemical society* 144.4 (1997): 1188-1194.
25. Andersson, Anna S., et al. "Thermal Stability of LiFePO4-Based Cathodes." *Electrochemical and Solid-State Letters* 3.2 (2000): 66-68.
26. Barboux, P., J. M. Tarascon, and F. K. Shokoohi. "The use of acetates as precursors for the low-temperature synthesis of LiMn2O4 and LiCoO2 intercalation compounds." *Journal of Solid State Chemistry* 94.1 (1991): 185-196.
27. Tsang, C., and A. Manthiram. "A new route for the synthesis of LiMn2O4 cathode: variation of composition, microstructure, and electrochemical behavior with synthesis temperature." *Solid State Ionics* 89.3-4 (1996): 305-312.
28. Hasegawa, Akira, KazunariYoshizawa, and TokioYamabe. "Crystal Orbital Overlap Population Analysis of the Capacity Fading of Metal-Substituted Spinel Lithium Manganate LiMn2 O 4." *Journal of the Electrochemical Society* 147.11 (2000): 4052-4057.
29. Armstrong, A. Robert, and Peter G. Bruce. "Synthesis of layered LiMnO 2 as an electrode for rechargeable lithium batteries." *Nature* 381.6582 (1996): 499-500.
30. Dahn, J. R., et al. "Rechargeable LiNiO2/carbon cells." *Journal of the Electrochemical Society* 138.8 (1991): 2207-2211.
31. Dahn, J. R., Ulrich von Sacken, and C. A. Michal. "Structure and electrochemistry of Li1±yNiO2 and a new Li2NiO2 phase with the Ni (OH) 2 structure." *Solid State Ionics* 44.1-2 (1990): 87-97.
32. Arai, H., et al. "Characterization and cathode performance of Li1− xNi1+ xO2 prepared with the excess lithium method." *Solid State Ionics* 80.3-4 (1995): 261-269.
33. Huang, S. Y., et al. "Rocking chair lithium battery based on nanocrystalline TiO2 (anatase)." *Journal of the Electrochemical Society* 142.9 (1995): L142-L144.
34. De Picciotto, L. A., and M. M. Thackeray. "Lithium insertion/extraction reactions with LiVO2 and LiV2O4." *Solid State Ionics* 18 (1986): 773-777.

35. De Picciotto, L. A., M. M. Thackeray, and G. Pistoia. "An electrochemical study of the systems Li1±xV2O4 and Li1−xVO2 (0□ x□ 1)." *Solid State Ionics* 28 (1988): 1364-1370.
36. Zachau-Christiansen, B., et al. "Lithium insertion in oxide spinels." *Solid State Ionics* 40 (1990): 580-584.
37. Pistoia, G., et al. "Further electrochemical studies on Li/LiV2O4 secondary cells." *Journal of power sources* 34.3 (1991): 199-206.
38. LI, Guohua, et al. "Synthesis and characterization of LiV2O4 as the cathode in secondary lithium batteries." *Denki Kagaku oyobi Kogyo Butsuri Kagaku* 64.3 (1996): 202-206.
39. Faran, O., and V. Volterra. "Metal-insulator transition in the LiV2O4− δ spinel system." *Solid state communications* 101.11 (1997): 861-864.
40. Kondo, S., D. C. Johnston, and L. L. Miller. "Synthesis, characterization, and magnetic susceptibility of the heavy-fermion transition-metal oxide LiV 2 O 4." *Physical Review B* 59.4 (1999): 2609.
41. Boivin, Edouard, et al. "Structural and electrochemical studies of a new Tavorite composition: LiVPO 4 OH." *Journal of Materials Chemistry A* 4.28 (2016): 11030-11045.
42. Barker, J., M. Y. Saidi, and J. L. Swoyer. "Electrochemical insertion properties of the novel lithium vanadium fluorophosphate, LiVPO4 F." *Journal of the Electrochemical Society* 150.10 (2003): A1394-A1398.
43. Ellis, Brian L., et al. "Structure and electrochemistry of two-electron redox couples in lithium metal fluorophosphates based on the tavorite structure." *Chemistry of Materials* 23.23 (2011): 5138-5148.
44. Sun, Xiaofei, et al. "Titanium doped LiVPO4F cathode for lithium ion batteries." *Solid State Ionics* 268 (2014): 236-241.
45. Yang, Bo, and Lin Yang. "Silver-coated LiVPO4F composite with improved electrochemical performance as cathode material for lithium-ion batteries." *Journal of Physics and Chemistry of Solids* 87 (2015): 228-232.
46. Yu, Zhihao, and Linhua Jiang. "Design and facile synthesis of nitrogen-doped carbon decorated LiVPO4F nanocrystals as superior cathode for lithium-ion batteries." *Solid State Ionics* 291 (2016): 20-25.
47. DOI: 10.5185/amlett.2019.2141
48. Hao, Yan-Jing, et al. "Influence of various complex agents on electrochemical property of Li4Ti5O12 anode material." *Journal of alloys and compounds* 439.1-2 (2007): 330-336.
49. Park, C. W., et al. "Synthesis and materials characterization of Li2MnO3–LiCrO2 system nanocomposite electrode materials." *Materials research bulletin* 42.7 (2007): 1374-1383.
50. Zhong, Shengkui, et al. "Preparation and electrochemical studies of Y-doped LiVPO 4 F cathode materials for lithium-ion batteries." *Journal of Wuhan University of Technology-Mater. Sci. Ed.* 24.4 (2009): 552-556.
51. Zhong, Sheng-Kui, et al. "Synthesis of LiVPO4F with high electrochemical performance by sol-gel route." *Transactions of Nonferrous Metals Society of China* 20 (2010): s275-s278.
52. Sivashanmugam, Arumugam, et al. "Novel Li4Ti5O12/Sn nano-composites as anode material for lithium ion batteries." *Materials Research Bulletin* 46.4 (2011): 492-500.
53. Rangaswamy, Puttaswamy, et al. "Enhanced electrochemical performance of LiVPO 4 F/f-graphene composite electrode prepared via ionothermal process." *Journal of Applied Electrochemistry* 47.1 (2017): 1-12.
54. Li, Qiyuan, et al. "Chemical reaction characteristics, structural transformation and electrochemical performances of new cathode LiVPO 4 F/C synthesized by a novel one-step method for lithium ion batteries." *RSC advances* 8.13 (2018): 7044-7054.
55. Zeng, Taotao, et al. "Effect of Environmental Temperature on the Content of Impurity Li3V2 (PO4) 3/C in LiVPO4F/C Cathode for Lithium-ion Batteries." *Frontiers in Chemistry* 6 (2018).
56. Krimmel, Alexander, et al. "Anomalous structural behaviour of Zn-doped LiV2O4." *Physica B: Condensed Matter* 350.1-3 (2004): E297-E299.
57. Lu, Yao, et al. "Ultrathin LiV2O4 Layers Modified LiNi0. 5Co0. 2Mn0. 3O2 Single-Crystal Cathodes with Enhanced Activity and Stability." *Advanced Materials Interfaces* (2019).
58. Cui, Ping, et al. "Preparation and characteristics of Sb-doped LiNiO2 cathode materials for Li-ion batteries." *Journal of Physics and Chemistry of Solids* 72.7 (2011): 899-903.
59. Bakenov, Zhumabay, and Izumi Taniguchi. "LiMnPO4 olivine as a cathode for lithium batteries." (2011).
60. Zheng, J. M., X. B. Wu, and Yong Yang. "A comparison of preparation method on the electrochemical performance of cathode material Li [Li0. 2Mn0. 54Ni0. 13Co0. 13] O2 for lithium ion battery." *ElectrochimicaActa* 56.8 (2011): 3071-3078.
61. Nayak, Prasant Kumar, et al. "Electrochemical and structural characterization of carbon coated Li1. 2Mn0. 56Ni0. 16Co0. 08O2 and Li1. 2Mn0. 6Ni0. 2O2 as cathode materials for Li-ion batteries." *ElectrochimicaActa* 137 (2014): 546-556.
62. Dai, Dongmei, et al. "Simultaneously improved capacity and initial coulombic efficiency of Li-rich cathode Li [Li0. 2Mn0. 54Co0. 13Ni0. 13] O2 by enlarging crystal cell from a nanoplate precursor." *Journal of Power Sources* 307 (2016): 665-672.
63. Zhou, Chun-xian, et al. "Cyclic performance of Li-rich layered material Li1. 1Ni0. 35Mn0. 65O2 synthesized through a two-step calcination method." *ElectrochimicaActa* 252 (2017): 286-294.
64. Yang, Puheng, et al. "Structure tuned Li1. 2Mn0. 6Ni0. 2O2 with low cation mixing and Ni segregation as high performance cathode materials for Li-ion batteries." *ElectrochimicaActa* 271 (2018): 276-283.
65. Chen, Min, et al. "Polyethylene glycol-assisted synthesis of hierarchically porous layered lithium-rich oxide as cathode of lithium ion battery." *Journal of Power Sources* 279 (2015): 197-204.
66. Fey, George Ting-Kuo, et al. "Improved electrochemical performance of LiCoO2 surface treated with Li4Ti5O12." *Journal of Power Sources* 174.2 (2007): 1147-1151.
67. Ge, Hao, et al. "Electrochemical characteristics of spinel Li4Ti5O12 discharged to 0.01 V." *Electrochemistry communications* 10.5 (2008): 719-722.

68. Su, Xiuli, et al. "Synthesis and electrochemical performance of nano-sized Li4Ti5O12 coated with boron-doped carbon." *ElectrochimicaActa* 196 (2016): 300-308.
69. Sheng, Suojiang, et al. "Al2O3-surface modification of LiCoO2 cathode with improved cyclic performance." *Journal of Electroanalytical Chemistry* 795 (2017): 59-67.
70. Tan, Long, et al. "Synthesis of novel high-voltage cathode material LiCoPO4 via rheological phase method." *Journal of Alloys and Compounds* 502.2 (2010): 407-410.
71. Deng, C., et al. "Synthesis and improved properties of nanostructured Li2MnSiO4/C via a modified sol–gel method." *Int J ElectrochemSci* 7 (2012): 4559-4566.
72. Xiao, Dichang, et al. "Hydrothermal preparation of iron-based orthosilicate cathode materials with different SiO2 particles and their electrochemical properties." *J ElectrochemSci* 8 (2013): 7581-7590.
73. Feng, Yiming, et al. "Understanding the improved kinetics and cyclability of a Li2MnSiO4 cathode with calcium substitution." *Inorganic chemistry* 57.6 (2018): 3223-3231.
74. Wagner, Nils P., et al. "Vanadium Substitution in Li2MnSiO4/C as Positive Electrode for Li Ion Batteries." *The Journal of Physical Chemistry C* 120.21 (2016): 11359-11371.
75. Xie, Man, et al. "Template-assisted hydrothermal synthesis of Li2MnSiO4 as a cathode material for lithium ion batteries." *ACS applied materials & interfaces* 7.20 (2015): 10779-10784.
76. Aravindan, Vanchiappan, et al. "Influence of carbon towards improved lithium storage properties of Li 2 MnSiO 4 cathodes." *Journal of Materials Chemistry* 21.8 (2011): 2470-2475.
77. Zhang, Shu, et al. "Cr-doped Li 2 MnSiO 4/carbon composite nanofibers as high-energy cathodes for Li-ion batteries." *Journal of Materials Chemistry* 22.29 (2012): 14661-14666.
78. Hu, Zhe, et al. "Li 2 MnSiO 4@ C nanocomposite as a high-capacity cathode material for Li-ion batteries." *Journal of Materials Chemistry A* 1.40 (2013): 12650-12656.
79. Deng, Hui, et al. "Effect of Ni substitution on structural stability, micromorphology, and electrochemical performance of Li 2 MnSiO 4/C cathode materials." *RSC Advances* 6.112 (2016): 111539-111548.
80. Choi, Sungho, et al. "Controlled shape with enhanced electrochemical performance of various ions doped Li2MnSiO4 cathode nanoparticles." *Materials Letters* 105 (2013): 113-116.
81. Muraliganth, T., K. R. Stroukoff, and ArumugamManthiram. "Microwave-solvothermal synthesis of nanostructured Li2MSiO4/C (M= Mn and Fe) cathodes for lithium-ion batteries." *Chemistry of Materials* 22.20 (2010): 5754-5761.
82. Duncan, Hugues, et al. "Novel Pn polymorph for Li2MnSiO4 and its electrochemical activity as a cathode material in Li-ion batteries." *Chemistry of materials* 23.24 (2011): 5446-5456.
83. Liu, Shuang-Shuang, et al. "Comparative study of the cathode and anode performance of Li2MnSiO4 for lithium-ion batteries." *ElectrochimicaActa* 188 (2016): 145-152.
84. Dominko, R., et al. "Li2MnSiO4 as a potential Li-battery cathode material." *Journal of Power Sources* 174.2 (2007): 457-461.
85. Wang, Chao, et al. "Enhanced electrochemical properties of F-doped Li2MnSiO4/C for lithium ion batteries." *Journal of Power Sources* 378 (2018): 345-352.
86. He, Guang, and ArumugamManthiram. "Nanostructured Li2MnSiO4/C Cathodes with Hierarchical Macro-/Mesoporosity for Lithium-Ion Batteries." *Advanced Functional Materials* 24.33 (2014): 5277-5283.
87. Wang, Fei, et al. "High performance Li2MnSiO4 prepared in molten KCl–NaCl for rechargeable lithium ion batteries." *ElectrochimicaActa* 119 (2014): 131-137.
88. Hwang, Chahwan, et al. "Synthesis, characterization, and electrochemical performance of V-doped Li2MnSiO4/C composites for Li-ion battery." *Materials Letters* 164 (2016): 270-273.
89. Zhang, S., et al. "Impacts of in situ carbon coating on the structural, morphological and electrochemical characteristics of Li2MnSiO4 prepared by a citric acid assisted sol–gel method." *Journal of Electroanalytical Chemistry* 689 (2013): 88-95.
90. Ji, Ran, et al. "Manipulating the Crystalline Structure and Electrochemical Performance of a Dilithium Manganese Silicate Cathode Material by Polyanion Doping." *ChemElectroChem* 3.11 (2016): 1805-1812.
91. Chen, Ruiyong, et al. "Structural Evolution of Li2Fe1-y Mn y SiO4 (y= 0, 0.2, 0.5, 1) Cathode Materials for Li-Ion Batteries upon Electrochemical Cycling." *The Journal of Physical Chemistry C* 117.2 (2013): 884-893.
92. Lai, Chunyan, et al. "Mo-doped Li2MnSiO4/C nanocomposite synthesized by citric acid-assisted sol-gel method with enhanced electrochemical properties." *Materials Letters* 139 (2015): 134-137.
93. Wu, Xia, et al. "Improving the structure stability and electrochemical performance of Li2MnSiO4/C cathode materials by Ti-doping and porous microstructure." *Journal of Alloys and Compounds* 735 (2018): 1158-1166.
94. Wang, Min, et al. "The high capacity and excellent rate capability of Ti-doped Li 2 MnSiO 4 as a cathode material for Li-ion batteries." *RSC Advances* 5.2 (2015): 1612-1618.
95. Wang, Yan-Chao, et al. "Solvothermal synthesis and electrochemical performance of Li2MnSiO4/C cathode materials for lithium ion batteries." *Journal of Alloys and Compounds* 614 (2014): 271-276.
96. Wagner, Nils P., et al. "Fe and V Substituted Li2MnSiO4/C As Potential Cathode Material for Li-Ion Batteries." *ECS Transactions* 64.22 (2015): 33-45.
97. Lee, Sol-Nip, et al. "Cu–Li2MnSiO4-polyaniline composite hybrids as high performance cathode for lithium batteries." *Journal of Alloys and Compounds* 630 (2015): 292-298.
98. Peng, Tao, et al. "Uniform coaxial CNT@ Li2MnSiO4@ C as advanced cathode material for lithium-ion battery." *ElectrochimicaActa* 291 (2018): 1-8.
99. Qiu, Shen, et al. "Template synthesis of mesoporous Li2MnSiO4@ C composite with improved lithium storage properties." *ElectrochimicaActa* 291 (2018): 124-131.
100. Dong, Yue, et al. "Synthesis of La-doped Li2MnSiO4 nano-particle with high-capacity via polyol-assisted hydrothermal method." ElectrochimicaActa 166 (2015): 40-46.

101. Cheng, Hong-Mei, et al. "Synthesis and structural stability of Cr-doped Li2MnSiO4/C cathode materials by solid-state method." Applied Surface Science 433 (2018): 1067-1074.
102. Kokalj, Anton, et al. "Beyond One-Electron Reaction in Li Cathode Materials: Designing Li2Mn x Fe1-x SiO4." *Chemistry of Materials* 19.15 (2007): 3633-3640.
103. Deng, C., et al. "Partial substitution of Mn/Si with V, Cr or Al in Li2MnSiO4 nanoparticle: Dependence of the physical and electrochemical properties on the substitution strategy." *Journal of Electroanalytical Chemistry* 719 (2014): 150-157.
104. Zhu, Hai, et al. "Nitrogen doped carbon layer of Li2MnSiO4 with enhanced electrochemical performance for lithium ion batteries." *ElectrochimicaActa* 295 (2019): 956-965.
105. Rangappa, Dinesh, et al. "Ultrathin nanosheets of Li2MSiO4 (M= Fe, Mn) as high-capacity Li-ion battery electrode." *Nano letters* 12.3 (2012): 1146-1151.
106. Luo, Shaohua, Ming Wang, and Weina Sun. "Fabricated and improved electrochemical properties of Li2MnSiO4 cathodes by hydrothermal reaction for Li-ion batteries." *Ceramics International* 38.5 (2012): 4325-4329.
107. Li, Xueliang, et al. "Ionothermal synthesis and characterization of Li2MnSiO4/C composites as cathode materials for lithium-ion batteries." *Ceramics International* 40.1 (2014): 289-296.
108. Song, Hee Jo, et al. "Li2MnSiO4 nanorods-embedded carbon nanofibers for lithium-ion battery electrodes." *ElectrochimicaActa* 180 (2015): 756-762.
109. Gummow, Rosalind J., et al. "Li2MnSiO4 cathodes modified by phosphorous substitution and the structural consequences." *Solid State Ionics* 259 (2014): 29-39.
110. Wang, Min, et al. "Structural evolution and electrochemical performance of Li 2 MnSiO 4/C nanocomposite as cathode material for li-ion batteries." *Journal of nanomaterials* 2014 (2014): 4.
111. ZHAO, Hongbin, et al. "Effect of Mg2+ doping on structure and electrochemical performance of lithium magnesium silicate." *Journal of The Chinese Ceramic Society* 39.7 (2011): 1084-1089.
112. Aravindan, Vanchiappan, et al. "Influence of carbon towards improved lithium storage properties of Li_2MnSiO_4 cathodes." Journal of Materials Chemistry 21.8 (2011): 2470-2475.
113. Liu, Jing, et al. "Facile solid-state synthesis of Li_2MnSiO_4/C nanocomposite as a superior cathode with a long cycle life." Journal of Power Sources 231 (2013): 39-43.
114. Peng, Zhenbo, et al. "PEG-assisted solid state synthesis and characterization of carbon-coated Li_2MnSiO_4 cathode materials for lithium ion battery." Int. J. Electrochem. Sci 8 (2013): 903-913.
115. Jin, Yun-Ho, et al. "Electrochemical Performances of Li_2MnSiO_4 Cathodes Synthesized by Mechanical Alloying Process." Journal of nanoscience and nanotechnology 15.3 (2015): 2418-2421.
116. Devaraj, S., et al. "Sol–gel derived nanostructured Li_2MnSiO_4/C cathode with high storage capacity." ElectrochimicaActa 102 (2013): 290-298.
117. Qu, Long, et al. "Synthesis and characterization of high capacity Li_2MnSiO_4/C cathode material for lithium-ion battery." Journal of Power Sources 252 (2014): 169-175.
118. Park, Kyung-Soo, et al. "Enhanced electrochemical performance of carbon-coated Li2MnSiO4 nanoparticles synthesized by tartaric acid-assisted sol–gel process." Ceramics International 40.7 (2014): 9413-9418.
119. Liu, Shuangke, et al. "High capacity Li2MnSiO4/C nanocomposite prepared by sol–gel method for lithium-ion batteries." Journal of power sources 232 (2013): 258-263.
120. Xie, Man, et al. "Template-assisted hydrothermal synthesis of Li2MnSiO4 as a cathode material for lithium ion batteries." ACS applied materials & interfaces 7.20 (2015): 10779-10784.
121. Pei, Yi, et al. "Chelate-induced formation of Li2MnSiO4nanorods as a high capacity cathode material for Li-ion batteries." Journal of Materials Chemistry A, 4.24 (2016): 9447-9454.
122. Jiang, Xiaolei, et al. "Hydrothermal synthesis of the Li2MnSiO4/C nanocomposite as a cathode material for lithium-ion batteries." Materials Letters 113 (2013): 9-12.
123. Hu, Zhe, et al. "Li2MnSiO4@C nanocomposite as a high-capacity cathode material for Li-ion batteries." Journal of Materials Chemistry A, 1.40 (2013): 12650-12656.
124. Mancini, M., et al. "Study on the stability of Li2MnSiO4 cathode material in different electrolyte systems for Li-ion batteries." ElectrochimicaActa 176 (2015): 679-688.
125. Molenda, Marcin, et al. "Stability of C/Li2MnSiO4 composite cathode material for Li-ion batteries towards LiPF6 based electrolyte." Solid State Ionics 262 (2014): 98-101.
126. Li, Xueliang, et al. "Ionothermal synthesis and characterization of Li2MnSiO4/C composites as cathode materials for lithium-ion batteries." Ceramics International40.1 (2014): 289-296.

Dr. Ambesh Dixit *is an Associate Professor at the Indian Institute of Technology Jodhpur (IIT Jodhpur), India, and has more than 15 years of experience in computational and experimental functional materials' physics. The particular emphasis is on the development of various technologies, including energy, water, and health. He is the first one in the scientific community to show that iron vanadate (FeVO4) is an intrinsic multiferroic system. Further, he has co-authored two books (i) Nanotechnology for Defence Applications (Springer) and (ii) Nanotechnology for Rural Development (Elsevier) and co-edited two books on Solar Energy (Springer). He has more than a hundred articles of international repute and two patents on his credit. He is an Editorial Board member of the Elsevier journal "Vacuum" and a life member of various societies such as Materials Research Society of India, Magnetic Society of India, Indian Carbon Society, and an annual American member Physical Society since 2007 and IEEE since 2019.*

Silicon based anode materials for Li-ion batteries – Importance, challenges and strategies

Manoj K. Jangid and Amartya Mukhopadhyay*

High Temperature and Energy Materials Laboratory, Department of Metallurgical Engineering and Materials Science, Indian Institute of Technology Bombay (IITB), Powai, Mumbai 400076, India.

**corresponding author; email: amartya_mukhopadhyay@iitb.ac.in; Phone: (+91) 22-2576 7612.*

Abstract

Higher Li-storage capacity and improved safety aspects, with respect to graphitic carbon, render Si an important anode material for the next generation Li-ion batteries as replacement for the presently used graphitic carbon. However, colossal volume changes (by up to ~400%) upon Li-alloying/de-alloying and limited Li-transport kinetics cause build-up of huge stresses and concomitant fracture/disintegration of Si (and loss in contact with current collector or rest of the electrode) during repeated electrochemical lithiation/delithiation cycles. These lead to rapid fade in Li-storage capacity within a few electrochemical lithiation/delithiation cycles and accrued surface reactions with the electrolyte at the freshly exposed fractured surfaces of Si; which are the major bottlenecks towards the development of stable Si-based electrode for practical Li-ion batteries. Of course, various strategies have been investigated to address the above issues, which include development of composite electrode materials (with 'Li-active/inactive' matrix/'buffer' materials), nanostructures/nano-architectures and porous Si electrodes. Such strategies reduce the severity of the stress development during lithiation/delithiation, but have other issues such as challenges associated with the development of the materials and exposure of enhanced surface to electrolyte where irreversible deleterious 'side' reactions take place. In the above contexts, the present review highlights the potential advantages of Si as anode material for Li-ion batteries, the mechanistic aspects concerning Li-storage in crystalline and amorphous forms of Si, the challenges-cum-bottlenecks associated with Si-based anodes and the strategies adopted (or looked into) for potentially addressing/suppressing the challenges.

Keywords: *Si-based anode, Li-ion batteries, cyclic stability, stress development*

Introduction

The limited Li-storage capacity (theoretical specific capacity of 372 mAh/g) and safety issues (Li-plating and dendrite formation) are the major disadvantages of graphitic carbon based anodes in the context of the development of safer Li-ion batteries, possessing high energy and power densities[1-3]. Hence, it is importantto developalternate anode materials with greaterLi-storage capacitiesandimproved safety aspects. In this regard, 'alloying reaction' based elements (*viz.*, Si, Sn, Ge and Al) and intermetallics (*viz.*, Cu_3Sn, Cu_6Sn_5, SbSn, etc.) are, to start with, deemed to be very suitable due to their significantly higher Li-storage capacities and slightly higherlithiation/delithiation potentials with respect to graphitic carbon (which will prevent Li-plating and dendrite formation) (see Fig. 1) [1-6]. In fact, it was as early as in 1971 thatDey*et al.*[6] demonstrated that Li can

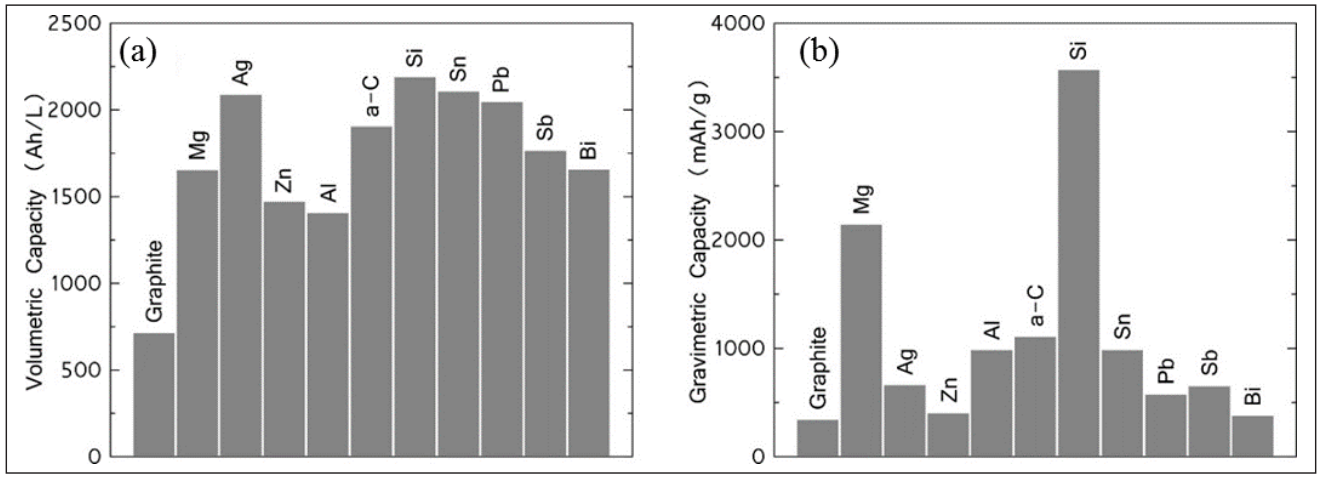

Fig. 1. Comparison of (a) volumetric and (b) gravimetric Li-storage capacities of different anode materials for Li-ion batteries [4].

reversibly form alloys with a few metallic materials under electrochemical conditions and these metals can be used as substitute for metallic Li anode in rechargeable batteries. The formation of Li based alloys is shown in eq. 1, below (here, M denotes either the metals or the alloys):

$$Li_xM \leftrightarrow xLi^+ + xe^- + M \quad (1)$$

Among the 'alloying reaction' based anode materials, the second most abundant element in the earth's crust, *viz.*, silicon (Si), having approximately 11 times higher gravimetric Li-storage capacity as compared to graphitic carbon (*viz.*, ~ 4200 mAh/g one of the highest) and alithiation/delithiation voltage of ~0.2 V *vs.* Li/Li^+ has been the most sought after next generation anode material for Li-ion batteries[1-5].

However, Si, as well as most of the 'alloying reaction' based anode materials have a major drawback, which is primarily related to huge volumetric changes upon Li-insertion/removal. For Si, this can be up to ~400% and causes colossal stress developments during lithiation/delithiationdue to external constraint towards dimensional changes (*viz.*, external stress) and also dimensional mismatch between co-existing regions within the same lattice/particle having different Li-concentrations (*viz.*, internal stress) [3,44].Such stresses causesevere mechanical degradation, including fracture of the active electrode particles/films and loss of contact with current collector. The fracture also leads to the exposure of fresh electrode surfaces to electrolyte, which act as sites for continued undesirable surface reactions with the electrolyte (primarily reduction of electrolyte species) and continued formation of solid electrolyte interface (SEI) layer; thus, raising the impedance of the cell. The above causes rapid fade in Li-storage capacity during electrochemical cycling and may render a Si-based electrode not useful after a few discharge/charge cycles. Over the last decade extensive research efforts have been directed towards addressing the above issues; primarily focusing on reduction in dimensional scale (for suppressing the Li-concentration gradient and minimizing absolute dimensional changes) and usage of 'buffer' (inter)layers (to possibly 'accommodate' dimensional changes or stress developments).

In the above contexts, this reviewfocuses on thevarious electro-chemo-mechanical aspects (*viz.*, inter-relationships between electrochemical aspects, stress developments, structural/mechanical instabilities and strategies for suppressing the same) of Si-based anodes for Li-ion batteries. It gets initiated by brief discussions on the potential advantages of replacing graphitic carbon based anode with Si-based anodes for Li-ion batteries and mechanistic aspects concerning electrochemical Li-storage in Si, highlighting the subtle differences between amorphous and crystalline Si in this regard. Following this, the challenges and bottlenecks towards realizing widespread development and usage of Si-based anodes have been discussed in fundamental terms, highlighting the issues associated with the huge volume changes upon lithiation/delithiation and the concomitant stress induced rapid fade in the Li-storage capacity upon multiple electrochemical lithiation/delithiation cycles. Subsequently, the strategies adopted to suppress such cyclic instability of Si-based electrode have been discussed. Towards the end the potential of Si as anode material for the upcoming Na-ion battery system and the associated issues are mentioned in brief, followed by a summary of the important aspects discussed in this review.

2. Mechanisms of Li-storage in crystalline and amorphous Si

As mentioned in the previous section, among the various 'alloying reaction' based metal anodes, Si is considered to be possibly the most promising candidate towards the replacement of graphitic carbonbased anodesin Li-ion batteries due to thevery high gravimetric and volumetric capacities (~4200 mAh/g and ~2400 mAh/cm^3, respectively; Fig. 1), wide-spread and abundant availability,

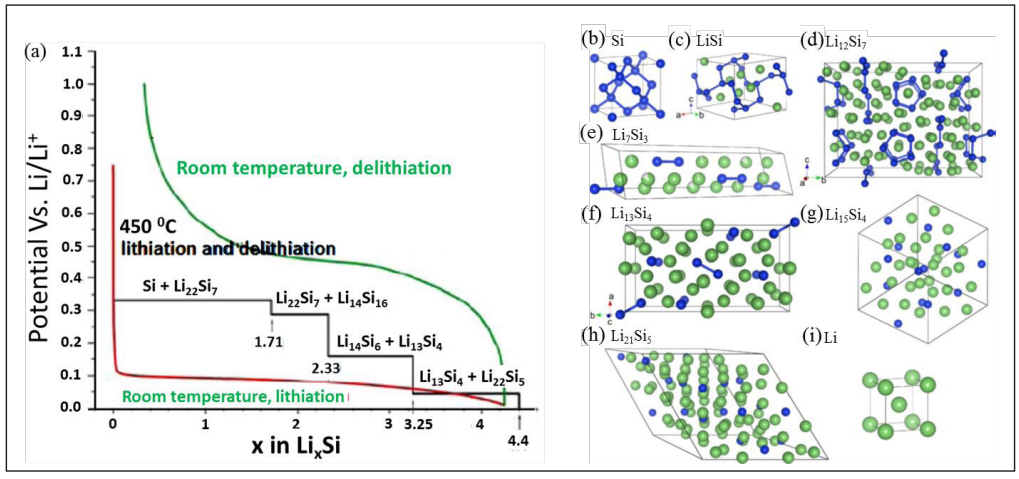

Fig. 2. (a) Typical galvanostatic discharge/charge profiles of Si when cycled in Li 'half cell' (lithiation and delithiation are depicted in red and green lines, respectively). The black line shows the different Li-Si phases that are predicted to form at 450 °C, along with the corresponding potentials vs. Li/Li$^+$[22]. Simulated structures of (b) Si, (c-h) different Li-Si phases and (i) Li metal [24].

safer lithiation/delithiation potentials and well-developed manufacturing/productiontechnology of Si[3-22]. For the first time, Sharma *et al.*[8], reported the formation of Si-Li binary phases at temperaturesabove 400 °C (Fig. 2a). However, later Wilson and Dahn demonstrated the possibility offormation of Si-Li alloys via electrochemical routealso at room temperature [23]. The alloying of Si with Li takes place by breaking of Si-Si bonds of the host matrix, followed by sequential formation of various Li-Si phases (*viz.*, $Li_{12}Si_7$, Li_7Si_3, $Li_{13}Si_4$, $Li_{15}Si_4$, $Li_{22}Si_5$ etc. [8-24]) within a fairly narrow potential range (as shown in Figs. 2a,b). The final Si-Li phase, *i.e.*, $Li_{22}Si_5$,corresponds to a maximum theoretical specific capacity of ~4200 mAh/g.

In order to understand the electro-chemo-mechanical aspects of Si-based anodes, it is important to understand the electrochemical Li-alloying/de-alloyingmechanism in both crystalline and amorphous Si types. The mechanismsin crystalline Si (c-Si) have been investigated by *in-situ* XRD[25,26]and *in-situ* TEM observations during electrochemical cycling[27,28]. In the pioneering work done by Li and Dahn[25], it was suggested that in the beginning, lithiation of c-Si occurs *via* a two-phase mechanism where unlithiated c-Si and highly lithiated amorphous Li_xSi phases co-exist, separated by a few nanometers thick reaction front (Figs. 3ato c) [5,25,29]. Further, *in-situ* TEM observations revealed

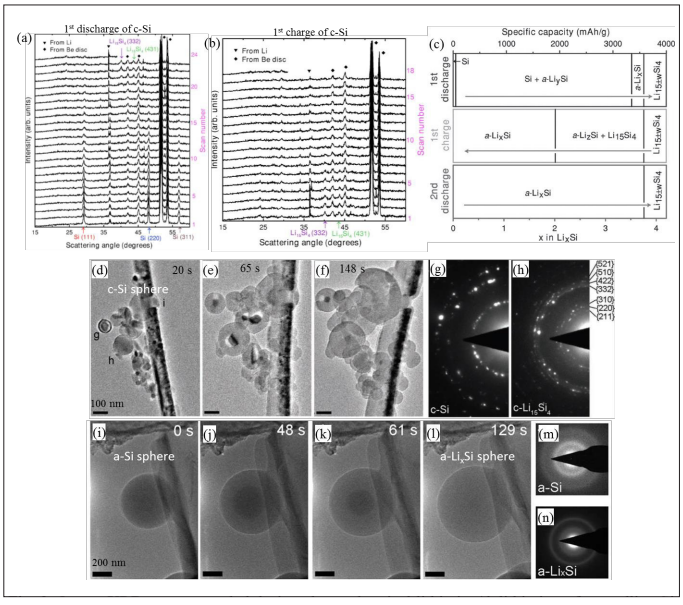

Fig. 3. In-situ XRD scans recorded during electrochemical lithiation/ delithiation of crystalline Si during the (a) 1st discharge and (b) 1st charge cycles; (c) mechanisms of Li-storage in crystalline Si [25]; (d-h) in-situ TEM observations and relevant SAED patterns obtained during lithiation of crystalline Si nanoparticles [29]. (i-n) in-situ TEM observations and relevant SAED patterns obtained during the lithiation of amorphous Si nanoparticles [31].

that this reaction front progressively moves towards the unlithiated c-Si core (Figs. 3dtoh) [29]. Accordingly, even when starting with a crystalline phase, Si turns amorphous during lithiation. However, when lithiated to potentials below ~0.05V vs. Li/Li^+ (during discharge against Li electrode; *viz.*, in Li 'half cell'), amorphous Li_xSi again turns crystalline, which ends up being the final lithiated phase. The reverse mechanisms take place during delithiation, with the higher lithiated Li_xSi and lesser lithiated Li_xSi phases being separated by a reaction front, which now moves from Li-rich phase to the lesser Li-containing phase, ultimately toformunlithiated amorphous Si (a-Si).Accordingly, theelectrochemical lithiation and delithiation reactions of c-Si can be summarized as below [30];

During lithiation (*i.e.*the discharge half cycle in Li 'half cells'):

$$Si\ (c) + \ xLi^+ + xe^- \rightarrow Li_xSi\ (a) + (3.75 - x)Li^+$$
$$(3.75 - x)e^- \rightarrow Li_{15}Si_4\ (c\ or\ a) \quad (2)$$

During delithiation (*i.e.* the charge half cycle in Li 'half cells'):

$$Li_{15}Si_4(c)\ \rightarrow Si(a) + yLi^+ + ye^-$$
$$+\ Li_{15}Si_4\ (residual) \quad (3)$$

Here, 'c' and 'a' are referred to crystalline and amorphous naturesof Si or Li_xSi, respectively.

Unlike in the case of c-Si, Li-storage mechanism in amorphous Si (a-Si) during the lithiation/delithiation was expected to be *via*a single phase solid-solution, without a truly sharp reaction front[5]. However, McDowell *et al.* [5,31], based on extensive *in-situ* TEM observations, indicated that the lithiation/delithiation of even a-Si takes place via a two-phase mechanism; *viz.*, both the unlithiated and lithiated a-Si phases co-existing and being separated by a reaction front. It may be noted that the final phaseupon 'complete' lithiation can be either crystalline or amorphous (*i.e.*, irrespective of the starting Si-type) depending upon the lower cut-off voltage. If the cut-off voltage is below ~0.05V vs.Li/Li^+ for lithiation, even a-Si will convert to crystalline phase ($Li_{15}Si_4$ and beyond)[25].

3. Issues and challenges with Si-based anodes

3.1. Challenges associated with cyclic stability, reversibility and rate capability

Si, irrespective of the crystalline or amorphous nature, experiences rapid fade in Li-storage capacity within initial

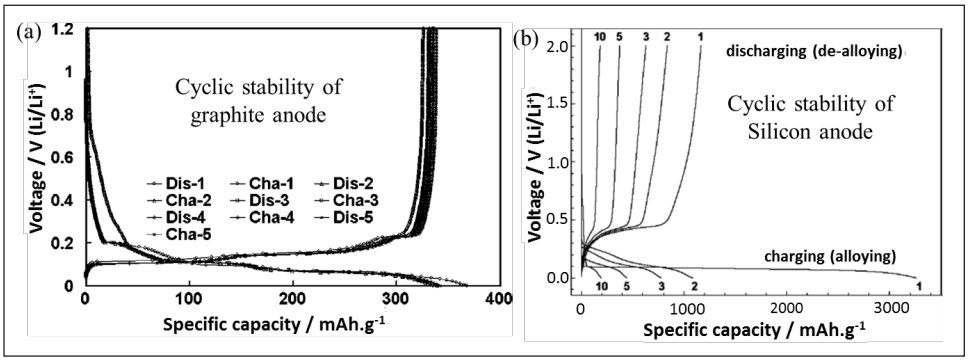

Fig. 4. (a) Galvanostatic discharge/charge profiles during initial electrochemical cycling of (a) graphite [33] and (b) Si (having particle size of ~10 μm) [11] in Li 'half cells'.

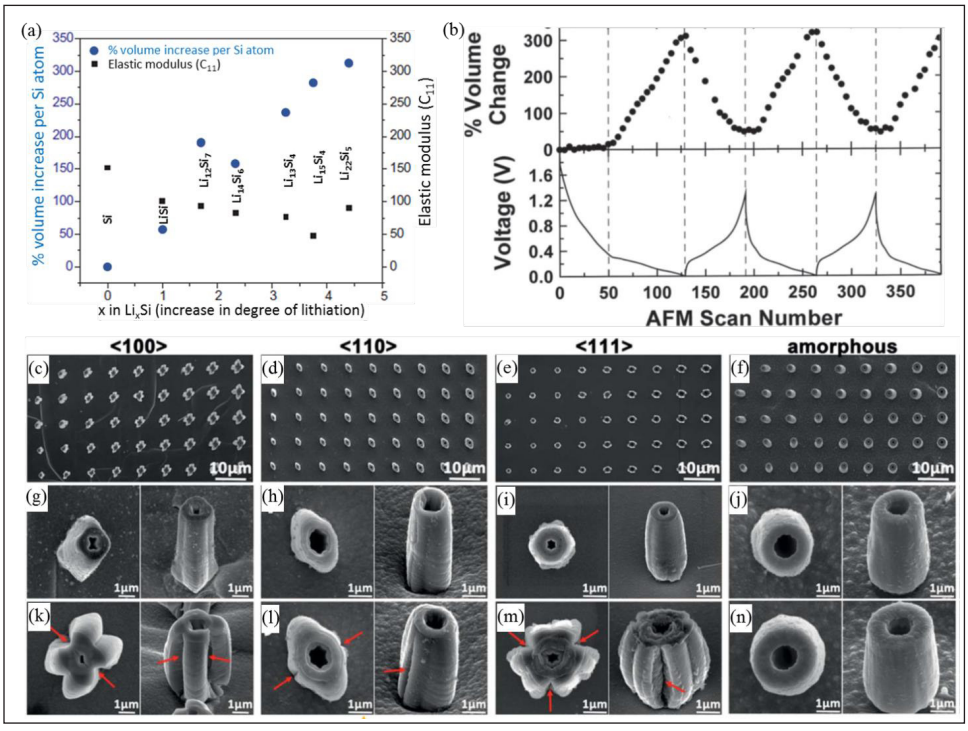

Fig. 5. (a) Variations of volume and elastic modulus with the increasing degree of lithiation of Si [3]. (b) Variations of voltage and volume (as measured by in-situ AFM scans) of Si during electrochemical lithiation/delithiation of patterned a-Si film [40]. Anisotropic and isotropic volume expansion observed during lithiation of (c-e,g-i,k-m) c-Si and (f,j,n) a-Si nanotube arrays, respectively; with anisotropic expansion, followed by fracturing of (c,g,k) <100>, (d,h,l) <110>, (e,i,m) <111> oriented c-Si nanotubes, being observed and (f,j,n) isotropic volume expansion observed for amorphous Si nanotubes without fracturing [41].

few cycles. A comparison of the galvanostatic cyclic stabilities during initial few cycles for graphite and Si-basedanodes is presented in Fig. 4. For, Si, almost 90% capacity fade is observed after only the first 10 cycles [3,5,9-11,16,18,19,22,30,32],but on the other handgraphitic carbonbased electrode shows excellent cyclic stability [1-3,33-36].

Furthermore, reversibility of lithiation and delithiation, *i.e.*, Coulombic Efficiency, is usually poor for Si, as compared to graphitic carbon. This is because, as mentioned above, fracture/disintegration of Si during each electrochemical lithiation/delithiation cycle exposes fresh surface to the electrolyte where irreversible surface reactions (including formation of solid electrolyte interface; SEI) keeps occurring even post the first cycle [3,7,37]. Additionally, the originally formed SEI layer on the surface of Si is also not stable (unlike in the case of, say, graphitic carbon) due to the huge volume changes during each lithiation and delithiation cycle [3,7,37]. Such continued occurrences of irreversible surface reactions keep consuming Li irreversibly from the cell and, thus, also contributes towards the decrease in the cell capacity in the case of a Li-ion 'full' cell.

On a different note, Li-insertion in Si isa relatively slower process as compared to graphitic carbon due to the lower Li-diffusivity (D_{Li})in Si (*viz.*, D_{Li} of just ~ 10^{-13} to 10^{-12} cm^2/s for Si [38,39], as compared toD_{Li} of ~ 10^{-9} to 10^{-7} cm^2/s for graphitic carbon [34-36]). From a more fundamental perspective, alloying is a relatively more complex and slow process, involving 'breakage/ distortion'of existing Si-Si bonds for forming new Si-Li bonds, as compared to intercalation (as for graphitic carbon). Accordingly, to improve the rate capability of Si-based anodes, 'Li transport distances' in Si 'host' matrix need to reduced. In other words, in the context of rate capability, reduction of the dimensional scale (say, particle size) of Si is desirable. However, the same will accrue the electrode/ electrolyte interfacial area and, accordingly, the occurrence of deleterious (irreversible) surface reactions.

3.2. Colossal volume changes during lithiation/ delithiation of Si

Since up to 4.4 atoms of Li can be stored forper singleatom of Si, accommodation of such amount of incoming Li-ions leads to~400% increase in volume (for$Li_{22}Si_5$) (see Fig. 5a)

[3-5,7-16]. Additionally, with increase in Li-content of Li_xSi, the elastic modulus (or stiffness)decreases. Beaulieu *et al.*[40] showed via*in-situ* atomic force microscopy (AFM) measurements during lithiation/delithiation of patterned a-Si films that thechange in height and volume of a-Si 'islands' is fairly linear with the degree of lithiation, with the same being reversible upon delithiation (Fig. 5b) [40]. The overall change in volume was measured to be ~300% [40]. Even though the volume change is isotropic in the case of a-Si, for c-Si the change in volume is anisotropic and depends on the crystallographic orientation [5,41]. Such anisotropic volumetric changes are due to differences in 'mobility' of Li atthedifferent crystallographic planes; *viz.*,[110] plane of c-Si possessthe fastest reactivity towards lithiation and, hence,c-Si exhibits preferential expansion along <110> direction.Similar observations were made by Lee*et al.*(with Si nanopillars)and Wang *et al.* (with Si nanotubes), whichshowed maximum expansion ofc-Si at the[110] surfaces upon lithiation(Figs. 5cton). The dimensional changes along the[110] and [100] directions were measured to be 245% and 49%, respectively.

In the context of fracture, upon lithiation, in the case of a-Si (which exhibits isotropic volume changes during lithiation/delithiation),firstly, the lattice gets broken into small Si clusters at relatively higher voltages (vs. Li/Li^+) during lithiation (in Li 'half' cells) and upon further lithiation the small clusters getfurther broken down into isolated Si atoms. When the potential goes below 0.05V *vs.* Li/Li^+, the metastable crystalline $Li_{15}Si_4$ phase is formed.With progress in lithiation/delithiation cycles (i.e., upon continued cycling), 'electrochemical sintering' or agglomeration or cluster formation of the broken down Si particles/islands have sometimes been observed [37]. A comparison of volumetric changes (in % with respect to the initial volume of Si), elastic modulus (i.e., C_{11}) and associated Li-storage capacity for the different Li_xSi phases is presented in Table 2.1.

Table 1.Various parameters related to different Li-Si phases (lattice type, percentage volume changeswith respect toinitial volume of Si, elastic modulus (C_{11}) and Li-storage capacity associated with particular Li_xSi phase) [3,24,44].

Phases (Li_xSi)	Lattice type	Change in volume of Si (%)	Longitudinal elastic modulus (C_{11})	Associated capacity (mAh/g)
Si	cubic	--	152	--
LiSi	tetragonal	56.95	101	954
$Li_{12}Si_7$	orthorhombic	115.23	93	1636
$Li_{13}Si_4$	orthorhombic	236.13	77	3100
$Li_{15}Si_4$	cubic	290	47	3579
$Li_{22}Si_5$	cubic	311.56	90	4198

3.3.Stress development in Si during lithiation/ delithiation

The volume expansion/contraction caused during Li-insertion/removal leads to stress development in the Si-based electrodes.Whileexpanding (by ~300-400%), theactive Si electrode material (particle/film) experiences constraints fromneighboring active particles, binder/ conducting additive, current collector etc.This constraining effect is a major cause for the stress development in Si and can be referred to as 'external stress' [3,7]. Additionally, Li-ion concentration gradients which get developed within the particle/film during lithiation/delithiation, which lead to the development of 'internal stress'; sometimes referred to 'diffusion induced stress'[3,7]. The different causes for stress developmentsin Si and other electrode materials have beenschematically illustrated in Fig. 6 [3,5,7].The severity of both the types of stresses, i.e., 'internal' or 'external' stress usually increases with the increase in the current density used for galvanostatic discharge/charge or rate of lithiation/delithiation.

The stress developments due to constraining effect will be discussed in the subsequent sections. In the context of 'internal stress', the development of concentration gradientscauses regions/lattices having different molar volumes, elastic properties, crystallographic orientation (in the case of c-Si) and Li-transport to co-exist (*i.e.*, be neighbors)within the same particle/film. Such internal mismatch leads to the development of the 'internal' or 'diffusion induced' stress (see Figs. 6dto g).In simple terms, during the course lithiation of a Si particle, the outer lithiated Li_xSi 'shell'(having greater Li-concentration) expands more compared to inner Si 'core' (having lesser Li-concentration). Accordingly, in the context of the model associated with 'two-phase lithiation' of Si particles, tensile hoop stress gets developed closer to the surface, with the unlithiated (or relatively less lithiated) core experiencing hydrostatic compressive stress [5,43]. It is also possible that the outer region undergoes plastic/viscous deformation, with the inner core still remaining elastic.A detailed literature on various techniques (primarily focused on curvature based techniques) used for real-time monitoring of stresses, structural evolution and other mechanistic aspects can be found in refs. [3,7].

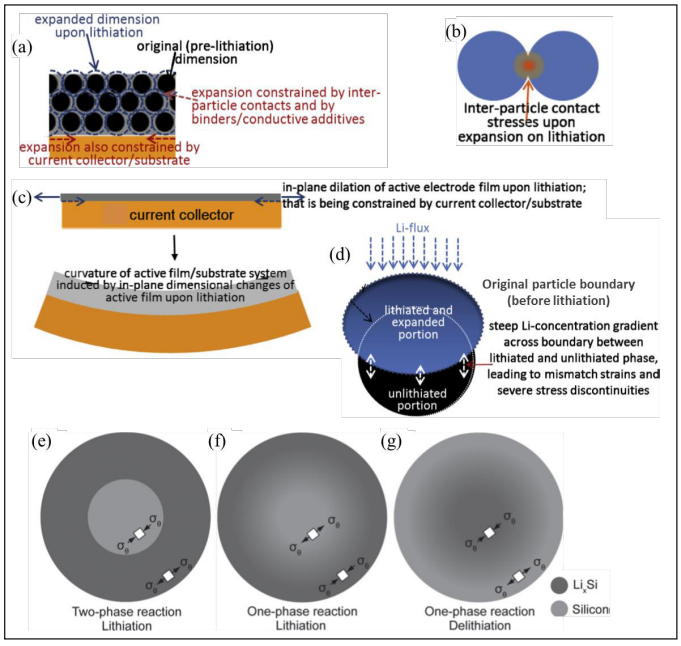

Fig. 6. Schematic representations of the various mechanisms of stress developments in electrode materials. (a) Constraining effect on expanding active particle from the neighboring active particles/binder/current collector; (b) Stress generation due to inter-particle interactions during volume expansion; (c) evolution of curvature due to constraints from the substrate or current collector during expansion of active film electrode; (d) stress developments due to Li-concentration gradient between different phases [3]. The hoop stresses in Si particles during two-phase and single-phase (de) lithiation processes, showing stress development in unlithiated and lithiated Si; (a) two phase lithiation of crystalline Si; (b) single phase lithiation of amorphous Si; (c) single phase delithiation of lithiated Si [5].

3.4. Structural degradation of Si-based anodes

In previous sections, it has been highlighted that due to the large Li-storage capacity of Si-based anodes, these undergo colossal volumetric changes and concomitantly large stress generation which collectively lead to premature and severe structural degradation of the Si anodesin the form of particle pulverization, cracking, fracture, film/particle delamination from current collector (*i.e.* loss of electronic contact), de-bonding from the polymer binder or conducting reinforcements,etc. (various modes of structural degradation are schematically depicted in Fig.7) [3-5,9-11,16,18,19,30,46]. More importantly, the majority of the irreversible capacity losses (poor Coulombic efficiency) is seen is during the initial electrochemical cycles and majorly due to the electrolyte decomposition/reduction (*i.e.* formation of SEI layer) and associated permanent trapping of Li-ion. The SEI layer is electronically insulating but it allows the diffusion of the Li-ions. Ideally, a thin and stable SEI layer is recommended to achieve stable electrochemical cycling during the extended electrochemical cycling. However, due to the structural

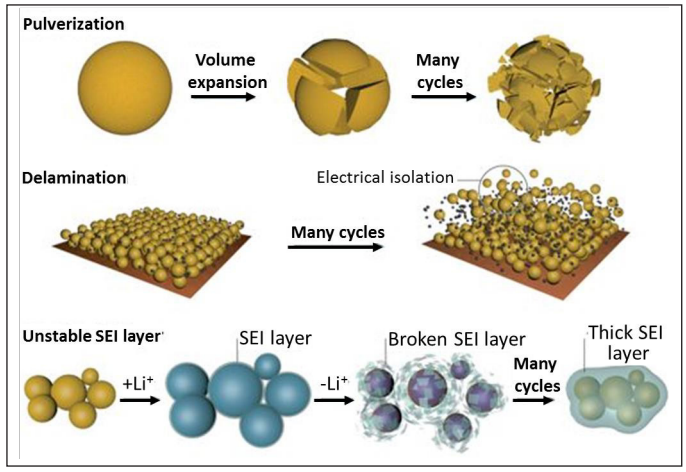

Fig. 7. Schematic representation of the various modes of structural instabilities related to Si and other 'alloying-reaction' based anodes [46].

degradation/instabilities, the SEI layer no more remains stable, it fractures and leads to exposure of fresh surfaces of Si where additional electrolyte decomposition/reduction occurs and new SEI layer reforms (similar to the initial electrochemical cycles). Therefore, due to the repeated cracking and exposure of fresh surfaces to the electrolyte, the SEI layer breaks, reforms and becomes thicken leading to continued irreversible capacity loss even beyond the initial few cycles.

4. Improving electrochemical and structural stabilities of Si-based anodes

In order to use Si-based materials as an anode in commercial batteries, various issues related to the volume accommodation, structural instabilities, and stress development arising during the electrochemical lithiation/delithiation must be addressed. Therefore, in the past few years, various methods/strategies have been used/adopted to improve the electrochemical cycling and structural stabilities, and rate capabilities of the Si-based anodes.Broadly, these can be classified in Si nanostructures [9,10,22,32], Si thin films and patterned Si films [9,10,12-15,22,32,46], Si composites with electrochemically active/inactive materials [48-52], porous Si architectures [16], Si/carbon composites [18-20,53] etc. (various strategies are presented in following sub-sections). In these strategies, the changes in the volume are either accommodated within the gaps between the active materials or by the 'buffer' materials.

4.1. Silicon nanostructures

As presented in Fig. 4b,Si particles having diameter of ~10 µm experience ~90% capacity fade only after 10 electrochemical cycles [11].The bulkier Si anodes not only suffer from poor structural-cum-electrochemical stabilities, but also from poor rate capabilities; which, in turn, exacerbate the 'internal stress' development due to concentration

gradients (see section 3.3) and further contribute towards the instabilities. Therefore, to overcome these issues, the use of Si-based nanostructures has been investigated extensively; and over time different types of Si-based nanostructures (*i.e.* nanoparticles, nanowires, nanorods, nanotubes, core-shell particles/wires etc.[9,10,22,32,54]) have been developed. When used for electrochemical Li-storage applications, they promise toreduce/minimize the absolute volume changes and associated stresses, leading to bettermaintainthe structural/mechanical integrities(see Fig. 8). WithSi-based nanostructures, not onlydoes the electrochemical cyclic and structural stabilities get improved,but also doesthe rate capabilitydue to the shorter Li-transportdistances as compare to the bulkier forms. In fact, it has been reported that cracking/fracturing upon lithiation/delithiation can potentially be totally suppressed for Si nanoparticles having diameter less than ~150 nm (Fig. 8a) [55].In the case of the Si nanowires, the empty space between nanowires has been claimed to effectively accommodate the volume expansion (see Figs. 8bandc) and, thus,suppress the stress development[54]. With the core-shell architecture comprised of c-Si core and a-Si shell in the case of Si nanowire, the crystalline core is expected to provide additional support and also act as secondary current collector from the base to the top, provided the electrochemical conditions are suitably tuned such that the c-core does not get lithiated[56,57]. Biologically inspired Si nano-architectures have also been developed to try and improve the stability of Si-based anodes. In one such studies, Liu et al.[58] have developed 'Si-pomegranates' type hierarchical nanostructure, which is made of single Si nanoparticle encapsulated by a thin hollow carbon layer, with several single units ensembled in one and coated by a thick carbon coating (see Figs. 8d,e). Such Si-based electrodewas reported to exhibit ~97% capacity retention after 1000 cycles. However, 'nanostructuring' of Si may also have negative impact by contributing towards accrued SEI formation during the initial few cycles due to the enhanced specific surface area [9,10,18,19,44]. Additionally, in the case of nanosized Si particles, particle agglomeration may be expected after a few electrochemical cycles, which mandates proper surface engineering of the nanostructures.

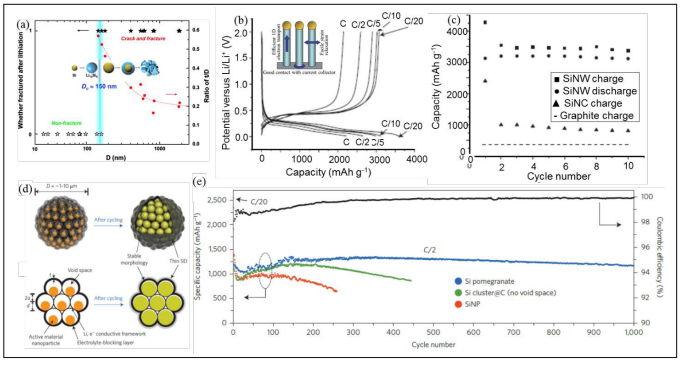

Fig. 8. (a) Relation between the possibilities of fracturing of Si particles, the thickness/diameter ratio (i.e., t/D ratio, where t is the thickness of Li_xSi) with respect to the diameter (D) of Si particles [55]. For Si nanowire electrodes (b) the rate capability (i.e., capacity obtained at different current densities or C-rates) and (c) electrochemical cyclic stability during the first 10 cycles [54]; (d) schematic representation of pomegranate inspired Si structure and volume accommodation by the same during lithiation; (e) comparison of the electrochemical cycling stabilities of Si pomegranates, nanoclusters and nanoparticles [58].

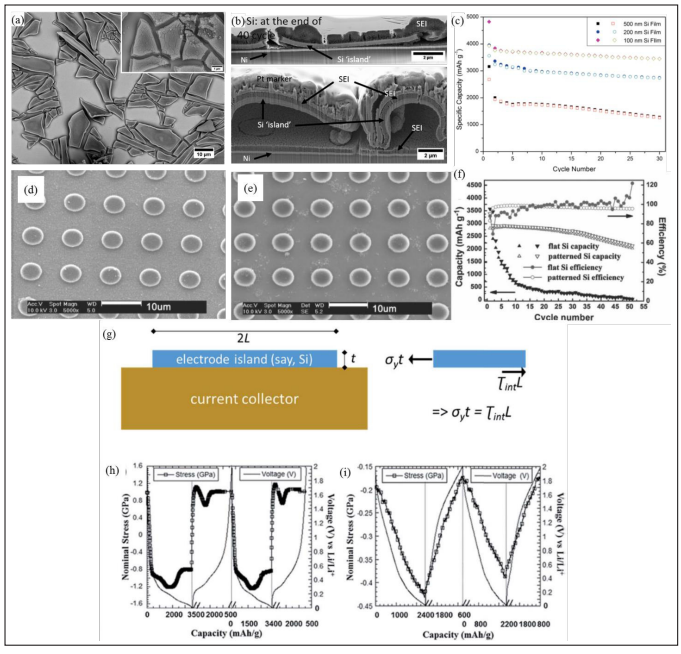

Fig. 9. SEM images obtained for 250 nm thick a-Si film electrode after 40 electrochemical lithiation/delithiation cycles in the (a) top view, (b) cross-section view modes [37]; (c) electrochemical cyclic stability of a-Si films having 500, 200 and 100 nm thickness [47]; SEM images of patterned Si film (d) before, (e) after electrochemical cycling; (f) electrochemical cyclic stability and Coulombic Efficiency obtained for continuous and patterned Si films during lithiation/delithiation [60]; (g) schematic representation of critical Si islands/pattern for interfacial sliding and (h,i) voltage and stress profiles with respect to capacity during two lithiation/delithiation cycles for continuous film and patterned Si film (square patterns of size 7 x 7 μm) [15].

4.2. Silicon thin and patterned films

Similar to bulkier Si particles, thick Si films (with thickness > ~250 nm) experience severe cracking and delamination from the current collector. By contrast, such instability can be minimized or even eliminated by reducing the thickness of the Si films, such thatcracking/delamination during electrochemical lithiation/delithiationis almost absent for Si films having thickness below ~100 nm. Above this 'critical' thickness, Si films get cracked into small islands; initially providing a 'cracked

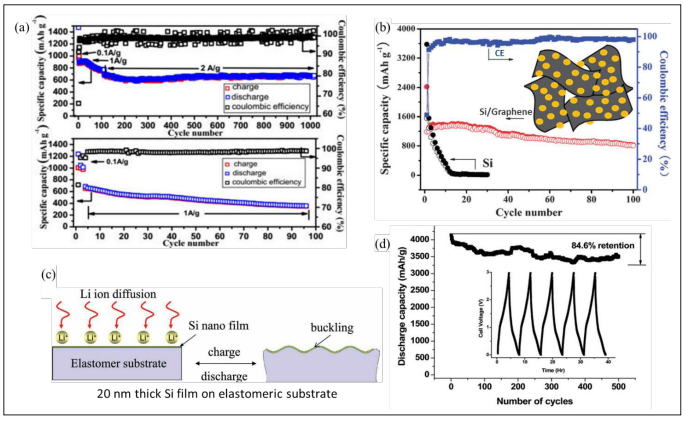

Fig. 10. Electrochemical cyclic stabilities (upon lithiation/delithiation) of (a) Si and Ga-Sn liquid metal composite [52], (b) Si/graphene composite electrode with uniform 'decoration' of Si nanoparticles on the graphene sheets [57]; (c) schematic representation of thin silicon film on elastomeric substrate and its buckling during electrochemical cycling; (d) cyclic stability of such thin Si film on elastomeric substrate [61].

mud' type of appearance (Figs. 9a,b) [12-15,46]. Eventually, with continued cycling, these 'islands' aggregate on the current collector and also delaminate [37,59].This occurs upon continued lithiation/delithiation primarily due to the incremental plastic deformation of the Si 'islands' [15,37,59], which possess lateral dimension beyond certain critical value (for a given thickness and adhesion strength at the Si/current-collector interface), as may be estimated by clever usage of 'shear-lag model' (see Figs.9dto g)[12-15,60]. Soni et al. [15] have demonstrated that Si 'islands'of lateral dimension ≤ 7 μm(and thickness of ~100 nm) on Cu current collector do not undergo plastic flow during lithiation/delithiation and is, accordingly, more stable in terms of retaining integrity upon repeated lithiation/delithiation in contrast to the continuous Si film of similar thickness (Figs. 9h,i).Furthermore, for continuous a-Si films, the magnitude of in-plane compressive stress (as measured in real-time during electrochemical lithiation/delithiation)goes up to ~2 GPa[14,15,37,59], whereas the patterned a-Si film was found to cause much lesser stress development, *viz.*, ~250 MPa[15].

4.3.Composite electrodes based on Silicon

Inactive-matrix composites: Suchcomposites consist of active Si particles/layers embedded in or co-existing with electrochemically inert matrix or 'buffer' layers[47-51,59]; for example, Si/NiTi electrodes [59], where NiTi (which is a shape memory alloy) is inactive towards lithiation. These Si-based composite anodes, in contrast to the 'pure' Si, exhibit lesser overall volume changes and lower stress developments; thus possessing superior cyclic stability, as compared to 'pure' Si. However, higher content of the inactive material increases the 'dead weight' of the electrode, which reduces the overall capacity; which renders it a compromise between overall capacity and cyclic stability.Furthermore, if the composite or electrode architecture is not carefully designed, the inactive matrix may lead to further 'slowing down' of the electron and ionic transport.

Active-matrix composites: Somewhat lesser compromise with respect to overall electrode capacity, while still improving the cyclic stability, is possible if the phase/material other than is also active towards reversible Li-storage for example, (for example, Ga-Sn alloy).In this case, both the phases, *i.e.*Si and the matrix/buffer, are active towards the lithiation/delithiation, but preferably at different potentials such that at a given time only one of the phases get lithiated (or delithiated) with the other acting as 'inactive' matrix/buffer. Additionally, 'matrix' materials like binary Ga-Sn metal, which covers the Si particles, may also act as self-healing matrix, thus preventing the agglomeration of Si particles healing the cracks (see Fig. 10a) [52].

4.4.Porous Si structure

Three-dimensional porous Si structures accommodate the volume expansion/contraction (occurring during lithiation/delithiation) very effectively by adjusting the increased volume in the pores/voids. Additionally, due to the porosity, the Li-diffusion length gets decreased which in turn increases the Li-ion diffusion; results in higher rate capabilities. But porous structures have disadvantages also, the low anode material loading and low volumetric capacities are few concerns with these porous structures [16].

4.5. Silicon-carbonnanocomposites

Use of various forms of carbon (as matrix or 'buffer' layers or reinforcements) to alleviate the stress development during electrochemical lithiation/delithiation of Sihas been extensively investigated over the last decade.The concerned carbon-based materials, such ascarbon nanotubes (CNTs), graphene, graphene oxide (GO), reduced graphene oxide (rGO), carbon powder, carbon fibers[18-20,53],possess very good electronic conductivity, excellent mechanical properties andflexibility. Furthermore, despite acting as 'active' materials towards reversible Li-storage themselves, the carbon-based materials undergosignificantly lower volume changes during electrochemical lithiation/delithiationand, by themselves, possessexcellent cyclic stability [3,42,43]. The above aspects render the carbon-based materials, as 'buffer'/reinforcement/matrix/additive in Si-based electrodes, promising towards 'accommodating' the volume changes and suppressing the stress developments during electrochemical lithiation/

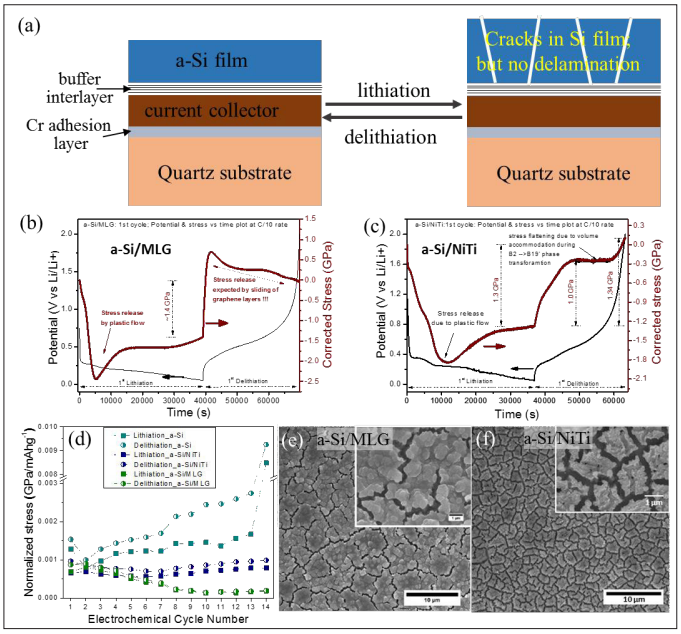

Fig. 11. (a) Schematic representation a-Si film electrode having 'buffer' interlayers. Voltage and in-situ monitored in-plane stress profiles, with respect to time, during the first lithiation/delithiation cycle of a-Si electrode in the presence of (b) multi-layered graphene (MLG) [37] and (c) NiTi interlayer [59]. (d) Comparison of magnitudes of the variations of the in-situ monitored stresses with electrochemical cycle numbers for a-Si, a-Si/MLG and a-Si/NiTi electrodes. Top-view SEM images obtained after 40 electrochemical lithiation/delithiation cycles of (e) a-Si/MLG and (f) a-Si/NiTi.

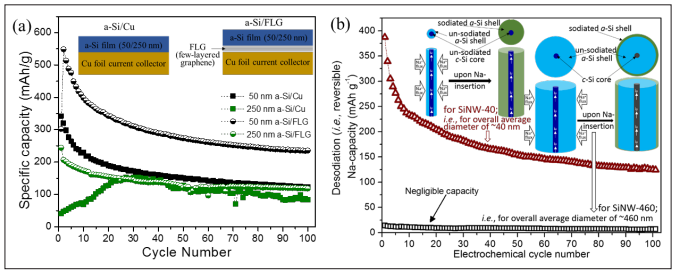

Fig. 12. Cyclic stabilities during electrochemical sodiation/desodiation of (a) 50 and 250 nm a-Si film electrodes in the absence and presence of few layers graphene (FLG) as interlayer [71], (b) Si nanowires having c-Si core and a-Si shell architecture and overall diameters of ~40 and ~460 nm [72].

delithiation of Si. Additionally, the presence of continuous conducting network of such carbon-based materialsalong with Si, leads to enhanced rate capability (due to significant improvement in the overall electronic conductivity) and also many a times help retain the electronic connectivity with broken fragments of Si; thus suppressing the loss of active material during lithiation/delithiation cycles.On a different note, when present as a thin coating on the surface of Si particles, the deleterious irreversible reactions of Si with the electrolyte (including the formation of thick SEI layer) is suppressed. In particular, in silicon-graphene composites, wrinkled graphene sheets have been reported to form a continuous network and cover the Si nanoparticles (Fig. 10b). The graphene sheets act as barrier towards suppressing the aggregation of Si nanoparticles upon volume expansion during lithiation and help maintaining the integrity of the overall electrode. With regard to stress development, it is believed that reversible sliding of constituent single graphene layers past one anotherhelps 'accommodate' some of the dimensional changes and hence 'buffer' the stress development. Additionally, in our work, we could establish that it is the weaker interface between Si and graphene (as compared to Si/Si or Si/current collector interfaces) that allows relatively constraint free reversible dimensional changes of Si upon lithiation/delithiation and, thus, helps maintain integrity over multiple cycles [59]. On a different note,nanosized gaps/spacespresent in Si/graphene composites and the flexible nature of graphene have been claimed to further help in'accommodating' the volume changes of Si nanoparticles; thus, leading to improved structural and electrochemical cyclic stability[57].

4.6.Silicon film on elastomeric substrate

Rigid substrates oppose the "free" expansion/contraction of Si film electrodes, but less stiff and more flexible substrates can potentially allow relatively constrain free dimensional changes of Si; thus minimize the stress developments due to such constraints. In this context, when Si films are present on'soft' substrates (such as Polydimethylsiloxane orPDMS), the volumetric strain developed in Si film during electrochemical lithiation/delithiation somewhat leads to buckling of the initially flat Si film (Figs. 10c,d). In this way, the stress developed in the Si film gets released/minimized by balancing the lithiation induced stress and buckling induced stress (release) (similar to that of a spring); which, in turn,suppresses cracking of Si and bestows it with superior cyclic stability (*viz.*, ~84 % capacity retention after 500 galvanostatic cycles) [60].

4.7.'Buffer' interlayers

In order to suppress the stress development and mechanical degradationofSi-based anodes, the effects of incorporation of'buffer' interlayers in-between the active electrode particles, active electrodefilm and current collector have been explored[20,37,59,61]. In fact, such architecture hasalso received considerable attention towards the development of stable thin film batteries with safer anodes, like Si. In this case, a thin film is employedin-between the active electrode film (for example, Si) and current collector, which serves as 'mechanical buffer'interlayer to mitigate/reduce the lithiation/delithiation induced stresses developed in the electrode (see Fig.11a).Depending on the interfacial characteristics, a weaker interface

between the active electrode material and interlayer may allow relatively constraint free dimensional changes of the active material during lithiation/delithiation and, thus minimize the development of normal stress in the active material. As seen in the case of Si film electrode, with multi-layered graphene (MLG) as 'buffer' interlayer (*viz.*, a-Si/graphene film electrode), the above, not only reduces the magnitude of the stress development, but also suppresses the occurrence of plastic flow upon lithiation of Si [37]. Such inferences were obtained based on real-times stress measurements (see Figs. 11bandd) using multi-beam optical stress sensor (MOSS) and detailed analysis of the *in-situ* data[37]. Such 'buffering action', in turn, preserved the integrity and contact of a-Si film electrode with the current collector (despite being laterally cracked into 'islands') after multiple lithiation/delithiation cycles (see Fig. 11e). On the other hand, 'buffer' interlayers, such as NiTi shape memory alloy (SMA; as one of the potential materials), which can show 'pseudoelasticity' or 'elastic' recovery of considerablestrain upon release of stress/load (by way of reversible B2↔B19′ phase transformation in the case of NiTi)[59,62,63]can 'accommodate' some of the dimensional changes of Si during lithiation/delithiation. This also suppresses the overall stress development and maintains the integrity of Si with the current collector (via the interlayer)[59].

5. Silicon as potential anode materialfor beyond Li-ion batteries

Despite the success and further promise of Li-ion battery systems as advanced electrochemical energy storage technique, due to the limited and highly localized sources of Li, alternative alkali metal-ion battery systems need to be explored and developed. Being a member of the same group in the periodic table, both Li and Na possess many similarities, which render Na-ion batteries as one of the best choices for battery chemistry beyond the Li-ion battery system. In the context of Na-ion batteries, it is important to note that Na-ions do not get intercalated in the interlayer spaces of constituent graphene layers of bulk graphitic carbon, which renders it absolutely necessary to find suitable non-graphitic anode material for the upcoming Na-ion battery system, with 'alloying-reaction' based anode materials being the forerunner. Here, it was surprisingthat Si was earlier believed to be inactive towards electrochemical Na-storage, despite the existence of Si-Na phase diagram showing thermodynamic feasibility of alloying[64,65]. As per such phase diagram, Na_1Si_1 should be the most sodium-rich phase of Na-Si alloy, which would correspond to a theoretical Na-storage capacity of 945 mAh/g [66]. Recently, a few theoretical studies indicated that one Si atom can host at most 0.76 Na (*i.e.* up to a composition of $Na_{0.76}Si$), leading to a theoretical capacity of ~725 mAh/g[67], with experimental research showing the possibility of the Na-storage in both amorphous Si (a-Si) [68,69] and crystalline Si (c-Si) [70], but only whenthey are in the form of nanoparticles. Overall, the literature on electrochemical sodiation/desodiation of Si was confusing and contradictory in nature.

The confusion has now been addressed based on systematic studies conducted by us [71], where thicknesses of a-Si film electrodes for electrochemical Na-alloying were varied, which proved that sodiation/desodiation is very much feasible in a-Si, but is severely 'transport limited', especially for a-Si dimensions beyond ~50 nm (Fig. 12a). Nevertheless, for dimension of ~50 nm, initial reversible Na-storage capacities of ~340 mAh/g can be obtained. The diffusion co-efficient of Na in such a-Si electrodes was estimated to be lesser than that of Li-diffusivity by ~6 orders of magnitude!In another study of ours withSi nanowires (SiNWs) having crystalline core and amorphous shell as part of the same structure, similar observations concerning dimensional effects were made(see Fig. 12b) [72]. SiNWs with amorphous shell thickness of ~8-10 nm (and overall diameter of ~40 nm) could get electrochemically sodiated/de-sodiated to a 1st cycle reversible Na-storage capacity of ~390 mAh/g. Interestingly, only the amorphous Si part (*i.e.*, the shell) was found to get sodiated, with the crystalline Si core not participating in the Na-alloying. Such observations tend to indicate that, sodiation of c-Si is possibly even more kinetically hindered (as compared to the amorphous counterpart), which also tends to support some of the earlier observations concerning 'inactiveness' of c-Si towards sodiation.

6. Summary

In this article, the importance of Si, as a potential anode material for Li-ion batteries, has been highlighted, followed by the challenges that have not yet rendered it feasible to develop stable anodes based primarily on Si. In a nutshell, replacement of graphitic carbon by Si as the anode material would lead to significant improvement of the energy density and safety aspects of Li-ion batteries. These are due to the higher Li-storage capacity of Si (*viz.*, by an order of magnitude) and the slightly higher electrochemical lithiation/delithiation potentials (vs. Li/Li^+) than graphitic carbon, respectively. However, colossal volume expansion/contraction (by up to ~400%) during Li-alloying/de-alloying and Li-transport limitation lead to huge stress development due to external constraints towards expansion/contraction and steep Li concentration gradient. Such external and internal stresses lead to mechanical instability, including fracture/disintegration, of active Si particles/films, loss in contact of the same with

current collector (and rest of the electrode) and alsodynamic fracture-cum-reformation of the supposed to be passivating SEI layer on the surface (which irreversibly consumes Li-ions and accrues the impedance) during repeated electrochemical lithiation/delithiation (*i.e.*, discharge/charge of cell). These lead to rapid fade in reversible Li-storage capacity of Si-based electrodes with a few discharge/charge cycles. In order to overcome this primary bottleneck towards the successful usage of Si as anode material, reduction of dimensional scale of nanosized-regime, development of innovative nanostructured/porous architectures and fabrication of composites with Li-active/inactive matrix/interlayer have been extensively investigated. Such strategies help, to a good extent, towards reducing the severity of the lithiation/delithiation induced stresses and enhancing the cyclic stability of Si-based electrodes for Li-ion cells. However, not only is the development of such innovative nanoscaled architectures and composites itself not too facile, but also nanoscaled Si exposes larger surface area to the electrolyte leading to the occurrence of excessive undesirable irreversible surface reactions. Furthermore, excessive usage of Li-'inactive' component in composite electrodes also negates the advantage of Si concerning bestowing higher energy density to the cell. Accordingly, even though considerable progress has been made with Si-based electrodes for rendering the same more stable upon repeated electrochemical lithiation/delithiation, further work needs to be done, in more practical perspective, to allow facile development of stable Si-based electrodes that do not lead to sacrifice with respect to the overall electrode capacity and irreversible capacity loss.

References

1. D. Deng, *Energy Sci. Eng.* 3 (2015) 385–418.
2. J.-M. Tarascon and M. Armand, *Nature* 414 (2001) 359–367.
3. A. Mukhopadhyay and B. W. Sheldon, *Prog. Mater. Sci.* 63 (2014) 58–116.
4. M. N. Obrovac and V. L. Chevrier, *Chem. Rev.* 114 (2014) 11444−11502.
5. M. T. McDowell, S. W. Lee, W. D. Nix, Y. Cui, *Adv. Mater.* 25 (2013) 4966−4985.
6. A. N. Dey, *J. Electrochem. Soc.* 118 (1971) 1547−1549.
7. M. K. Jangid and A. Mukhopadhyay, *J. Mater. Chem. A*7 (2019) 23679-23726.
8. R. A. Sharma and R. N. Seefurth, *J. Electrochem. Soc.* 123 (1976) 1763−1768.
9. Y. Jin, B. Zhu, Z. Lu, N. Liu, J. Zhu, *Adv. Energy Mater.* 7 (2017) 1700715.
10. U. Kasavajjula, C. Wang, A. J. Appleby, *J. Power Sources* 163 (2007) 1003–1039.
11. J. H. Ryu, J. W. Kim, Y.-E. Sung, S. M. Oh, *Electrochem. Solid-State Lett.* 7 (2004) A306−A309.
12. V. A. Sethuraman, M. J. Chon, M. Shimshak, V. Srinivasan, P. R. Guduru, *J. Power Sources* 195 (2010) 5062–5066.
13. M. J. Chon, V. A. Sethuraman, A. McCormick, V. Srinivasan, P. R. Guduru, *PRL* 107 (2011) 045503.
14. S. K. Soni, B. W. Sheldon, X. Xiao, A. F. Bower, M. W. Verbrugge, *J. Electrochem. Soc.* 159 (2012) A1520−A1527.
15. S. K. Soni, B. W. Sheldon, X. Xiao, M. W. Verbrugge, D. Ahn, H. Haftbaradaran, H. Gao, *J. Electrochem. Soc.* 159 (2012) A38−A43.
16. M. Ge, X. Fang, J. Rong, C. Zhou, *Nanotechnology* 24 (2013) 422001.
17. L. Su, Y. Jing, Z. Zhou, *Nanoscale* 3 (2011) 3967–3983.
18. J. Wang, T. Xu, X. Huang, H. Li, T. Ma, *RSC Adv.* 6 (2016) 87778–87790.
19. F. Luo, B. Liu, J. Zheng, G. Chu, K. Zhong, H. Li, X. Huang, L. Chen, *J. Electrochem. Soc.* 162 (2015) A2509−A2528.
20. S. Basu, S. Suresh, K. Ghatak, S. F. Bartolucci, T. Gupta, P. Hundekar, R. Kumar, T.-M. Lu, D. Datta, Y. Shi, N. Koratkar, *ACS Appl. Mater. Interfaces* 10 (2018) 13442−13451.
21. G. Radhakrishnan, P. M. Adams, B. Foran, M. V. Quinzio, M. J. Brodie, *APL Mater.* 1 (2013) 062103.
22. H. Wu and Y. Cui, *Nano Today* 7 (2012) 414–429.
23. A. M. Wilson and J. R. Dahn, *J. Electrochem. Soc.* 142 (1995) 326−332.
24. V.L. Chevrier, J.W. Zwanziger, J.R. Dahn, *J. Alloys Compd.* 496 (2010) 25–36.
25. J. Li and J. R. Dahn, *J. Electrochem. Soc.* 154 (2007) A156−A161.
26. T. D. Hatchard and J. R. Dahn, *J. Electrochem. Soc.* 151 (2004) A838−A842.
27. P. Limthongkul, Y.-I. Jang, N. J. Dudney, Y.-M. Chiang, *Acta Mater.* 51 (2003) 1103–1113.
28. X. H. Liu, J. W. Wang, S. Huang, F. F. Fan, X. Huang, Y. Liu, S. Krylyuk, J. Yoo, S. A. Dayeh, A. V. Davydov, S. X. Mao, S. T. Picraux, S. L. Zhang, J. Li, T. Zhu, J. Y. Huang, *Nat. Nanotechnol.* 7 (2012) 749–756.
29. M. T. McDowell, I. Ryu, S.W. Lee, C. Wang, W. D. Nix, Y. Cui, *Adv. Mater.*24 (2012) 6034–6041.
30. D. Ma, Z. Cao, A. Hu, *Nano-Micro Lett.* 6 (2014) 347–358.
31. M. T. McDowell, S. W. Lee, J. T. Harris, B. A. Korgel, C. Wang, W. D. Nix, Y. Cui, *Nano Lett.*13 (2013) 758−764.
32. H. Li, X. Huang, L. Chen, Z. Wu, Y. Liang, *Electrochem. Solid-State Lett.* 2 (1999) 547−549.
33. H. Yang, H. Bang, K. Amine, J. Prakash, *J. Electrochem. Soc.* 152 (2005) A73−A79.
34. M. D. Levi and D. Aurbach, *J. Phys. Chem. B* 101 (1997) 4641−4647.
35. K. Persson, V. A. Sethuraman, L. J. Hardwick, Y. Hinuma, Y. S. Meng, A. van der Ven, V. Srinivasan, R. Kostecki, G. Ceder, *J. Phys. Chem. Lett.* 1 (2010), 1176−1180.
36. N. A. Kaskhedikar and J. Maier, *Adv. Mater.* 21 (2009) 2664–2680.
37. M. K. Jangid, F. J. Sonia, R. Kali, B. Ananthoju, A. Mukhopadhyay, *Carbon* 111 (2017) 602-616.
38. N. Ding, J. Xu, Y.X. Yao, G. Wegner, X. Fang, C.H. Chen, I. Lieberwirth, *Solid State Ion.* 180 (2009) 222–225.

39. M. Pharr, K. Zhao, X. Wang, Z. Suo, J. J. Vlassak, *Nano Lett.* 12 (2012) 5039−5047.
40. L. Y. Beaulieu, T. D. Hatchard, A. Bonakdarpour, M. D. Fleischauer, J. R. Dahn, *J. Electrochem. Soc.* 150 (2003) A1457−A1464.
41. C. Wang, J. Wen, F. Luo, B. Quan, H. Li, Y. Wei, C. Gu, J. Li, *J. Mater. Chem. A*7 (2019) 15113-5122.
42. A. Mukhopadhyay, F. Guo, A. Tokranov, X. Xiao, R. H. Hurt, B. W. Sheldon, *Adv. Funct. Mater.* 23 (2013) 2397–2404.
43. Z. Cui, F. Gao, J. Qu, *J. Mech. Phys. Solids* 60 (2012) 1280–1295.
44. H. Xianhua, H. Shejun, R. Qiang, Z. Zhiwen, *Rare Metal Mat. Eng.* 39 (2010) 2079-2083.
45. V.B. Shenoy, P. Johari, Y. Qi, *J. Power Sources195 (2010) 6825–6830.*
46. J. W. Choi and D. Aurbach, *Nat. Rev. Mater.* 1 (2016) 16013.
47. J. Li, A. K. Dozier, Y. Li, F. Yang, Y.-T. Cheng, *J. Electrochem. Soc.* 158 (2011) A689−A694.
48. X. Zuo, J. Zhu, P. Müller-Buschbaum, Y.-J. Cheng, *Nano Energy* 31 (2017) 113–143.
49. J.-B. Kim, H.-Y. Lee, K.-S. Lee, S.-H. Lim, S.-M. Lee, *Electrochem. Commun.* 5 (2003) 544–548.
50. I.-S. Kim, P. N. Kumta, G. E. Blomgren, *Electrochem. Solid-State Lett.* 3 (2000) 493−496.
51. Y. He, X. Yu, Y. Wang, H. Li, X. Huang, *Adv. Mater.* 23 (2011) 4938–4941.
52. Y. Wu, X. Huang, L. Huang, X. Guo, R. Ren, D. Liu, D. Qu, J. Chen, *ACS Appl. Energy Mater.* 1 (2018) 1395−1399.
53. X. Shen, Z. Tian, R. Fan, L. Shao, D. Zhang, G. Cao, L. Kou, Y. Bai, *J. Energy Chem.* 27 (2018) 1067–1090.
54. C. K. Chan, H. Peng, G. Liu, K. McIlwrath, X. F. Zhang, R. Huggins, Y. Cui, *Nat. Nanotechnol.* 3 (2008) 31-35.
55. X. H. Liu, L. Zhong, S. Huang, S. X. Mao, T. Zhu, J. Y. Huang, *ACS Nano* 6 (2012) 1522–1531.
56. M. K. Jangid, S. Sinha, A. S. Lakhnot, F. J. Sonia, A. Kumar, R. O. Dusane, A. Mukhopadhyay, *Electrochim. Acta* 297 (2019) 381-391.
57. M. Zhou, F. Pu, Z. Wang, T. Cai, H. Chen, H. Zhang, S. Guan, Phys. *Chem. Chem. Phys.* 15 (2013) 11394–11401.
58. N. Liu, Z. Lu, J. Zhao, M. T. McDowell, H.-W. Lee, W. Zhao, Y. Cui, *Nat. Nanotechnol*. 9 (2014) 187-192.
59. M. K. Jangid, R. Lakra, V. Srihari, H. K. Poswal, M. Aslam, P. Pant, A. Mukhopadhyay, *ACS Appl. Energy Mater.* 2019, 2, 8181−8196.
60. Y. He, X. Yu, Y. Wang, H. Li, X. Huang, *Adv. Mater.* 23 (2011) 4938–4941.
61. C. Yu, X. Li, T. Ma, Ji. Rong, R. Zhang, J. Shaffer, Y. An, Q. Liu, B. Wei, H. Jiang, *Adv. Energy Mater.* 2 (2012) 68–73.
62. H. Jung, Y.-U. Kim, M.-S. Sung, Y. Hwa, G. Jeong, G.-B. Kim, H.-J. Sohn, *J. Mater. Chem.* 21 (2011) 11213−11216.
63. P. S. Lobo, J. Almeida, L. Guerreiro, *Procedia Eng.* 114 (2015) 776–783.
64. S. Komaba, Y. Matsuura, T. Ishikawa, N. Yabuuchi, W. Murata, S. Kuze, *Electrochem. Commun.* 21 (2012) 65–68.
65. L.D. Ellis, B.N. Wilkes, T.D. Hatchard, M.N. Obrovac, *J. Electrochem. Soc.* 161 (2014) A416−A421.
66. H. Morito, T. Yamada, T. Ikeda, H. Yamane, *J. Alloys Compd.* 480 (2009) 723−726.
67. S.C. Jung, D.S. Jung, J.W. Choi, Y. -K. Han, *J. Phys. Chem. Lett.* 5 (2014) 1283−1288.
68. Q. Zhao, Y. Huang, X. Hu, *Electrochem. Commun.* 70 (2016) 8−12.
69. C.-H. Lim, T.-Y. Huang, P.-S. Shao, J.-H. Chien, Y.-T. Weng, H.-F. Huang, B. J. Hwang, N.-L. Wu, *Electrochim. Acta* 211 (2016) 265−272.
70. Y. Xu, E. Swaans, S. Basak, H.W. Zandbergen, D.M. Borsa, F.M. Mulder, *Adv. Energy Mater.* 6 (2016) 1501436.
71. M. K. Jangid, A. Vemulapally, F. J. Sonia, M. Aslam, A. Mukhopadhyay, *J. Electrochem. Soc.* 164 (2017) A2559-A2565.
72. M. K. Jangid, A. S. Lakhnot A. Vemulapally, F. J. Sonia, S. Sinha, R. O. Dusane, A. Mukhopadhyay, *J. Mater. Chem. A* 6 (2018) 3422–3434.

Amartya Mukhopadhyay, *presently, Associate Professor at the Department of Metallurgical Engineering and Materials Science, IIT Bombay, completed his Doctoral in Materials research from the University of Oxford, UK, in 2009. He did his post-doctoral Research at Brown University, USA, for a couple of years. His research interests include materials for electrochemical energy storage and engineering ceramics. Among his major accomplishments, he has been awarded with the 'IIT Bombay Research Dissemination Award 2018', 'INAE Young Engineer Award 2016', 'ASM-IIM North America Visiting Lectureship 2016', 'IIT Bombay Young Investigator Award 2014' and 'Dr. R. L. Thakur Memorial Award' (as Young Scientist) by the 'Indian Ceramic Society' in 2013.*

Dr. Manoj K. Jangid *did his graduation in the area of electrochemical energy storage in 2019 and later, worked as Senior Research Fellow in the department of Metallurgical Engineering and Materials Science, Indian Institute of Technology Bombay (India). He did his Bachelors' and Masters' degrees (with honours) in Nanotechnology and Nanomaterials in 2012 from University of Rajasthan (India). He did his masters' degree project from CSIR-National Chemical Laboratory, Pune (India) in organic field-effect transistors. He is a prospective post-doctoral researcher at Michigan University Ann Arbor (2021). He isthe recipient ofthe prestigious 'Excellence in Ph.D. Research Award' (2020) from Indian Institute of Technology Bombay. His research interests are interface engineering, understanding stress developments in electrodes, and development of new electrode materials for Li-/Na/K-ion batteries*

A review on vanadium based oxides nanomaterials as an electrode for lithium ion battery

K. N. Manukumar[a], G. Nagaraju[a*] and Balaji P. Mandal[b]

[a] *Energy Materials Research Laboratory, Department of Chemistry, Siddaganga Institute of Technology, Tumakuru- 572103, India*

[b] *Chemistry Division, Bhabha Atomic Research Centre, Mumbai- 400085*

Abstract

Vanadium oxides, alkali and transition metal substituted/doped vanadates are being considered as promising cathode materials for lithium-ion battery owing to its multiple valence states (V^{2+} to V^{5+}), layered structure, low cost, high abundance, large discharge capacities and rich structural chemistry. The synthetic strategies and electrochemical battery performance of vanadium oxide nanostructures like vanadium dioxide (VO_2), vanadium pentoxide (V_2O_5), alkali metal and transition metal vanadates nanomaterials are summarized. This review will provide comprehensive knowledge of vanadium-based nanomaterials and shed light on their potential applications in emerging energy storage.

1. Introduction:

Energy is a critical global issue and the most focused research area in modern science and technology [1]. Fossil fuels occupy more than an 80% share in primary energy consumption in the world which causes air and water pollution, greenhouse effects from CO_2 emissions and other severe environmental problems [2]. In 2015, 195 nations signed ambitious commitments in Paris to reduce their emissions of greenhouse gasses, indicating emerging requirement for alternative ways to minimize the usage of fossil fuels [3]. Thus, exploring new materials and innovative strategies for energy conversion is of vital importance [4, 5]. Over the past years, nanotechnology has been engaged in numerous inspirations to solve several long-standing problems in energy conversion fields [6]. For example, slow solid-state diffusion, low energy density, and unstable cycling performance are major challenges that prevent further development of lithium-ion batteries (LIBs). In recent reports, nanostructures can shorten the transportation distance of ions or electrons, yielding a faster solid state diffusion in electrochemical energy conversion systems [7]. In addition, nanostructures own higher specific surface areas to provide more active positions for the interaction with other molecules or ions [8]. Vanadium is a highly abundant element in the earth crust and its oxides have been well known for multi-oxidation states (V^{2+} to V^{5+}) and various crystalline structures including VO_2 [9-13], V_2O_5 [14-16], $Na_xV_2O_5$ [17-19] , $Fe_2V_4O_{13}$ [20-22], ZrV_2O_7 [23, 24]. Moreover, unique chemical, electrical and optical properties enable vanadium oxides to find promising applications in energy conversion fields [10, 25]. The research pertaining to vanadium oxides have been summarized by several researchers in this area. For example, Whittingham et al. [26] and Bahlawane et al. [27] gave comprehensive reviews of synthesis of vanadium oxide compounds through hydrothermal and gas phase routes respectively. Chen et al.[28] and O'Dwyer et al.[29] systematically discussed the role of vanadium oxides in LIBs. Recently, Xie group has reported two excellent reviews about the synthesis of vanadium oxides for energy-related applications [10, 30]. Even though considerable scientific contributions of the above-mentioned reviews, most of them focus on energy storage/saving related applications. Vanadium oxides in the form of nanostructures are promising in converting natural resources, such as chemical, solar and thermal energies into widely used electrical power. Therefore, a literature survey is required to summarize the rapid development of novel vanadium oxide nanostructures in the energy-conversion-related field. In this review, it is aimed to summarize the recent advances in the development of synthesis strategies for vanadium oxide nanostructures and major achievements in solving the existing problems related to energy conversion comprehensively. A brief introduction, summary of different synthesis methods and structural properties of various vanadium oxide nanostructures has been given. Finally, the applications of vanadium oxides based in energy conversion and storage devices has been discussed.

2. Design and Synthesis of vanadium based nanomaterials:

Vanadium-based oxides possess multiple valence states. They can be divided into vanadium oxides and vanadate. Nanostructured vanadium oxide with controllable oxidation state and polymorph is highly

desired but very difficult to synthesize. In this Section, the synthesis strategies for different vanadium oxides in various nanostructures will be discussed.

2.1 Synthesis of VO_2 Nanostructures

VO_2 exhibits several polymorphic structures namely most stable rutile-type VO_2 (R) and monoclinic VO_2 (M) as well as metastable tetragonal VO_2 (A), monoclinic VO_2 (B), tetragonal VO_2 (C) , monoclinic VO_2 (D) and paramontroseite VO_2 (P) [31-34]. Ji and coworkers selectively prepared tetragonal VO_2(A) by controlling the pressure during the hydrothermal synthesis [35]. Li and coworkers reported the ultra-long VO_2(A) nanobelts synthesized hydrothermally using V_2O_5 sol as precursor and polyethylene glycol as both surfactant and reducing agent [36]. 1-D VO_2(A) nanostructures could also be prepared via an one-step hydrothermal method using $VOSO_4$ and NH_4OH as precursors [37]. Liangmiao et. al prepared monocrystalline VO_2(A) nanoplates synthesized *via* a one-pot hydrothermal process [38]. Emmanuel et.al [39] synthesised vanadium oxide aerogels as a precursor for preparing nanotextured VO_2[B] by low temperature heat treatment under vacuum. Nagaraju et.al [13] reported the metastable VO_2(B) bundles of nanorods and microspheres synthesized through a simple hydrothermal method by dispersing V_2O_5 in aqueous quinol. Jayalakshmi et.al [40] synthesised VO_2(B) nanorods by hydrothermal method using $NaVO_3$ precursor and sodium oxalate as a reducing agent. Yifu et.al [41] articulated the controlled synthesis of 3-D porous VO_2(B) hierarchical spheres with various interiors for energy storage. Hagrman et.al [42] prepared a novel polymorph VO_2(C) by dehydration of the new layered vanadium oxide hydrate, $VO_2.0.5\ H_2O$. Diana et.al [43] synthesised different morphologies and sizes of VO_2(D) particles via hydrothermal synthesis using ammonium metavanadate (NH_4VO_3) or vanadium pentoxide (V_2O_5) as a vanadium precursor. Yifu et. al [44] synthesised 3-D porous VO_2(B) hierarchical spheres with various interiors (solid spheres and hollow spheres) by a template-free method. Swagatika et.al [45] synthesised VO_2(D) plate-like structures by a simple hydrothermal process using ammonium metavanadate as vanadium precursor. Scheme 1 depicts the Growth mechanism of vanadium oxides nanostructures at different concentration of NaOH [46].

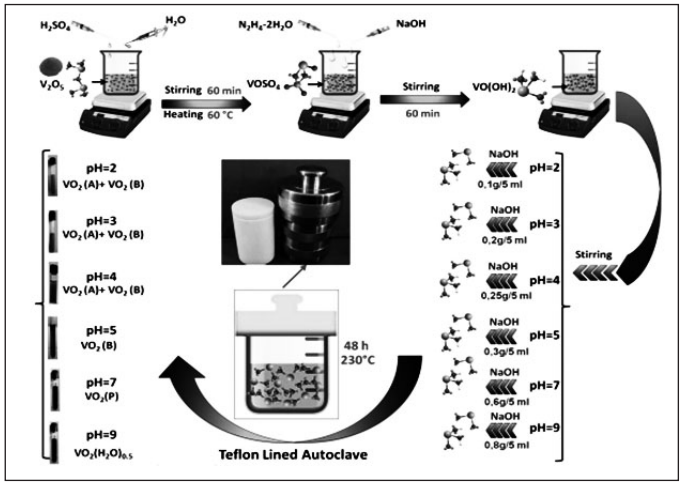

Scheme 1. Growth mechanism of vanadium oxides nanostructures at different concentration of NaOH

Yang et.al [47] reported VOOH hollow nanourchins which could be converted topochemically to paramontroseite VO_2 hollow nanourchins without altering the size and original appearance during the annealing process. Chang et.al [48] reported paramontroseite VO_2 which has been successfully obtained using a simple chemical reaction route for aqueous lithium ion battery application.

2.2 Synthesis of V_2O_5 Nanostructures

V_2O_5 is probably the most studied vanadium oxides due to its layered structures for energy conversion applications. However, few limitations, such as poor conductivity, slow electrochemical kinetics, and irreversible electrochemical transformations, severely hindered the development of V_2O_5 based electrode materials. Nanostructures have been studied to overcome the above mentioned problems. In this section, the fabrication strategies of nanostructured V_2O_5 will be discussed. The complexity, rich chemistry, crystallinity, and morphology have made V_2O_5 a very interesting material for research. It should be mentioned that Livage, the pioneer of the so-called "chimie douce", played a key role to promote the development of vanadium chemistry[49]. Jiangyan et al.[50] reported multi-shelled V_2O_5 hollow microspheres prepared via an anion-adsorption mechanism. Nagaraju et al.[51] V_2O_5 nanobelts have been prepared via hydrothermal treatment of commercial V_2O_5 in acidic (HCl/H_2SO_4) medium at relatively low temperature (160 ◦C).

Nagaraju et al . [52] reported the hydrothermal synthesis of V_2O_5 nanorings without using any surfactant rather by the acidification of sodium metavanadate solution and SEM images has been shown in Figure.1.

Zhang et al. [53] reported 3D porous V_2O_5 hierarchical microspheres via additive-free solvothermal method and subsequent calcination. Nagaraju et al. [54] reported synthesis of V_2O_5 nanoparticles *via* a simple low temperature hydrothermal method using ammonium vanadate and quinol.

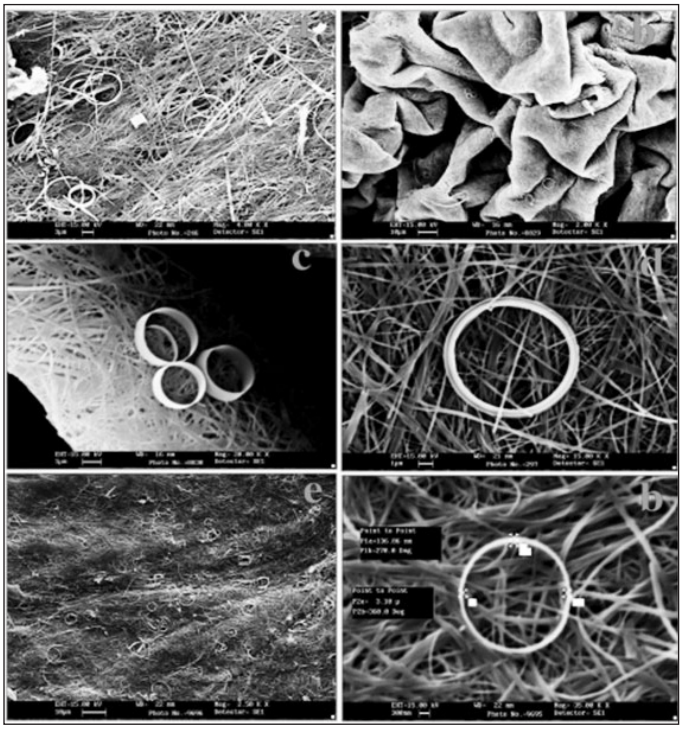

Figure 1. SEM images of the nanorings/nanoribbons prepared at (a) 130 C for 1 day, (b, c) 130 C for 2 days, (d) 150 C for 1 day and (e, f) 150 C for 2 days.

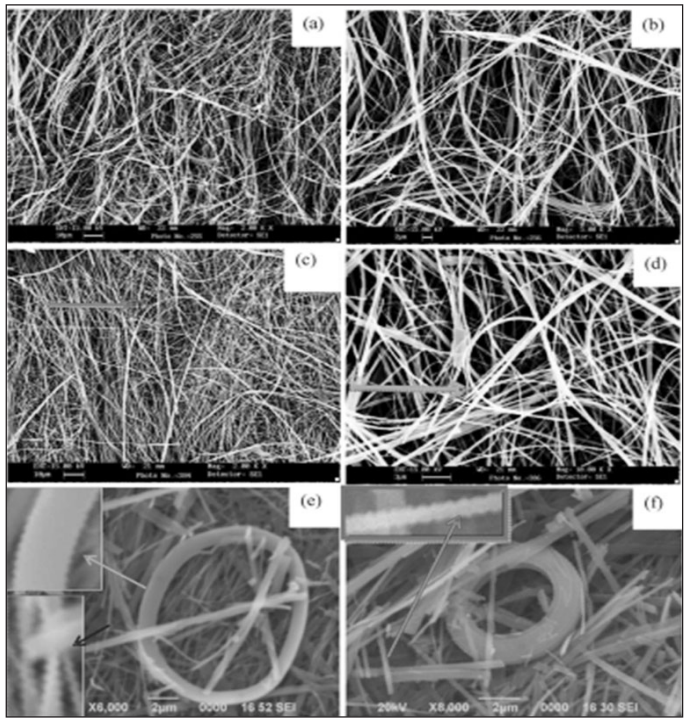

Figure 2. SEM images of $Na_{0.3}V_2O_5$ nanofibers/nanorings prepared at 200 °C for (a and b) 3 days, (c and d) 4 days and (e and f) 5 days.

2.3 Synthesis of Alkali metal and Transition metal vanadates

Alkali metal and transition metal vanadates have been widely studied as potential cathode materials for battery systems [55-57]. Nagaraju [58] reported simple one step hydrothermal method to synthesize $Na_{0.3}V_2O_5$ nanofibers/ nanorings without using any surfactant at 200 °C in 3-5 days which could be predicted in scheme 2 and SEM images has been depicted in Figure 2.

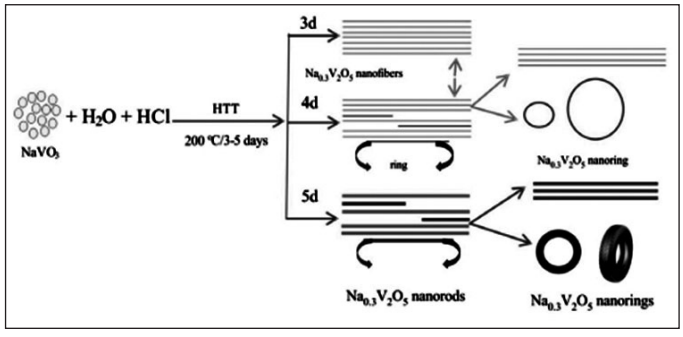

Scheme 2. Possible schematic growth diagram of $Na_{0.3}V_2O_5$ nanofibers/ nanorings.

$Na_{0.33}V_2O_5 \cdot 1.5H_2O$ nanorings/nanorods and $Na_{0.33}V_2O_5 \cdot 1.5H_2O$ /reduced graphene oxide (RGO) composites have been prepared through a facile hydrothermal route in acidic medium at 200 °C for 2 days [59]. $Na_{0.28}V_2O_5$ nanobelts could be synthesize at 130°C in two days in acidic medium (H_2SO_4) without using any surfactant. Xuexia et al.[55] reported β-Na0.33V2O5 synthesized *via* a sol-gel method followed by annealing at high temperatures. Fe2V4O13 nanoparticles were prepared using iron nitrate and ammonium vanadate as oxidizer and sucrose as the fuel [59]. Qidong et al [59]synthesised superstructure ZrV_2O_7 nanofibres as cathode materials for Li-ion batteries Shreenivasa et al. [60]synthesised porous ZrV_2O_7 as cathode material for lithium ion battery via solution combustion method.

3. Applications of Vanadium based oxides nanomaterials in lithium ion battery

Vanadium oxides have been extensively studied as cathode materials in the past studies since Whittingham first reported in 1976 [61].Their unusual layered structures, which allows ions or small molecules embedded between the layers, serve as a high capacity cathode material for lithium-ion batteries. In this section, the battery performance of vanadium based oxides nanomaterials will be discussed.

3.1 Electrochemical stuudies of VO_2 Nanostructures

Figure 3a shows cyclic voltammogram of VO_2(B) electrode with a scan rate of 0.5 mVs^{-1} in a voltage range of

1.5–4 V [13]. The cathodic peak located at around 2.2 V corresponds to the voltage platform of the discharge process, in which Li^+ is intercalated into the $VO_2(B)$ electrode, whereas the anodic peak located at around 2.7 V corresponds to the charge process, in which Li^+ is deintercalated from the $VO_2(B)$ electrode.

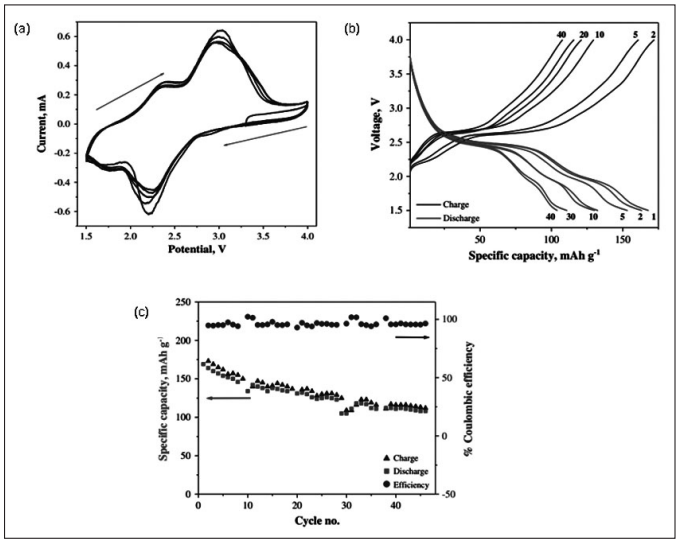

Figure 3. (a) Cyclic voltammogram of $VO_2(B)$ electrode, (b) Voltage–capacity profiles of $VO_2(B)$ and (C) Charge–discharge vs. cycle number, and Coulombic efficiency of $VO_2(B)$

The insertion/extraction behavior of lithium ions thus can be tentatively expressed as

$$VO_2 + Li^+ + e^- \rightarrow Li_1VO_2 \text{ (2.09 V)} \quad \text{--- (1)}$$

$$Li_1VO_2 \rightarrow VO_2 + Li^+ + e^- \text{ (3.38 V)} \quad \text{--- (2)}$$

The cathodic/anodic peaks in the CV were in good agreement with the plateaus observed in the voltage–capacity profiles. The electrochemical properties of $VO_2(B)$ bundles of nanorods as cathode in lithium ion storage were tested via charge– discharge measurement at a current density of 0.1 mA g^{-1} as shown in Figure 3b. In Figure 3c, the average Coulombic efficiency at different currents is no less than 85% from the first cycle to the 47th, and the enhanced Li insertion properties were relevant to the increased crystallinity of the material.

Mesoporous $VO_2(B)$ and its rGO composite exhibited better performance as shown in Figure 4 [12]. The enhanced performance in electrical energy storage system reveals the effectiveness of rGO in the composite, as it enhances the conductive electron pathway to overcome the intrinsic limits of single phase $VO_2(B)$.

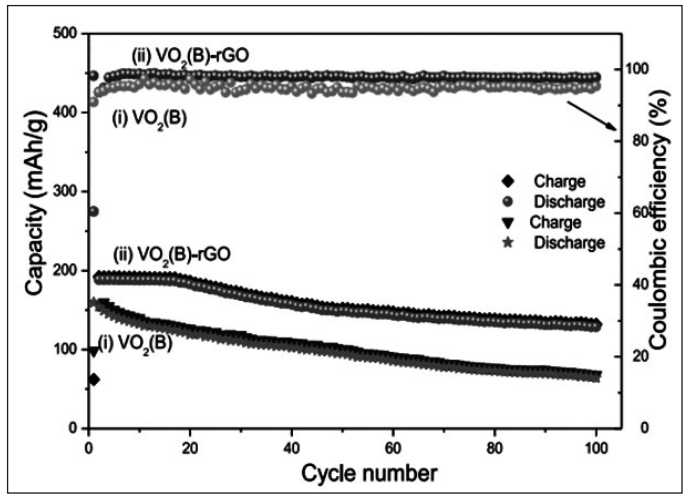

Figure 4. Charge–discharge vs. cycle number, and Coulombic efficiency of $VO_2(B)$

3.2 Electrochemical performance of V_2O_5 Nanostructures

The electrochemical analysis shows an initial discharge capacity of 360 $mAhg^{-1}$ and its almost stabilized capacity is reached to 250 $mAhg^{-1}$ after 55 cycles [51] . Possible reaction mechanism for the formation of orthorhombic V_2O_5 nanobelts is proposed.

$$\alpha\text{-}V_2O_5 + Li^+ + e^{-1} \rightarrow \delta\text{-}LiV_2O_5 \text{ at 3.2 V} \quad \text{---(3)}$$

$$\delta\text{-}LiV_2O_5 + Li^+ + e^{-1} \rightarrow \gamma\text{-}Li_2V_2O_5 \text{ at 2.1 V} \quad \text{--- (4)}$$

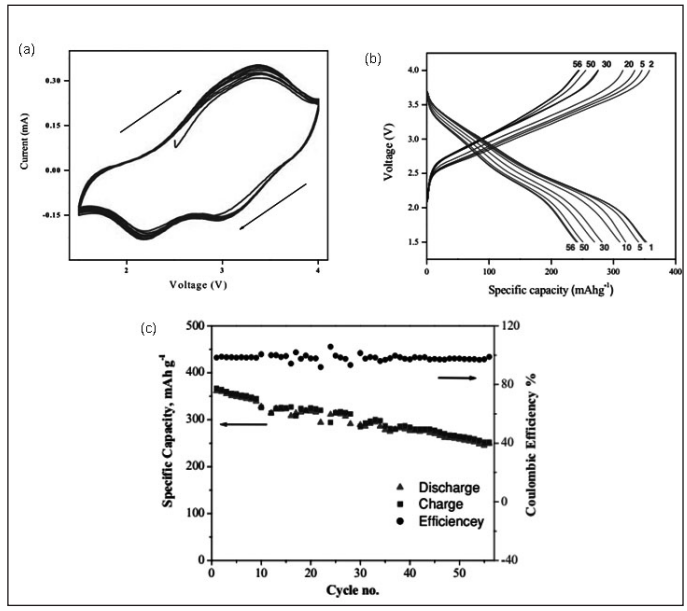

Figure 5. (a) Cyclic voltammogram of V_2O_5 nanobelts electrode, (b) Voltage–capacity profiles of V_2O_5 nanobelts and (C) Charge–discharge vs. cycle number, and Coulombic efficiency of V_2O_5 nanobelts

Electrochemical performance of V_2O_5 nanorings/nanoribbons exhibited better performance is shown in Figure 6 [52].

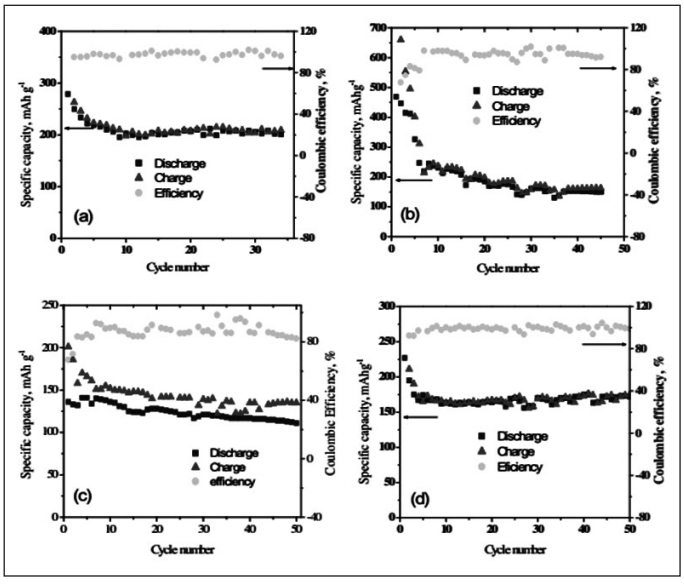

Figure 6. Discharge and charge capacity, Coulombic efficiency of the V_2O_5 nanorings/nanoribbons prepared at (a) 130°C for 1 day, (b) 130 °C for 2 days, (c) 150 °C for 1 day and (d) 150 °C for 2 days at a current density of 100 mA g^{-1}

Recent report on V_2O_5 nanoparticles from our group delivered better battery performance and is shown in Figure 7 [54] and Figure 8 [62]

3.3 Electrochemical performance of Alkali metal and Transition metal vanadates

The $Na_{0.3}V_2O_5$ nanofibers/rings exhibited an initial discharge specific capacity of 182 mAh g^{-1} and a stabilized

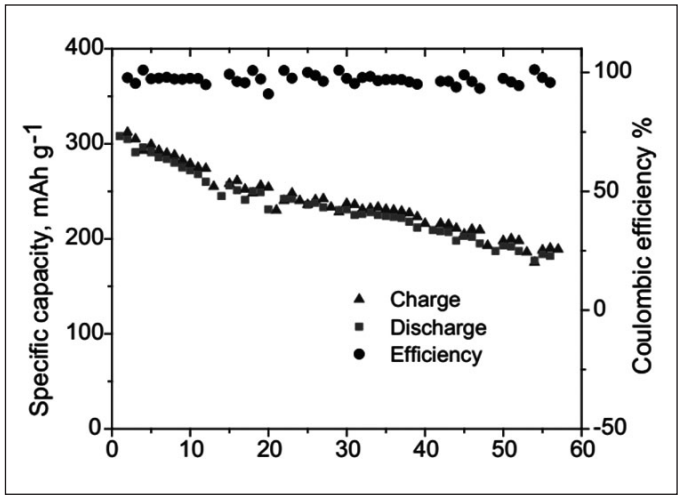

Figure 7. V_2O_5 nanoparticles cycling stability and Coulombic efficiency over 60 cycles at 0.1 mA g^{-1}

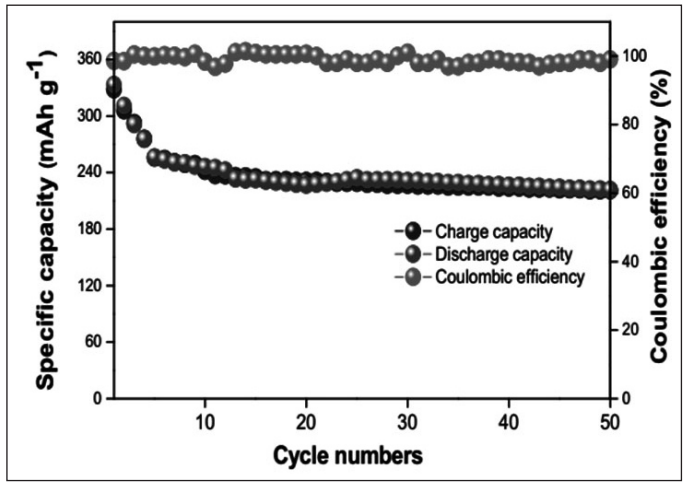

Figure 8. Cyclic performance and coulombic efficiency of EGCG-assisted V_2O_5 NPs

capacity of 179 mAh g^{-1} even after 50 cycles and shown in Figure 9 [58].

The insertion/extraction behavior of lithium ions thus can be predicted as

$$Na_{0.3}V_2O_5 + Li^+ + xe^{-1} \rightarrow Li_xNa_{0.3}V_2O_5 \qquad \text{----(5)}$$

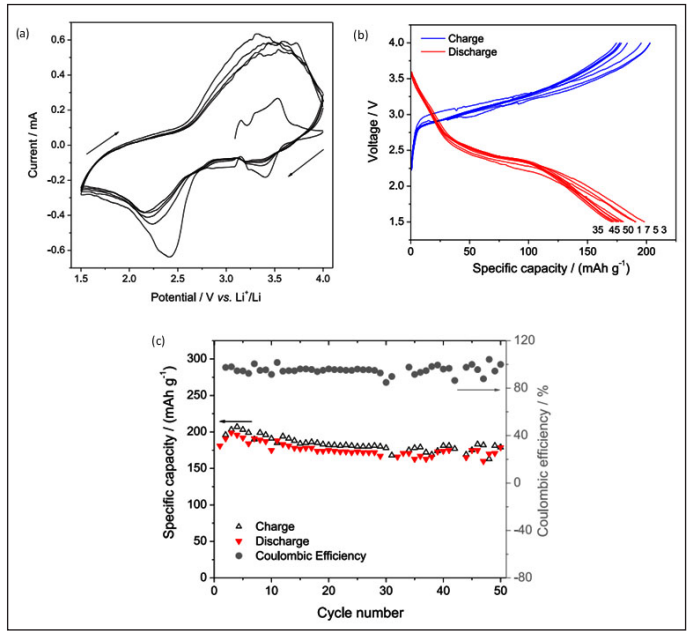

Figure 9. (a) Cyclic voltammogram of $Na_{0.3}V_2O_5$ nanofibers/rings electrode, (b) Voltage–capacity profiles of $Na_{0.3}V_2O_5$ nanofibers/rings and (C) Charge–discharge vs. cycle number, and Coulombic efficiency of $Na_{0.3}V_2O_5$ nanofibers/rings

$Na_{0.33}V_2O_5 \cdot 1.5H_2O$ nanorings/nanorods and $Na_{0.33}V_2O_5 \cdot 1.5H_2O$ /reduced graphene oxide (RGO) composites delivered better battery performance and shown in Figure 10 [63]

The electrochemical performance of $Na_{0.28}V_2O_5$ nanorings/nanobelts has been presented in in Figure 11 [64].

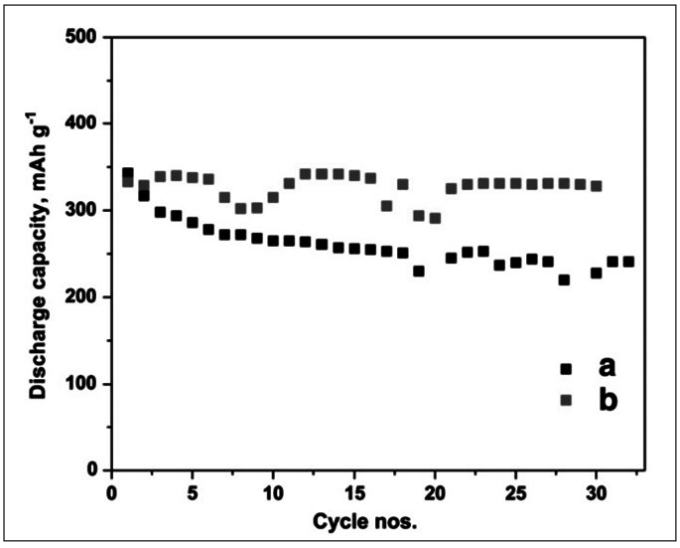

Figure 10. Specific capacity vs cycle no. (a) $Na_{0.33}V_2O_5 \cdot 1.5H_2O$ nanorings/nanorods and (b) $Na_{0.33}V_2O_5 \cdot 1.5H_2O$ /RGO composite.

The probable electrochemical reaction mechanism for $Na_{0.28}V_2O_5$ nanorings/nanobelts could be as follows

$$Na_{0.28}V_2O_5 + 0.33Li^+ + 0.33e^{-1} \rightarrow Li_{0.33}Na_{0.28}V_2O_5$$

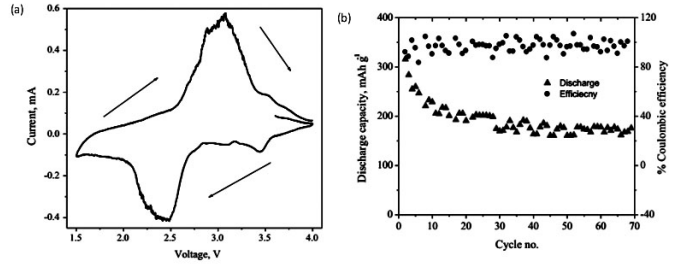

Figure 11. (a) Cyclic voltammogram of $Na_{0.28}V_2O_5$ nanorings/nanobelts electrode and (b) Charge–discharge vs. cycle number, and Coulombic efficiency of $Na_{0.28}V_2O_5$ nanorings/nanobelts

at 3.45 V ---(6)

$$Li_{0.33}Na_{0.28}V_2O_5 + 0.33Li^+ + 0.33e^{-1} \rightarrow Li_{0.66}Na_{0.28}V_2O_5$$

at 3.1 V ---(7)

$$Li_{0.66}Na_{0.28}V_2O_5 + 1Li^+ + 1e^{-1} \rightarrow Li_{1.66}Na_{0.28}V_2O_5$$

at 2.5 V ---(8)

$Na_{0.28}V_2O_5$ in nanobelt form exhibited better battery performance as shown in Figure 12 [65]

Porous ZrV_2O_7 delivered excellent discharge capacity of 159 mAh g^{-1} and 126 mAh g^{-1} at C/10 and 1 C [60]. The cyclic voltammetric behavior of porous ZrV_2O_7 has been

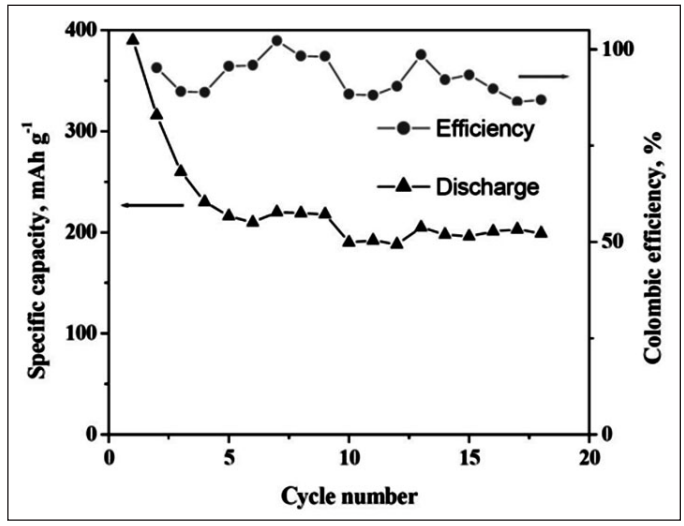

Figure 12. Discharge capacity vs. cycle number, coulombic efficiency of $Na_{0.28}V_2O_5$ nanobelts.

studied at scan rate of 0.1 mV/s between the voltage 1.5 and 4 V, and the results of which are shown in Figure 13a. The peaks that appeared, in first cycle at 3.2 V and 3.7 V, correspond to the reduction of $V^{+5} \rightarrow V^{+4}$ and oxidation of $V^{+4} \rightarrow V^{+5}$ during lithium intercalation and de-intercalation. However, the reduction peak at 3.2 V in the subsequent cycle disappears. The observed slight difference in the CV result compared to the reported may be due the difference in the size of ZrV_2O_7 and purity of the sample. Based on CV results, the intercalation/deintercalation of Li^+ into the porous ZrV_2O_7 matrix may be expressed as follows

$$ZrV_2O_7 + xLi^+ + xe^- \rightarrow Li_xZrV_2O_7 \quad ---(9)$$

The cyclic performance of porous ZrV_2O_7 at 0.1 C rate in the voltage range 1.5–4 V is shown in Figure 13 b. The first discharge cycle shows the capacity of 147 $mAhg^{-1}$. Generally, the fading of capacity observed between first and the subsequent cycles was ascribed to the formation of the SEI film caused by electrode and electrolyte side reactions [35] and structural distortion. After 37th cycle, the discharge capacity becomes constant up to 50 cycles, where it is about 159$mAhg^{-1}$.

$Fe_2V_4O_{13}$ nanoparticles were tested as cathode material for lithium secondary battery and charge/discharge results show that the 154 $mAhg^{-1}$ is retained after 50 th cycle.

The cyclic voltammograms (CV) of the $Fe_2V_4O_{13}$ coin cell was recorded at scan rate of 0.1 mVs-1 in the potential range 1.5 -4 V vs Li/Li^+. It is evident from Figure 14a that two broad reduction peaks centered at 2.7 and 2.0 V appeared in the initial lithiation (first three cycles). However, these two reduction peaks vanishes in the following cycles and it may due to the structural

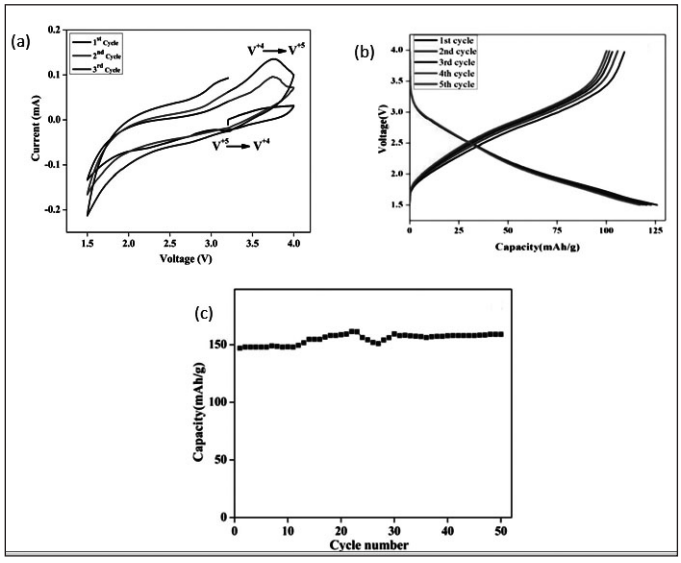

Figure 13 (a) Cyclic-volatammograms of the ZrV_2O_7 recorded between the voltage 1.5 and 4 V, at scan rate of 0.1 mV/s, (b) Charge-discharge curves of ZrV_2O_7 at a 1 C and (c) Cycle performance of ZrV_2O_7 at 0.1 C rate

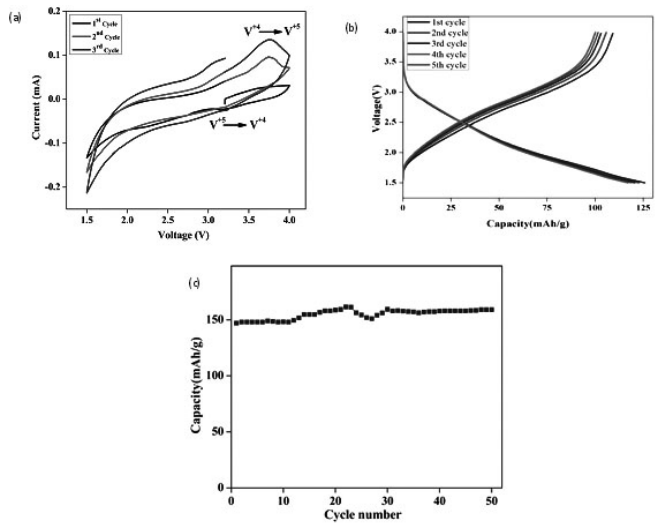

Figure 14 (a) Cyclic-volatammograms of the $Fe_2V_4O_{13}$ nanoparticles recorded between the voltage 1.5 and 4 V, at scan rate of 0.1 mV/s, (b) Charge-discharge curves of $Fe_2V_4O_{13}$ nanoparticles at a 0.1 C and (c) Cycle performance of $Fe_2V_4O_{13}$ nanoparticles at 0.1 C rate

degradation of $Fe_2V_4O_{13}$ during the lithiation process. Electrochemical performance of the $Fe_2V_4O_{13}$ nanoparticles in half-cell configuration, including the charge/discharge voltage profile and cycling performance between 1.5 and 4.0 V vs. Li^+/Li is shown in Figure14b and Figure14c. It is observed that the initial discharge capacity (254 $mAhg^{-1}$), gradually decreases and reaches 154 $mAhg^{-1}$ at 50 cycles. That is the $Fe_2V_4O_{13}$ films retained ~60% of their initial capacity after 50 cycles. Though the retention capacity of the $Fe_2V_4O_{13}$ films was less but it is close to the retention capacity of the commercialized $LiCoO_2$ and $LiMn_2O_4$, where these materials exhibit the retention capacity of about 70% after 50 cycles at 1C rate.

Conclusion

The emerging electrochemical energy storage devices will definitely play vital roles in the future energy landscape of the world. The innovation of electrode materials is determinant for the development of emerging electrochemical energy storage devices. Vanadium-based electrode materials have a big family with a large number of members with various compositions, structures and properties, which provides huge possibilities for exploring and identifying new electrode materials for emerging energy storage. In this review, a comprehensive overview of the progresses of promising vanadium-based nanomaterials for emerging metal-ion batteries is presented.

Acknowledgement:

One of the reviewers Nagaraju Ganganagappa greatly thank BRNS-BARC, DAE (No.:37(2)/14/25/2015/BRNS) Bombay, Govt. of India for financial sponsorship.

References

1. Chu, S. and A. Majumdar, *Opportunities and challenges for a sustainable energy future.* nature, 2012. **488**(7411): p. 294.
2. Kang, B. and G. Ceder, *Battery materials for ultrafast charging and discharging.* Nature, 2009. **458**(7235): p. 190.
3. Ivanova, M., *Good COP, bad COP: Climate reality after Paris.* Global Policy, 2016. **7**(3): p. 411-419.
4. Zhang, Q., et al., *Nanomaterials for energy conversion and storage.* Chemical Society Reviews, 2013. **42**(7): p. 3127-3171.
5. Lewis, N.S., *Toward cost-effective solar energy use.* science, 2007. **315**(5813): p. 798-801.
6. Aricò, A.S., et al., *Nanostructured materials for advanced energy conversion and storage devices.* Nature Materials, 2005. **4**: p. 366.
7. Cao, A.-M., et al., *Self-Assembled Vanadium Pentoxide (V2O5) Hollow Microspheres from Nanorods and Their Application in Lithium-Ion Batteries.* Angewandte Chemie International Edition, 2005. **44**(28): p. 4391-4395.
8. Bruce, P.G., B. Scrosati, and J.-M. Tarascon, *Nanomaterials for Rechargeable Lithium Batteries.* Angewandte Chemie International Edition, 2008. **47**(16): p. 2930-2946.
9. Goodenough, J.B., *Anomalous properties of the vanadium oxides.* Annual Review of Materials Science, 1971. **1**(1): p. 101-138.
10. Wu, C., F. Feng, and Y. Xie, *Design of vanadium oxide structures with controllable electrical properties for energy applications.* Chemical Society Reviews, 2013. **42**(12): p. 5157-5183.
11. Mai, L., et al., *Nanoscroll Buffered Hybrid Nanostructural VO2 (B) Cathodes for High–Rate and Long-Life Lithium Storage.* Advanced materials, 2013. **25**(21): p. 2969-2973.
12. Jayalakshmi, T., K. Nagaraju, and G. Nagaraju, *Enhanced lithium storage of mesoporous vanadium dioxide(B) nanorods by*

reduced graphene oxide support. Journal of Energy Chemistry, 2018. **27**(1): p. 183-189.

13. Ganganagappa, N. and A. Siddaramanna, *One step synthesis of monoclinic VO2 (B) bundles of nanorods: Cathode for Li ion battery.* Materials Characterization, 2012. **68**: p. 58-62.
14. Wang, J., et al., *Multi-shelled metal oxides prepared via an anion-adsorption mechanism for lithium-ion batteries.* Nature Energy, 2016. **1**(5): p. 16050.
15. Zhou, G., et al., *Nanowires for Electrochemical Energy Storage.* Chemical Reviews, 2019. **119**(20): p. 11042-11109.
16. Nagaraju, G., et al., *Vanadium pentoxide nanobelts: One pot synthesis and its lithium storage behavior.* Crystal Research and Technology, 2012. **47**(8): p. 868-875.
17. Nagaraju, G. and G.T. Chandrappa, *Solution phase synthesis of Na0.28V2O5 nanobelts into nanorings and the electrochemical performance in Li battery.* Materials Research Bulletin, 2012. **47**(11): p. 3216-3223.
18. Nagaraju, G., et al., *Na0.33V2O5·1.5H2O nanorings/nanorods and Na0.33V2O5·1.5H2O/RGO composite fabricated by a facile one pot synthesis and its lithium storage behavior.* Solid State Ionics, 2012. **227**: p. 30-38.
19. Cai, Y., et al., *Na0.282V2O5: A high-performance cathode material for rechargeable lithium batteries and sodium batteries.* Journal of Power Sources, 2016. **328**: p. 241-249.
20. Adarakatti, P.S., et al., *Fe2V4O13 Nanoparticles Based Electrochemical Sensor for the Simultaneous Determination of Guanine and Adenine at Nanomolar Concentration.* Electroanalysis, 2018. **30**(9): p. 1971-1982.
21. Li, P., et al., *Direct Growth of Fe2V4O13 Nanoribbons on a Stainless-Steel Mesh for Visible-Light Photoreduction of CO2 into Renewable Hydrocarbon Fuel and Degradation of Gaseous Isopropyl Alcohol.* ChemPlusChem, 2013. **78**(3): p. 274-278.
22. Lakkepally, S., et al., *A new and effective approach for Fe2V4O13 nanoparticles synthesis: Evaluation of electrochemical performance as cathode for lithium secondary batteries.* Journal of Alloys and Compounds, 2018. **737**: p. 665-671.
23. Shreenivasa, L., et al., *Engineering of highly conductive and mesoporous ZrV2O7: a cathode material for lithium secondary batteries.* Journal of Solid State Electrochemistry, 2019. **23**(4): p. 1201-1209.
24. Kuang, Q., et al., *Sol-gel synthesized zirconium pyrovanadate as a high-capacity cathode for rechargeable Li batteries.* Electrochimica Acta, 2015. **170**: p. 229-233.
25. Xu, X., et al., *Vanadium-Based Nanomaterials: A Promising Family for Emerging Metal-Ion Batteries.* **n/a**(n/a): p. 1904398.
26. Chirayil, T., P.Y. Zavalij, and M.S. Whittingham, *Hydrothermal Synthesis of Vanadium Oxides.* Chemistry of Materials, 1998. **10**(10): p. 2629-2640.
27. Bahlawane, N. and D. Lenoble, *Vanadium Oxide Compounds: Structure, Properties, and Growth from the Gas Phase.* Chemical Vapor Deposition, 2014. **20**(7-8-9): p. 299-311.
28. Cheng, F. and J. Chen, *Transition metal vanadium oxides and vanadate materials for lithium batteries.* Journal of Materials Chemistry, 2011. **21**(27): p. 9841-9848.
29. McNulty, D., D.N. Buckley, and C. O'Dwyer, *Synthesis and electrochemical properties of vanadium oxide materials and structures as Li-ion battery positive electrodes.* Journal of Power Sources, 2014. **267**: p. 831-873.
30. Wu, C. and Y. Xie, *Promising vanadium oxide and hydroxide nanostructures: from energy storage to energy saving.* Energy & Environmental Science, 2010. **3**(9): p. 1191-1206.
31. Li, M., et al., *Hydrothermal Synthesis of VO2 Polymorphs: Advantages, Challenges and Prospects for the Application of Energy Efficient Smart Windows.* Small, 2017. **13**(36): p. 1701147.
32. Zhong, L., et al., *Phase Evolution of VO2 Polymorphs during Hydrothermal Treatment in the Presence of AOT.* Crystal Growth & Design, 2017. **17**(11): p. 5927-5934.
33. Morrison, V.R., et al., *A photoinduced metal-like phase of monoclinic VO₂ revealed by ultrafast electron diffraction.* Science, 2014. **346**(6208): p. 445-448.
34. Shvets, P., et al., *A review of Raman spectroscopy of vanadium oxides.* Journal of Raman Spectroscopy, 2019. **50**(8): p. 1226-1244.
35. Ji, S., F. Zhang, and P. Jin, *Selective formation of VO2(A) or VO2(R) polymorph by controlling the hydrothermal pressure.* Journal of Solid State Chemistry, 2011. **184**(8): p. 2285-2292.
36. Li, M., et al., *Synthesis, field-emission and electric properties of metastable phase VO2 (A) ultra-long nanobelts.* Dalton Transactions, 2011. **40**(41): p. 10961-10965.
37. Dai, L., et al., *VO2 (A) nanostructures with controllable feature sizes and giant aspect ratios: one-step hydrothermal synthesis and lithium-ion battery performance.* RSC Advances, 2012. **2**(12): p. 5265-5270.
38. Zhang, L., et al., *Synthesis and formation mechanism of VO2(A) nanoplates with intrinsic peroxidase-like activity.* RSC Advances, 2015. **5**(75): p. 61371-61379.
39. Baudrin, E., et al., *Preparation of nanotextured VO2 [B] from vanadium oxide aerogels.* Chemistry of materials, 2006. **18**(18): p. 4369-4374.
40. Jayalakshmi, T., K. Nagaraju, and G. Nagaraju, *Enhanced lithium storage of mesoporous vanadium dioxide (B) nanorods by reduced graphene oxide support.* Journal of energy chemistry, 2018. **27**(1): p. 183-189.
41. Zhang, Y., et al., *Controlled synthesis of 3D porous VO 2 (B) hierarchical spheres with different interiors for energy storage.* Inorganic Chemistry Frontiers, 2018. **5**(11): p. 2798-2810.
42. Hagrman, D., et al., *A New Polymorph of VO2Prepared by Soft Chemical Methods.* Journal of Solid State Chemistry, 1998. **138**(1): p. 178-182.
43. Teixeira, D., et al., *Particle size, morphology and phase transitions in hydrothermally produced VO 2 (D).* 2017. **41**(17): p. 9216-9222.
44. Zhang, Y., et al., *Controlled synthesis of 3D porous VO 2 (B) hierarchical spheres with different interiors for energy storage.* 2018. **5**(11): p. 2798-2810.
45. Kamila, S., et al., *Combined Experimental and Theoretical Insights into Energy Storage Applications of a VO2 (D)–Graphene Hybrid.* 2019. **123**(39): p. 24280-24288.
46. Derkaoui, I., et al., *Facile growth of varied phases and morphologies of vanadium oxides nanostructures: Structural and electrical properties.* Superlattices and Microstructures, 2019. **127**: p. 11-19.
47. Xu, Y., L. Zheng, and Y.J.D.T. Xie, *From synthetic montroseite VOOH to topochemical paramontroseite VO 2 and their*

applications in aqueous lithium ion batteries. 2010. **39**(44): p. 10729-10738.

48. Wu, C., et al., *Synthetic paramontroseite VO 2 with good aqueous lithium–ion battery performance.* 2008(33): p. 3891-3893.
49. Yao, J., et al., *Revitalized interest in vanadium pentoxide as cathode material for lithium-ion batteries and beyond.* 2018. **11**: p. 205-259.
50. Wang, J., et al., *Multi-shelled metal oxides prepared via an anion-adsorption mechanism for lithium-ion batteries.* 2016. **1**(5): p. 16050.
51. Nagaraju, G., et al., *Vanadium pentoxide nanobelts: one pot synthesis and its lithium storage behavior.* 2012. **47**(8): p. 868-875.
52. Nagaraju, G., et al., *Vanadium oxide nanorings: Facile synthesis, formation mechanism and electrochemical properties.* 2016. **83**: p. 542-549.
53. Zhang, C., et al., *Additive-free synthesis of 3D porous V2O5 hierarchical microspheres with enhanced lithium storage properties.* Energy & Environmental Science, 2013. **6**(3): p. 974-978.
54. Nagaraju, G., et al., *Synthesis of $$\hbox {V}_{2} \hbox {O}_{5}$$V2O5nanoparticles: cathode materials for lithium-ion batteries.* 2019. **42**(3): p. 88.
55. Song, X., et al., *Uniform β-Na0. 33V2O5 nanorod cathode providing superior rate capability for lithium ion batteries.* 2019. **31**(9): p. 094001.
56. Steunou, N. and J. Livage, *Rational design of one-dimensional vanadium(v) oxide nanocrystals: an insight into the physico-chemical parameters controlling the crystal structure, morphology and size of particles.* CrystEngComm, 2015. **17**(36): p. 6780-6795.
57. Cheng, F. and J.J.J.o.M.C. Chen, *Transition metal vanadium oxides and vanadate materials for lithium batteries.* 2011. **21**(27): p. 9841-9848.
58. Nagaraju, G.J.J.o.t.B.C.S., *Ultra long single crystalline Na0. 3V2O5 nanofibers/nanorings synthesized by a facile one pot green approach and their lithium storage behavior.* 2013. **24**(10): p. 1662-1668.
59. Li, Q., et al., *Superstructure ZrV 2 O 7 nanofibres: thermal expansion, electronic and lithium storage properties.* 2016. **18**(47): p. 32160-32168.
60. Shreenivasa, L., et al., *Engineering of highly conductive and mesoporous ZrV 2 O 7: a cathode material for lithium secondary batteries.* 2019. **23**(4): p. 1201-1209.
61. Whittingham, M.S.J.J.o.T.E.S., *The role of ternary phases in cathode reactions.* 1976. **123**(3): p. 315-320.
62. Udayabhanu, et al., *Epigallocatechin gallate (EGCG)–assisted combustion synthesis of V2O5 nanoparticles for Li-ion battery.* 2019.
63. Nagaraju, G., et al., *Na0. 33V2O5 · 1.5 H2O nanorings/nanorods and Na0. 33V2O5 · 1.5 H2O/RGO composite fabricated by a facile one pot synthesis and its lithium storage behavior.* 2012. **227**: p. 30-38.
64. Nagaraju, G. and G.T.J.M.R.B. Chandrappa, *Solution phase synthesis of Na0. 28V2O5 nanobelts into nanorings and the electrochemical performance in Li battery.* 2012. **47**(11): p. 3216-3223.
65. Nagaraju, G.J.Z.f.a.u.a.C., *Hydrothermal Synthesis of Na0. 28V2O5 Nanobelts and their Electrochemical Behavior in Lithium Batteries.* 2012. **638**(14): p. 2286-2291.

	**Manukumar K. N.** *obtained his M.Sc.(Chemistry) in 2014 from Kuvempu University, Shankaraghtta, Karnataka. Currently, he is pursuing Ph.D.under the supervision of Dr.G.Nagarajuat Energy Materials Laboratory, Department of Chemistry, SiddagangaInstitute of Technology, Tumakuru. His research interests are anode materials for lithium ion battery and efficient photocatalyst for photocatalytic hydrogen generation.*
	**Nagaraju Ganganagappa** *recived his M.Sc. (2000) and Ph.D. degree (2009) from Bangalore University, Bangalore. He is currently Asst. Professor at Energy Materials Research Laboratory, Dept. of Chemistry, Siddaganga Institute of Technology, Tumakuru. His research interests are graphene chemistry, anode materials for lithium ion battery, Hydrogen generation via photocatalytic water splitting reaction, Electrochemical sensor, Photocatalytic degradation of organic dyes.*
	**Dr. Balaji P Mandal** *completed MSc from University of Burdwan, West Bengal in 2003. He was awarded the PhD degree in Chemistry in 2009 by Mumbai University. He did his postdoctoral research in development of new electrodes for Li ion battery at Wayne State University, USA. He was awarded DAE-Young Scientist award in 2012. He has been awarded membership of National Academy of Science, India and also he has received DAE-SSPS Young Achiever Award in 2017. Presently he is involved in development of battery materials. He has transferred the technology for synthesis of electrode materials for litium ion battery to different Indian companies for commercialization. Dr Mandal has authored more than 65 scientific papers in the journals of international repute.*

Recent Advances in 3D GO Sponge as Sulfur Host and interlayer for lithium–sulfur batteries

Dipa Dutta Pathak [a*], Balaji Prasad Mandal [a,b]
[a] *Chemistry Division, Bhabha Atomic Research Centre, Mumbai-400085, India*
[b] *Homi Bhabha National Institute, Mumbai-400094, India*
E-mail: drdipa01@gmail.com, bpmandal@barc.gov.in, Tel: +91-22-25592201

Abstract

Lithium-sulfur (Li-S) batteries are one type of promising next-generation energy storage devices. Remarkable efforts have been dedicated for developing conductive well-engineered cathode to improve active materials utilization and cycling stability. This review starts with a concise discussion of the working principles, brings out the challenges and briefly describes the potential strategies to overcome these challenges for commercialization of Li-S batteries. Among the different well engineered sulfur hosts, 3D graphene sponges have recently captured significant importance in battery research. Here, we have summarized current developments of 3D graphene based materials as sulfur host and interlayers. Superiority of such materials for diminishing the shuttling of lithium polysulfide (LiPS) and improving active materials (sulfur) utilization has been discussed. We have summarised the challenge that need to be addressed for 3D graphene sponge-based cathode in Li-S batteries. A new strategy has also been proposed to improve the electrochemical performance, which shed light on commercials application of 3D graphene sponge-based cathode in high performance Li-S batteries.

1. Introduction

The ever increasing consumption of fossil fuels to meet the modern day energy demand has resulted in a significant increase in emission of greenhouse gasses, worsening the global warming threat. Renewable and clean energy sources such as wind and solar must be a good alternative but these discontinuous energy sources need alternate systems for energy storage. Furthermore, electrified vehicles can efficiently mitigate the urban environmental pollution by replacing gasoline-based vehicles. Rechargeable battery can offer an encouraging solution for vehicle electrification and renewable energy storage. The rechargeable lithium ion battery is recognized as a promising choice for energy storage systems and has revolutionized the portable electronic industry since its commercialization.[1-3] Despite the fact that Li-ion batteries have the highest energy density among rechargeable batteries, they still fall short to meet many modern day applications like vehicle electrification. Relatively lower specific capacities of cathode materials (~150 mAh g^{-1} for layered oxides and ~170 mAh g^{-1} for $LiFePO_4$) compared to those of the anode (370 mAh g^{-1} for graphite and 4200 mAh g^{-1} for Si) have been a limiting factor to the energy density of these batteries.[4],[5] Thus, there is a huge impulse for the improvement of high capacity energy storage solutions. Lithium–Sulfur batteries with their high theoretical capacity represent proficient alternative energy storage for various applications ranging from stationary grid storage to electric vehicles.

2. Advantages of Li-S battery

Elemental sulfur (S), grab special attention as a cathode material because of its high theoretical capacity (1675mAh g^{-1}) with a high theoretical specific energy of 2600 Wh kg^{-1}, on the presumption of the complete reaction of lithium with sulfur to form Li_2S.[6],[7] The theoretical capacity of S is five times higher than those of traditional cathode materials based on transition metal oxides or phosphates. Moreover, natural abundance of sulfur (~ 3% of earth's mass) makes the cathode material low cost, and it is also environmental friendly.[4],[8] More importantly, low operating voltage (~ 2.1 V) of Li-S batteries could offer safety advantages over the high-voltage intercalation cathodes (>3.3 V) and also strengthen the safety of the large format cells.[1] In addition, it has ability to produce useful energy at high temperatures upto 300 ^oC.

3. Working principle of Li–S batteries

Like other Li-ion batteries, a typical Li–S battery consists of a cathode, anode and separator in electrolyte solution as shown in figure 1(a). The Li-S battery is basically Li metal batteries which use Li metal as anode and sulfur containing materials as cathode with organic liquid or solid electrolytes. The electrochemistry of the cathode of Li–S batteries, is multistep process as depicted in figure 1(b).The overall electrochemical reaction can be described as: during the discharge process, at the anode lithium is oxidized into lithium ions by releasing one electron while in cathode side sulfur is reduced to lithium sulphide (Li_2S) by

accepting lithium ions and electrons. When the sulfur (S_8) is subjected to reduction (during discharge), two plateaus appear in the discharge curve. First, reduction of elemental sulfur to higher-order polysulfides (Li_2S_x, (x=8, 6, 5 and 4) and then again high-order polysulfides to low-order polysulfides (Li_2S_x, 1 < x< 4) and finally Li_2S.[9]

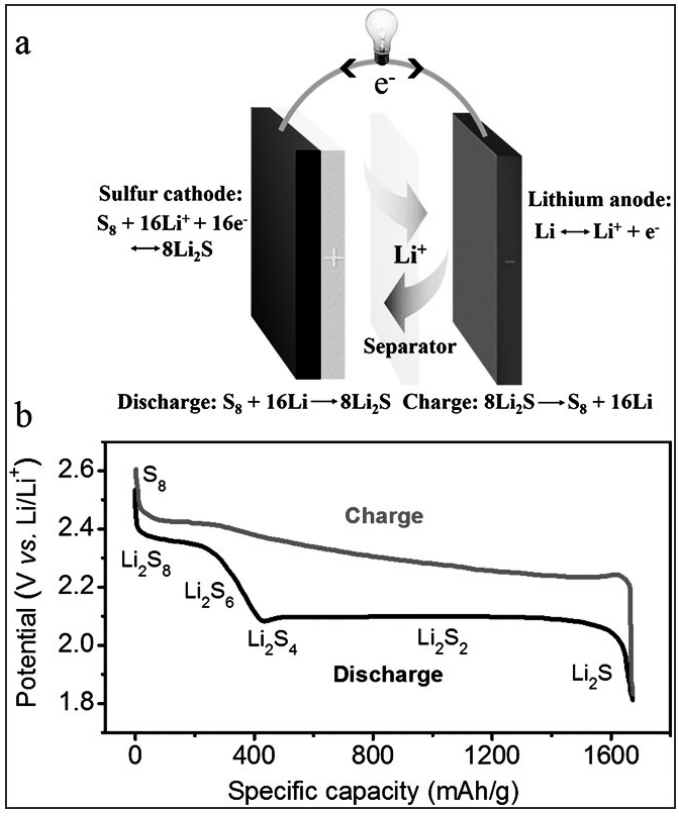

Figure 1: (a) Schematic diagram of a typical Li–S cell and (b) a typical 2-plateau charge/discharge voltage profile of lithium–sulfur batteries in ether-based electrolytes.[Reproduced from Ref. 9 with permission from The Royal Society of Chemistry]

4. Bottleneck for commercialization

Practical shortcomings of the Li−S technologies are hampering their employment in practical application. Very low electronic conductivity of sulfur (5× 10^{-30} S/cm at 25 °C) and intermediate lithium polysulfides formation deteriorates the electrochemical performance of the cell. Another major issue associated with Li-S battery is high solubility of the intermediate products (lithium polysulfides Li_2S_x (x=8, 6, 5 and 4)) in liquid electrolyte and their migration to the lithium anode side. This "shuttle effect" of polysulfides results into low coulombic efficiency, capacity fading and cathode pulverization.[10],[11] Furthermore, a part of the soluble polysulfides are strongly reduced to insoluble Li_2S and then deposited on the both side of the electrode.[12] These insoluble agglomerates on both electrodes can lead to degradation of the electrode structure, unreachability of the active components onto the electrode and increased cell impedance. The metal anode suffers growth of Li dendrites, which may leads to short circuit risk. In addition, a solid electrolyte interphase (SEI) layer is formed on Li anode due to Li electrolyte interaction, causing significant irreversible capacity loss.[13] Due to dissolution of polysulfide, the viscosity of the electrolyte increases lowering the ionic conductivity and clogging the separator membrane.[14] Furthermore, increase in volume of sulfur cathode (~80%) during lithiation/de-lithiation process due to the density differences of sulfur 2.06 g/cm^{-3} and lithium sulfide (1.66 g cm^{-3}); resulted mechanical distortion of cathode, fast capacity loss and limits the cycle life.[15] These accumulative effects are reflected in the poor cycle life, low specific capacity, and electrode pulverization of Li-S battery upon charge/discharge cycling.

During last decade, mainstream Li-S battery research have been dedicated on addressing the nonconductive nature of S/Li_2S, "shuttle effect" of polysulfides and the volume expansion during lithiation. Various techniques were adopted to address these issues namely,

(1) To increase conductivity of sulfur by embedding it into various carbon matrices.[4],[6],[15]

(2) Use metal oxide additives to strengthen binding of the intermediate polysulfides, which significantly reduces the shuttling effect of polysulfides.[16-18]

(3) Wrap sulfur with conducting polymer, which form a strong membrane that can accommodate the stress generated by volume expansion and keep away sulfur from direct contact with electrolytes.[1],[19-21]

However, it is worth noting that such cathode modification leads to further limitation of low areal sulfur loading (<2 mg cm^{-2}) and as reported the amount of active mass loading in the composite electrode is less than 70 wt. %.[8],[21-23] These "double low" issues significantly diminish the advantage of Li–S batteries. Recently, three dimensional (3D) sulfur host materials are being explored as an efficient agent to improve the energy density of Li-S batteries by improving the sulfur loading and sulfur content on the cathode host. Herein, we summarize the notable advances of 3D graphene oxide (GO) based sulfur host cathodes and interlayers of Li–S batteries. The lithium polysulfide (LiPS) trapping behaviour of functionalized 3D GO sponge and corresponding electrochemical performance improvement is systematically brought out in this report.

5. Engineered 3D sulfur host to overcome drawbacks

The ideal cathode host material for Li-S batteries should have (i) high electrical conductivity, (ii) stable material structure to sustain the strain generated by the volume changes during cycling, (iii) electrochemical affinity for sulfur and (iv)ability to accommodate high

loading of active mass. Considering the abovementioned criteria, carbonaceous materials are the most suitable host of sulfur for Li–S batteries. In addition, carbonaceous materials can physically entrap lithium polysulfides to mitigate capacity fading and improve longevity. Among the conductive carbonaceous materials, graphene is a two-dimensional (2D) material with superior electrical conductivity, mechanical strength, and high surface area making it a useful matrix to anchor sulfur for electrochemical energy storage applications. [24] However, due to 2D open structure graphene fails to trap the polysulfides resulting in low coulombic efficiency and capacity fading. Therefore, it is required to engineer a three-dimensional (3D) structure of graphene that provides all the features of graphene. Considerable efforts have been dedicated to design 3D graphene oxide sulfur host for improving the electrochemical performance of Li–S batteries. The sulfur impregnating into the 3D structure can be achieved by melt-diffusion and liquid infiltration method. This review summarizes the 3D graphene oxide based framework as cathode host and interlayer between cathode and separator.

5.1 GO Sponge based cathode host

5.1.1 Bare GO sponge

Hydrothermal synthesis of GO sponge: In 2014, Lu and co-workers [25] prepared a self-supporting graphene sponges using hydrothermal reduction followed by freeze dying. The as prepared GO sponges showed a 3D well interconnected porous network. Figure 2a shows the photographs of freeze dry graphene hydrogel. Sulfur was impregnated into pores of synthesised graphene sponges through a heat treatment of mixtures of sulfur and GO sponge at 155 ^{O}C for 10 h. The pores are filled with sulfur while the graphene sponge maintains essential electrical contacts between carbon and the insulating sulfur and ensure Li–ion access within the cathode. This 3D electrode have high areal mass loading of 12 mg sulfur/cm^2; approximately 6–12 times higher than that of previously reported.[26-28] The high areal specific capacity of the cathode (4.53 mAh cm^{-2} after 300 cycles) and slow decay rate (0.08% per cycle at 0.1C) after 300 cycles represents a significant step toward the cathode host engineering. These accomplishments have encouraged many researchers to realize the potential of structural engineering of graphene for Li–S batteries. An additional demonstration of an N-doped 3D graphene host (NG) for sulfur was studied by Wutthiprom et al. [29] The sulfur loading process onto NG achieved by the above mentioned heat treatment method. In addition to the modification of the cathode, the group also introduced an interlayer of graphitic carbon nitride (g-C3N4) coated on carbon fiber paper (CFP) for effective LiPS trapping. The resulting as-fabricated Li-S battery provided outstanding stability over 400 cycles with a reversible capacity of 1271 mAhg^{-1}at 0.1C. The capacity fading (only 0.068% per cycle) was much smaller than the self-supporting graphene sponges reported by Lu and co-workers. [25]

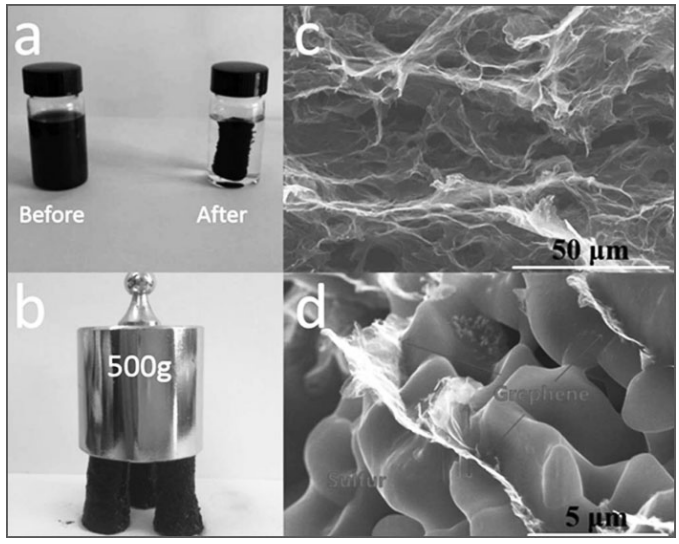

Figure 2: (a) Photographs of a 3.5 mg mL^{-1} homogeneous GO aqueous dispersion before and after hydrothermal reduction at 180 ^{O}C for 18 h; (b) photograph of three strong GO hydrogel allowing supporting weight; (c) SEM image of the interior microstructures of the GO sponges and (d) SEM image of interior microstructures of the S-GS with 80 wt.% sulfur.[Reproduced from Ref. 25 , This work is licensed under a Creative Commons Attribution-NonCommercial-NoDerivs 3.0 Unported License]

Another important work on GO sponge was reported by Jiang et al.,[24] they studied the effect of hydrothermal temperature (120, 150 and 180 ^{o}C) on the active mass loading onto the cathode host. The results indicate that sulfur loading increases suddenly along with the hydrothermal temperature rising from 120 to 150 ^{o}C. However, with further increase in the temperature to 180^{o}C, the loading does not increases enough due to the rapid increase of the viscosity of liquid sulfur. The group fabricated 3D porous graphene / sulphur nano composite by using mixture of GO dispersion and sulfur dissolved in carbon disulfide (CS_2) solution. As a result, active nano-sulfur was deposited within GO architectures. This hybrid material was found to deliver a specific capacity of 716.2 mAhg^{-1} at a current density of 100 mA g^{-1}after 50 cycles. Beside the wide application of GO sponge synthesised by hydrothermal technique followed by freeze dying as cathode host in Li-S battery, Fang's group [28] demonstrated fabrication of 3D GO structure without any special drying techniques. They reported alkali-free fabrication approach for graphene-based aerogel through hydrothermal reaction and heat treatment. The sulfur

loading on the aerogel was 1-3 mg cm^{-2}, which was much lower than the other reported studied.[25],[30] The thus fabricated 3D structure could not completely take care of the "double low" issue of Li-S batteries.

Recently, Fang et al. [30] reported a strategic fabrication method of binary graphene foam (BGF) sulfur host for Li-S batteries. BGF constituents, both N-doped graphene and highly porous graphene were prepared by freeze drying method. The author systematically investigated the individual component effect on the performance of the cell. Strong ionic attraction between electron-rich N and terminated Li in LiPS resulted strong chemical adsorption of LiPS on the N-doped graphene. On the other hand, the highly porous graphene not only improved the conductivity and provided ample pores for high sulfur loading but also accommodated the volumetric changes. With these advantages, Li-S batteries with the S/BGF cathode exhibited high specific discharge capacity of 1256 $mAhg^{-1}$, corresponding to a high areal capacity of 10.3 mAh cm^{-2}.

Chemical vapour deposition (CVD) method for synthesis of GO sponge: 3D graphene sponge synthesized by CVD method gathered attention due to its outstanding conductivity and high specific surface area and used as an efficient cathode host in Li-S battery. Xi et al. [31] reported an interconnected binder free 3D structure of few-layered graphene (FLG) synthesised by CVD method on Ni foam as a well-engineered cathode host. Sulfur solution infiltration method was used for the loading of the active materials onto the 3D FLG foam architecture. The battery exhibited excellent electrochemical reversibility and high capacity retention for up to 400 cycles. On the other hand, Zhang and co-worker [32] believed that sulfur loading on the 3D graphene sponge (3D-GS) by simple melt diffusion method was not a realistic approach to prevent the dissolution of LiPS. The group synthesized 3D-GS via CVD from a nickel catalyst template but adopted a novel design inspired by micro-pump for sulfur loading on 3D-GS. They immersed the 3D-GS with Ni template on the interface of oil-water two phase liquid seal system. Sulfur containing n-pentane solution was oil phase and $FeCl_3$ solution acted as water phase. The suction of sulfur-containing solution into 3D-GS was driven by the pressure differences generated between vacuum cavities due to Ni etching. As a result, after the evaporation of sulfur containing solution, the sulfur homogeneously anchored on the interior of 3D-GS structure. At a rate of 1C, the 3D-GS@S electrode delivered an initial capacity of 1010 $mAhg^{-1}$ and maintain at ~500 $mAhg^{-1}$ after 160 cycles. The researchers' suggested that this one step sulfur loading method could be applied to other 3D cathode host materials for high energy density rechargeable batteries.

To achieve much higher sulfur loading and overcome the "double low" issue, Hu and co-worker [23] combined the advantages of graphene foam, reduced graphene oxide (RGO), porous materials, and 3D porous interconnected architecture. The group reported the fabrication of CVD –grown graphene foam tangled with RGO aerogel (GF–RGO) and used the hierarchical macrostructure as a current collector. The structure not only provided abundant sites for high sulfur loading (14.36 mg cm^{-2}) with high sulfur content (89.4 wt%) simultaneously but also used as electrolyte reservoir. The sufficient pores effectively accommodated the stress generated during volumetric expansion of sulfur particles. Consequently, the GF–RGO/S cathodes (sulfur loading of 9.8 mg $cm^{-2}$and sulfur content of 83 wt%) exhibits a high areal capacity of 10.3 mA h cm^{-2} at 0.2 C rate with a good cycling stability. Further, it is suggested that such hybrid tangled network can also be used for Li-ion batteries and supercapacitors for high loading of suitable active materials.

5.1.2 GO sponge based composite

Presently, 3D GO sponge based composites have been receiving much attention as effective sulfur host due to synergetic effect of GO sponge and the other component. In 2014, Zhao et al. [33] reported a facile fabrication of 3D RGO/ultrathin MnO_2 nanosheet porous aerogel composites for sulfur host matrix in Li–S batteries. Nano sized S are evenly decorated into the 3D scaffold structure by a very straightforward solvothermal reaction process.

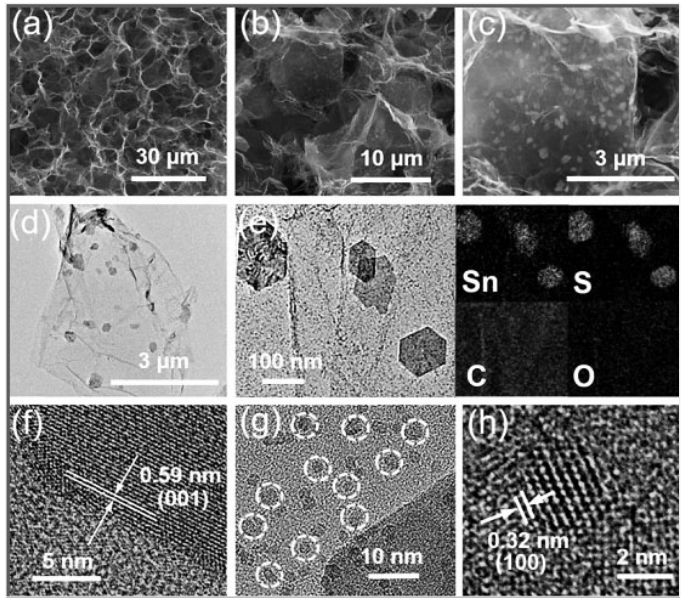

Figure 3: (a–c) SEM images of the SnS_2-ND@G aerogel. (d–e) TEM images of the SnS_2-ND@G aerogel and corresponding EDX elemental mapping results. (f–h) HRTEM images of SnS_2 nano-dots in the SnS_2-ND@G aerogel. [Reproduced from Ref. 27 with permission from The Royal Society of Chemistry]

The RGO component not only serves as an electron and ion transport passageway but also provided physical adsorption site for LiPS. The ultrathin MnO_2 nanosheets offer strong trapping sites for LiPS intermediates. As a result of this multifunctional cathode, 3D RGO/ultrathin MnO_2 nanosheet porous S- aerogel prepared cell exhibited high and stable specific discharge capacities over 200 cycles with outstanding high rate capability.

In addition, Manthiram group presented a new SnS_2 nano-dots embedded graphene aerogel (SnS2-ND@G) 3D structure as a proficient sulfur host (shown in figure 3) in 2018. [27] The hierarchically porous cathode host could load up to 10 mg/cm^2 sulfur; which is about 75 wt% of the 3D structure. Moreover, this work demonstrated homogeneous deposition of SnS_2 in the 3D matrix and significantly overcomes the flaws of previously studied physical incorporation of metal-compound in carbon matrix. [34] Due to the synergistic effect of chemical adsorption of LiPs on SnS_2 nano-dot and the physical entrapment on graphene, the SnS_2-ND@G aerogel architecture exhibits extraordinarily superior LiPS trapping ability with enhanced electrochemical stability. Consequently, a high initial specific capacity of 1234 mA h g^{-1} with a high capacity retention after 300 cycles was reported.

Another study by He and co-worker [35] also demonstrated the superiority of using binary component instead of single GO sponge as sulfur host. 3D carbon nanotubes (CNT)/graphene-sulfur (3DCGS) sponge with high sulfur content (~80.1%) was synthesized by a simple solvothermal reaction. The presence of CNT manipulated the pore size distribution within the cathode, which provided sufficient space of sulfur and polysulfides. The capacity decay of the battery was as low as 0.08% per cycle with a specific capacity of 877 mAhg^{-1} for the whole electrode at 0.2 C current rate.

5.2 3D GO sponge as separator

3D GO structures are also used as an interlayer between cathode and separator in bare form or can be coupled with other carbonaceous materials. Li et al. [36] fabricated three-dimensional (3D) reduced graphene oxide (RGO)/ activated carbon (AC) film by a simple hydrothermal method followed by mechanical pressing. The synthesized film acts as an interlayer for effectively trapping different polysulfide species. As a consequence, the Li-S cells with the interlayer display a notable initial discharge capacity of 1078 mAhg^{-1} and maintained at 655 mAhg^{-1} after 100 cycles. Furthermore, the researcher suggested that as RGO/AC interlayer has high specific area and abundant pores, the stress generated due to volume expansion are buffered to sufficient extent.

In another study, 3D interconnected reduced graphene oxide aerogel (GA) was used as a host of sulfur (S@GA cathode) as well as one of the component of interlayer. [26] GA together with nitrogen-rich graphitic carbon nitride (GCN) used as interlayer to accommodate

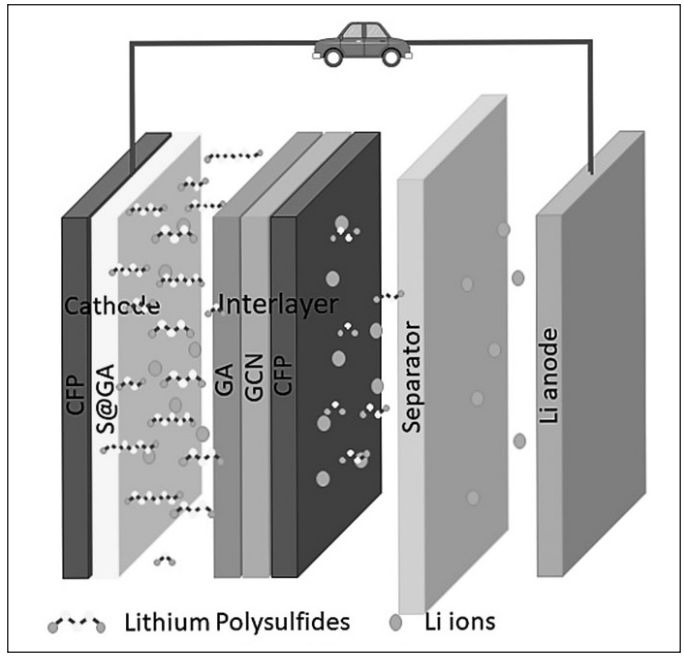

Figure 5: A schematic of a lithium sulfur battery with the S@GA cathode and the GA/GCN interlayer. [26]

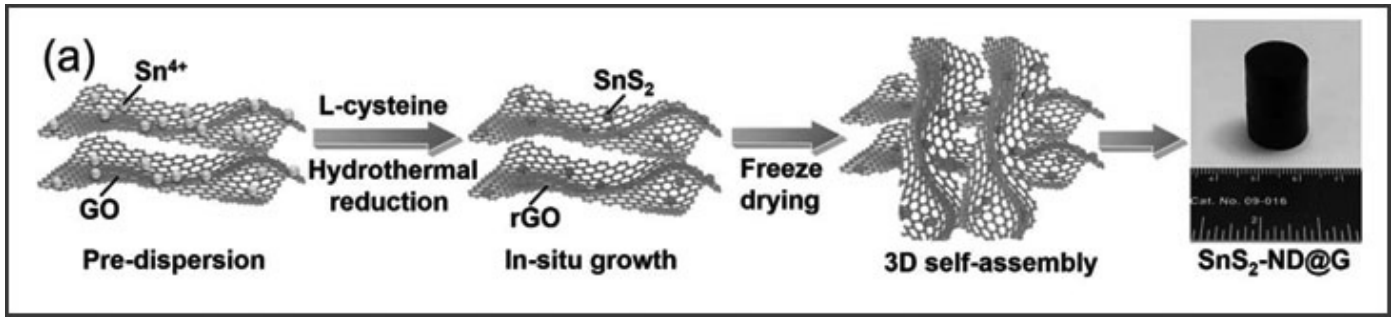

Figure 4: (a) Schematic illustration of the fabrication procedure and digital photo of the SnS_2-ND@G aerogel. [Reproduced from Ref. 27 with permission from The Royal Society of Chemistry]

the soluble LiPS. The GA/GCN interlayer was prepared by a layer-by-layer coating of the carbon fiber paper (CFP) substrate. Figure 5 represents the schematic of Li-S batteries component fabricated in this work including the sulfur loaded GA (S@GA coated on CFP) and the layer-by-layer GA/GCN/CFP interlayer. The group also investigated the adsorptive LiPS species on the interlayer by an ex situ X-ray photoelectron spectroscopy. This work demonstrated that the chemical bonds of sulfur related species on interlayer surface ensured effective LiPS adsorption. For active materials loading on cathode host (GA), conventional melt diffusion process was used. The insertion of interlayer between separator and cathode resulted 75% increase in the specific capacity. After 800 cycles, it shows a very low capacity fading of 0.056% per cycle. The group suggested that the Li-S battery with S@GA as cathode and GA/GCN as interlayer may be practically used in high-energy applications as it can efficiently overcome many drawback of the current Li-S batteries.

6. Summary and perspectives

Undoubtedly, 3D GO sponge sulfur host with high sulfur loading are crucial for the fabrication of advanced sulfur cathodes for practical use of Li-S batteries. Researchers are making remarkable contribution on improving electrochemical stability of high sulfur loaded cathode. The components of battery are engineered such a way that the cathode and interlayer can efficiently trap the LiPS and mitigate the challenges of "shuttle effect". A variety of GO sponge based cathode and interlayer materials are developed in last decade; which can address the "double low" issue of Li-S batteries. This review highlighting various synthesis methods of GO sponge, sulfur impregnation into the structure and finally the enhancement of electrochemical performance.

To meet modern world needs, high sulfur content cathodes with a high areal capacity are need of the hour. But on the other hand, lean electrolyte volume with low electrolyte/sulfur (E/S) ratio is also crucial for practical realisation of high energy density. Generally, for Li–S batteries with high E/S ratio (> 10 $\mu L/mg_S$), 50 wt.% of the whole cell come from electrolyte. [37] The effect of E/S ratio on the real energy density becomes preeminent when the areal sulfur loading increases (> 5mg/cm^2). The researcher while designing cathode had generally focussed on the principle drawback of the Li-S batteries. However, lean electrolyte batteries with high sulfur loading have not received enough attention. To improve the overall energy density, 3D sponge architecture having high sulfur loading with lean electrolyte volume is the need of the hour.

Reference

1. Y. Fu, A. Manthiram, Core-shell structured sulfur-polypyrrole composite cathodes for lithium-sulfur batteries, RSC Adv., 2 (2012) 5927-5929.
2. Y. Fu, Y.-S. Su. A. Manthiram, Sulfur-Polypyrrole Composite Cathodes for Lithium-Sulfur Batteries, J. Electrochem. Soc., 159 (2012) A1420-A1424.
3. H. Cheng, S. Wang, Recent progress in polymer/sulphur composites as cathodes for rechargeable lithium–sulphur batteries, J. Mater. Chem. A, 2 (2014) 13783-13794.
4. H. Wang, Y. Yang, Y. Liang, J.T. Robinson, Y. Li, A. Jackson, Y. Cui, H. Dai, Graphene-Wrapped Sulfur Particles as a Rechargeable Lithium–Sulfur Battery Cathode Material with High Capacity and Cycling Stability, Nano Lett., 11 (2011) 2644-2647.
5. H. Wu, Y. Cui, Designing nanostructured Si anodes for high energy lithium ion batteries, Nano Today, 7 (2012) 414-429.
6. L. Wang, Y. Zhao, L. Thomas Morgan, R. Byon Hye, In Situ Synthesis of Bipyramidal Sulfur with 3D Carbon Nanotube Framework for Lithium–Sulfur Batteries, Adv. Funct. Mater., 24 (2013) 2248-2252.
7. M. Sun, S. Zhang, T. Jiang, L. Zhang, J. Yu, Nano-wire networks of sulfur–polypyrrole composite cathode materials for rechargeable lithium batteries, Electrochem. Commun., 10 (2008) 1819-1822.
8. X. Zhou, F. Chen, J. Yang, Core@shell sulfur@polypyrrole nanoparticles sandwiched in graphene sheets as cathode for lithium–sulfur batteries, J. Energy Chem., 24 (2015) 448-455.
9. Z.W. Seh, Y. Sun, Q. Zhang, Y. Cui, Designing high-energy lithium–sulfur batteries, Chem. Soc. Rev., 45 (2016) 5605-5634.
10. Q. Wang, J. Jin, X. Wu, G. Ma, J. Yang, Z. Wen, A shuttle effect free lithium sulfur battery based on a hybrid electrolyte, Phys. Chem. Chem. Phys., 16 (2014) 21225-21229.
11. L. Xiao, Y. Cao, J. Xiao, B. Schwenzer, M. H. Engelhard, L. V. Saraf, Z. Nie, G. J. Exarhos, J. Liu, A Soft Approach to Encapsulate Sulfur: Polyaniline Nanotubes for Lithium-Sulfur Batteries with Long Cycle Life, Adv. Mater., 24 (2012) 1176-1181.
12. G. Li, S. Wang, Y. Zhang, M. Li, Z. Chen, J. Lu, Revisiting the Role of Polysulfides in Lithium-Sulfur Batteries, Adv. Mater., 30 (2018) 1705590.
13. G. Ma, Z. Wen, Q. Wang, C. Shen, J. Jin, X. Wu, Enhanced cycle performance of a Li–S battery based on a protected lithium anode, J. Mater. Chem. A, 2 (2014) 19355-19359.
14. R. Kumar, J. Liu, J.-Y. Hwang, Y.-K. Sun, Recent research trends in Li–S batteries, J. Mater. Chem. A, 6 (2018) 11582-11605.
15. W. Kong, L. Sun, Y. Wu, K. Jiang, Q. Li, J. Wang, S. Fan, Binder-free polymer encapsulated sulfur–carbon nanotube composite cathodes for high performance lithium batteries, Carbon, 96 (2016) 1053-1059.
16. J. Balach, J. Linnemann, T. Jaumann, L. Giebeler, Metal-based nanostructured materials for advanced lithium–sulfur batteries, J. Mater. Chem. A, 6 (2018) 23127-23168.
17. X. Ji, S. Evers, R. Black, L.F. Nazar, Stabilizing lithium–sulphur cathodes using polysulphide reservoirs, Nat. Commun., 2 (2011) 325.
18. M.-S. Song, S.-C. Han, H.-S. Kim, J.-H. Kim, K.-T. Kim, Y.-M. Kang, H.-J. Ahn, S.X. Dou, J.-Y. Lee, Effects of Nanosized

Adsorbing Material on Electrochemical Properties of Sulfur Cathodes for Li/S Secondary Batteries, J. Electrochem. Soc., 151 (2004) A791-A795.

19. Y. Fu, A. Manthiram, Orthorhombic Bipyramidal Sulfur Coated with Polypyrrole Nanolayers As a Cathode Material for Lithium–Sulfur Batteries, J. Phys. Chem. C, 116 (2012) 8910-8915.
20. G. Yuan, H. Wang, Facile synthesis and performance of polypyrrole-coated sulfur nanocomposite as cathode materials for lithium/sulfur batteries, J. Energy Chem., 23 (2014) 657-661.
21. Y. Yang, G. Yu, J.J. Cha, H. Wu, M. Vosgueritchian, Y. Yao, Z. Bao, Y. Cui, Improving the Performance of Lithium–Sulfur Batteries by Conductive Polymer Coating, ACS Nano, 5 (2011) 9187-9193.
22. S. Karuppiah, B. Kalimuthu, M.A. Nazrulla, S. Krishnamurty, K. Nallathamby, An effective polysulfide trapping polar interlayer for high rate Li–S batteries, J. Mater. Chem. A, 7 (2019) 10067-10076.
23. G. Hu, C. Xu, Z. Sun, S. Wang, H.-M. Cheng, F. Li, W. Ren, 3D Graphene-Foam–Reduced-Graphene-Oxide Hybrid Nested Hierarchical Networks for High-Performance Li–S Batteries, Adv. Mater., 28 (2016) 1603-1609.
24. Y. Jiang, M. Lu, X. Ling, Z. Jiao, L. Chen, L. Chen, P. Hu, B. Zhao, One-step hydrothermal synthesis of three-dimensional porous graphene aerogels/sulfur nanocrystals for lithium–sulfur batteries, J. Alloys Compd, 645 (2015) 509-516.
25. S. Lu, Y. Chen, X. Wu, Z. Wang, Y. Li, Three-dimensional sulfur/graphene multifunctional hybrid sponges for lithium-sulfur batteries with large areal mass loading, Sci. Rep.,4, (2014) 4629.
26. J. Wutthiprom, N. Phattharasupakun, M. Sawangphruk, Designing an interlayer of reduced graphene oxide aerogel and nitrogen-rich graphitic carbon nitride by a layer-by-layer coating for high-performance lithium sulfur batteries, Carbon, 139 (2018) 945-953.
27. L. Luo, S.-H. Chung, A. Manthiram, A three-dimensional self-assembled SnS2-nano-dots@graphene hybrid aerogel as an efficient polysulfide reservoir for high-performance lithium–sulfur batteries, J. Mater. Chem. A, 6 (2018) 7659-7667.
28. K. Zhang, F. Qin, Y. Lai, J. Li, X. Lei, M. Wang, H. Lu, J. Fang, Efficient Fabrication of Hierarchically Porous Graphene-Derived Aerogel and Its Application in Lithium Sulfur Battery, ACS Appl. Mater. Interfaces, 8 (2016) 6072-6081.
29. J. Wutthiprom, N. Phattharasupakun, J. Khuntilo, T. Maihom, J. Limtrakul, M. Sawangphruk, Collaborative design of Li–S batteries using 3D N-doped graphene aerogel as a sulfur host and graphitic carbon nitride paper as an interlayer, Sustain. Energy Fuels, 1 (2017) 1759-1765.
30. R. Fang, S. Zhao, K. Chen, D.-W. Wang, F. Li, Binary graphene-based cathode structure for high-performance lithium-sulfur batteries, J. Phys.: Energy, 2 (2020) 015003.
31. K. Xi, P.R. Kidambi, R. Chen, C. Gao, X. Peng, C. Ducati, S. Hofmann, R.V. Kumar, Binder free three-dimensional sulphur/few-layer graphene foam cathode with enhanced high-rate capability for rechargeable lithium sulphur batteries, Nanoscale, 6 (2014) 5746-5753.
32. Q. Zhang, S. Tan, X. Kong, Y. Xiao, L. Fu, Synthesis of sulfur encapsulated 3D graphene sponge driven by micro-pump and its application in Li–S battery, J. Materiomics, 1 (2015) 333-339.
33. X. Zhao, H. Wang, G. Zhai, G. Wang, Facile Assembly of 3D Porous Reduced Graphene Oxide/Ultrathin MnO2 Nanosheets-S Aerogels as Efficient Polysulfide Adsorption Sites for High-Performance Lithium–Sulfur Batteries, Chem. Eur. J., 23 (2017) 7037-7045.
34. L. Ma, H. Yuan, W. Zhang, G. Zhu, Y. Wang, Y. Hu, P. Zhao, R. Chen, T. Chen, J. Liu, Z. Hu, Z. Jin, Porous-Shell Vanadium Nitride Nanobubbles with Ultrahigh Areal Sulfur Loading for High-Capacity and Long-Life Lithium–Sulfur Batteries, Nano Lett., 17 (2017) 7839-7846.
35. J. He, Y. Chen, P. Li, F. Fu, Z. Wang, W. Zhang, Three-dimensional CNT/graphene–sulfur hybrid sponges with high sulfur loading as superior-capacity cathodes for lithium–sulfur batteries, J. Mater. Chem. A, 3 (2015) 18605-18610.
36. H. Li, L. Sun, Y. Zhang, T. Tan, G. Wang, Z. Bakenov, Enhanced cycle performance of Li/S battery with the reduced graphene oxide/activated carbon functional interlayer, J. Energy Chem., 26 (2017) 1276-1281.
37. M. Zhao, B.-Q. Li, H.-J. Peng, H. Yuan, J.-Y. Wei, J.-Q. Huang, Lithium–Sulfur Batteries under Lean Electrolyte Conditions: Challenges and Opportunities, Angew. Chem. Int. Ed., 59 (2020) 12636-12652.

	**Dr Dipa Dutta** *Pathak after completing her M.Sc. in Physics from Banaras Hindu University, received her Ph.D in Materials Science from Indian Institute of Technology Bombay in 2017. She has been awarded the "Excellence in Thesis Work" from IIT Bombay for outstanding research contribution. As part of her post-doctoral research she worked on development of cathode material for L-S batteries, as SERB-NPDF till 2019. She is currently working as a DST INSPIRE faculty at Bhabha Atomic Research Centre. Her research interests include design and fabrication of electrode materials of Li-ion and Li-S batteries. Her research findings have been published in reputed peer-reviewed international journals and well-received.*
	**Dr. Balaji P Mandal** *completed MSc from University of Burdwan, West Bengal in 2003. He was awarded the PhD degree in Chemistry in 2009 by Mumbai University. He did his postdoctoral research in development of new electrodes for Li ion battery at Wayne State University, USA. He was awarded DAE-Young Scientist award in 2012. He has been awarded membership of National Academy of Science, India and also he has received DAE-SSPS Young Achiever Award in 2017. Presently he is involved in development of battery materials. He has transferred the technology for synthesis of electrode materials for litium ion battery to different Indian companies for commercialization. Dr Mandal has authored more than 65 scientific papers in the journals of international repute.*

SOCIETY FOR MATERIALS CHEMISTRY (SMC)
(Reg. No. - Maharashtra, Mumbai/1229/2008/GBBSD)
c/o Chemistry Division
Bhabha Atomic Research Centre, Mumbai 400 085

APPLICATION FOR MEMBERSHIP

Please enroll me as a Life member of the *Society for Materials Chemistry* (**SMC**). My particulars are as follows:

Name :_____

Educational Qualifications :_____

Field of Specialization :_____

_____

Official Address :_____

_____

Telephone No. (Off.) :_____

Residential Address :_____

_____

Telephone No. (Res.) :_____

Address for Correspondence : Home/Office (Please tick one of the options)

E-mail Address :_____

Subscription Details

Mode of Payment : Cheque/DD/Cash
(Cheque/DD should be drawn in favor of "*Society for Materials Chemistry*" for Rs. 1000/- payable at Mumbai. For out-station *non-multi-city* cheques, please include Rs.50/- as additional charge for bank clearance.

Number :
Dated :
Drawn on Bank & Branch :
Amount :
Place:
Date: Signature

Registration Number: _____ (To be allotted by SMC office)

Printed by:
Ebenezer Printing House
Unit No. 5 & 11, 2nd Floor, Hind Service Industries
Veer Savarkar Marg, Shivaji Park Sea-Face, Dadar (W), Mumbai - 400 028
Tel.: 2446 2632 / 2446 3872 Tel Fax: 2444 9765 E-mail: outworkeph@gmail.com

In this issue

Published by

Society for Materials Chemistry

C/o. Chemistry Division

Bhabha Atomic Research Centre, Trombay, Mumbai 40085

e-mail: socmatchem@gmail.com, Tel: 91-22-25592001